

# Quasi-Integrals and the Origin of Bursting pH Oscillations in an Enzyme Model System

## Dissertation

zur Erlangung des akademischen Grades

**doctor rerum naturalium**  
**(Dr.rer.nat.)**

genehmigt durch

die Fakultät für Naturwissenschaften  
der Otto-von-Guericke-Universität Magdeburg

von **Dipl. Phys. Ronny Straube (geb. Möschke)**

geb. am **17. September 1975** in **Borna**

Gutachter: PD Dr. Marcus J.B. Hauser  
Prof. Dr. Dietrich Flockerzi  
PD Dr. Markus Bär

eingereicht am: 28. Juni 2005

verteidigt am: 21. Februar 2006



# Contents

<b>Contents</b>	<b>i</b>
<b>1. Introduction</b>	<b>1</b>
1.1. The hemin – hydrogen peroxide – sulfite system . . . . .	8
1.2. Outline of the thesis . . . . .	12
<b>I. Quasi-Integrals and Slow Manifolds in Reaction Networks</b>	<b>15</b>
<b>2. Singular Perturbation Theory</b>	<b>17</b>
2.1. A motivating example . . . . .	17
2.2. ODE systems with ‘small’ parameters . . . . .	19
<b>3. Quasi-Integrals</b>	<b>23</b>
3.1. Quasi-integrals in the hemin system . . . . .	23
3.2. Using quasi-integrals for model reduction . . . . .	26
3.3. Quasi-integrals in general reaction networks . . . . .	29
<b>4. Local Bifurcations in the Hemin System</b>	<b>33</b>
4.1. Two-parameter continuation in $k_0$ and $k_8$ . . . . .	33
4.2. Bifurcations along a one-parameter path . . . . .	35
4.3. Comparison between the 6-d system and its 3-d approximation . . . . .	37
<b>5. Summary and Discussion</b>	<b>39</b>
<b>II. The Origin of Bursting Behavior in the Hemin System</b>	<b>41</b>
<b>6. Dynamics and Bursting Oscillations in the Hemin System</b>	<b>43</b>
6.1. Change of coordinates . . . . .	43
6.2. A period doubling route to chaos . . . . .	44
6.3. Bursting oscillations . . . . .	46
<b>7. Slow-Fast Analysis – The Method</b>	<b>51</b>
7.1. Cartoon of the slow-fast structure of the hemin system . . . . .	51
7.2. A classification scheme for bursting behavior . . . . .	53

<b>8. The Slow-Fast Structure of the Hemin System</b>	<b>55</b>
8.1. Slow-fast analysis at a fixed value of $k_0$	56
8.2. Two-parameter continuation in $p$ and $k_0$	58
8.2.1. A transition in the bursting behavior	61
8.3. The origin of quasi-periodic behavior in the hemin system	63
8.3.1. A torus with unusual phase flow	63
8.3.2. Slow-fast analysis of the phase flow on the torus	64
<b>9. Summary and Discussion</b>	<b>69</b>
<b>III. Appendix</b>	<b>71</b>
<b>A. Dynamical Systems and Bifurcation Theory in a Nutshell</b>	<b>73</b>
A.1. Dynamical systems	73
A.1.1. The geometrical approach	75
A.1.2. Invariant sets, attractors, etc.	75
A.1.3. Hartman-Grobman and stable manifold theorem	76
A.1.4. Periodic orbits and Poincaré maps	79
A.2. Bifurcation theory	80
A.2.1. Center manifold theorem	83
A.2.2. Parameter dependent systems and normal forms	84
A.3. Local bifurcations in one-parameter families	86
A.3.1. Bifurcations of equilibria	87
A.3.2. Bifurcations of limit cycles	88
A.4. Local bifurcations in two-parameter families	91
A.4.1. Cusp bifurcation	92
A.4.2. Bogdanov-Takens bifurcation	92
A.4.3. Bautin bifurcation	93
A.5. Global bifurcations	94
A.5.1. Saddle homoclinic bifurcation	94
A.5.2. Saddle-node homoclinic bifurcation	96
<b>B. Investigation Methods and Parameter Settings</b>	<b>97</b>
B.1. The method of numerical continuation	97
B.2. Parameters and settings in the hemin system	99
B.3. Parameters and settings in the PO system	100
<b>C. Quasi-Integrals in the Peroxidase – Oxidase System</b>	<b>103</b>
<b>Bibliography</b>	<b>109</b>
<b>Danksagung</b>	<b>119</b>
<b>Deutsche Zusammenfassung</b>	<b>121</b>

# 1. Introduction

The field of nonlinear dynamics has attracted much attention during the past century since the seminal work of Poincaré [1] who studied the stability of planetary motions in the framework of classical Newtonian mechanics. Already at the end of the 19th century he noticed that small perturbations of integrable Hamiltonian systems may lead to unpredictable long-time behavior due to ‘small divisor’ resonant terms showing up in a perturbation series approach. The work of Poincaré marked the beginning of a period during which the perception began to prevail that irregular behavior in conservative systems is the rule rather than the exception. This period culminated in the works of Kolmogorov [2], Arnold [3] and Moser [4] who came up with the celebrated KAM theorem. For the case that the integrable, and therefore regular motion, occurs on a 2-torus where the frequencies are sufficiently incommensurable, the theorem basically says that the torus will persist under small perturbations. In the case that the frequencies are commensurable, small perturbations will cause the torus to decompose into smaller tori which again may be stable according to the KAM theorem. However, the motion in phase space between the tori is completely irregular and for sufficiently large perturbations *all* tori and therefore all regular behavior is destroyed.

Unlike conservative systems, where the total energy is a constant of motion, many real world systems belong to the class of so-called *dissipative systems* since they permanently dissipate energy into heat, for example, or rely on a steady exchange of energy and/or matter with the environment in order to operate properly. It has been a mystery for a long time how living organisms circumvent the second law of thermodynamics. Now we know that they represent open systems that continuously maintain a certain distance to thermodynamical equilibrium and thus, the second law is not applicable to them in the usual sense.

The distance to equilibrium can usually be controlled by parameters or boundary conditions modeling the environmental surrounding of the system under investigation. In particular, it is possible to bar an open system from reaching the thermodynamical equilibrium. Close to the equilibrium, the dynamics of the system follows linear relations among generalized fluxes and forces that cause the system to approach a unique stable nonequilibrium state. The states, close to the equilibrium, form the so-called thermodynamical branch (cf. Fig. 1.1) since it emanates continuously from the state of thermodynamical equilibrium. However, Nicolis and Prigogine [5] showed that when open systems are driven farther away from thermodynamical equilibrium, nonlinear processes may destabilize the thermodynamical branch giving rise to new stable nonequilibrium states which they termed *dissipative structures*. They further showed that for such structures to occur, a certain critical distance to equilibrium must be exceeded.

## 1. Introduction

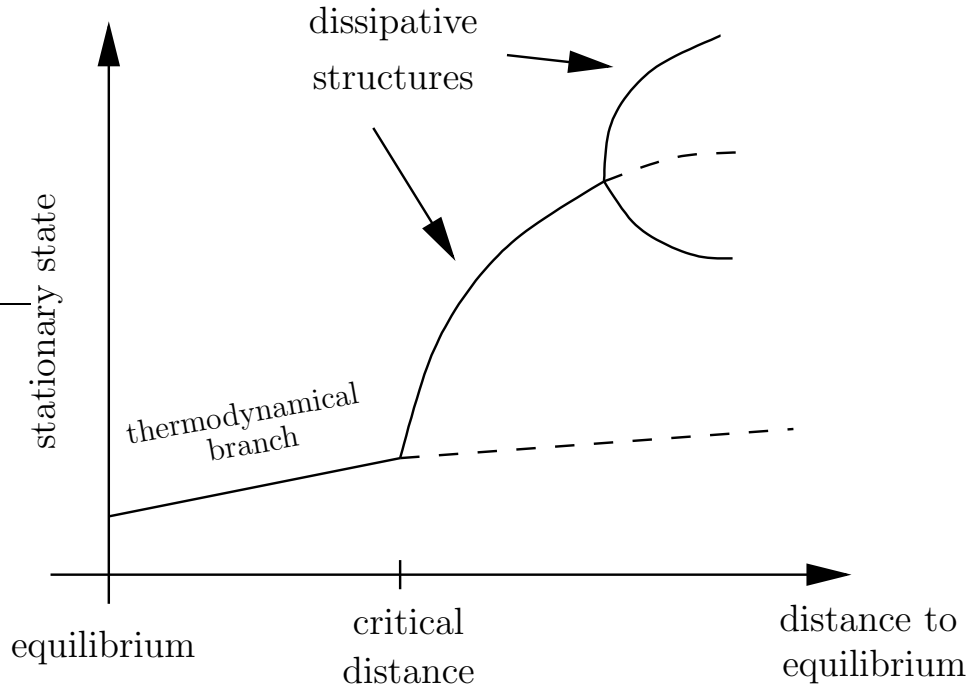


Figure 1.1.: Dissipative structures emerge far away from thermodynamical equilibrium as a critical parameter value is exceeded. Beyond that point the thermodynamical branch is unstable and nonlinear phenomena drive the system towards new stable nonequilibrium states. (stable states  $\leftrightarrow$  solid lines, unstable states  $\leftrightarrow$  dashed lines)

Today we know that the nonlinear behavior of a system is a further necessary condition for the occurrence of dissipative structures. The mathematical language in which nonlinear phenomena are frequently formulated is that of dynamical systems theory, i.e. one has to specify a suitable phase space  $X$  together with an evolution law for the state of the system. In the case that the evolution law is deterministic, the state of the system at time  $t$  is completely determined by a one-parameter group of transformations  $\varphi_t : X \rightarrow X$  according to  $x_t = \varphi_t x_0$  once the initial state  $x_0 \in X$  of the system is known. In general, one distinguishes two kinds of dynamical systems – continuous-time systems with  $t \in \mathbb{R}$  being a continuously varying parameter and discrete-time systems where  $t \in \mathbb{Z}$  is an integer. In the continuous-time case, the one-parameter group of transformations is also called a *flow* which is typically obtained as a solution of an initial value problem of a system of ordinary or partial differential equations depending on whether the system under consideration is spatially homogeneous or not.

Dissipative structures are frequently observed as a result of *self-organizing* processes in space or time where the individual entities of an ensemble spontaneously begin to act in a cooperative manner as soon as a relevant parameter of the system exceeds a

certain critical value. As a result, new properties of the system as a whole emerge which were not yet seen in the individual entities. These new system-theoretical aspects were combined by Haken [6] with the methods of nonlinear dynamics to establish a new field of research called *Synergetics*. Here the new emergent macroscopic features of a complex system, consisting of many subunits each of which follows a certain microscopic dynamics, are described close to the transition from individual to collective behavior by only very few degrees of freedom, so-called *order parameters*. As an example for temporal self-organization, consider an optical resonator containing an active medium whose atoms are excited by an external energy supply. Below a certain energy pump-rate, all atoms emit light just randomly resulting in a low power output of the system. However, above a certain threshold, the atoms start to synchronize their oscillation phases and the power output is high – the system works as a *laser*.

A distinct feature of dissipative systems, as compared to conservative ones, is that in the former bounded regions in phase space may shrink during the temporal evolution in which case all trajectories starting in that region are attracted by lower dimensional phase space objects such as points, curves or tori which would result in a regular motion of the system. In addition, it was found that the long-time dynamics of a dissipative system may occur on quite complicated sets in phase space. These sets can be of *fractal* nature which is the reason why they were called *strange attractors*. The behavior of trajectories on such an attractor is highly irregular or *chaotic*. For example, trajectories whose initial conditions on a chaotic attractor vary only slightly will diverge exponentially fast from each other in the course of the temporal evolution and thus, may lead after finite time to completely different behavior. As a consequence, it is practically impossible to forecast the long-time behavior of real world chaotic system since its initial conditions are only known with finite accuracy.

One of the first numerical evidences for the existence of a chaotic attractor was reported by Lorenz [7] in 1963 who studied a nonlinear three variable system of ordinary differential equations that was derived from a 2-dimensional convective fluid system by a Galerkin projection of suitable Fourier modes. In the same year, Smale [8] constructed his famous horseshoe map which is a simple 2-dimensional map that expands small phase space volumes in one direction while it contracts them in the orthogonal direction. Such maps may be induced by the flow of a continuous-time dynamical system on a suitable Poincaré section where they can occur in conjunction with a homoclinic orbit of the Poincaré map [9]. The horseshoe map has a very complicated invariant set exhibiting the structure of a direct product between two Cantor sets. If the dynamics is only considered on the invariant Cantor set, one finds the essential properties of chaotic behavior such as the ‘sensitive dependence on the initial conditions’ mentioned above. In addition, the invariant set of the horseshoe map contains a countable infinity of periodic points which are all of saddle-type, a countable infinity of homoclinic and heteroclinic orbits and a noncountable infinity of nonperiodic points. Thus, the typical (i.e. for almost all initial conditions) behavior of trajectories on the invariant set is highly irregular.

Although the invariant Cantor set of the horseshoe map is *not* an attractor, the map has an important property which is the reason why it is still considered as the prototypical example of a chaotic system: that is its *structural stability*. This means

## 1. Introduction

that if the horseshoe map is slightly perturbed, the invariant Cantor set as well as the properties of the dynamics on this set will persist. In this sense, the notion of structural stability can be used to define the phenomena of a system that are observable in numerical or real experiments which are always subject to small perturbations. Thus, a natural question to ask is: What is the ‘typical’ behavior of trajectories in a given dynamical system and how does it change as parameters in the system are varied? In this context, ‘typical’ means that the corresponding behavior is observed for a large set of initial conditions and/or parameter values. For example, a system could have a chaotic attractor for parameter values that form a set of Lebesgue measure zero in parameter space which, therefore, would not be observable in experiments. On the other hand, it is often the regular periodic behavior of a system which is of much more practical relevance than to know that a system has an invisible chaotic attractor.

Of particular interest are complex oscillatory states such as *mixed-mode* or *bursting* oscillations which are frequently observed in chemical and biological systems where they are of potential relevance for signal transduction processes. These periodic states exhibit a special waveform which can be described as a repeating pattern of  $L$  large amplitude oscillations that are followed by  $S$  small ones. Due to this property, mixed-mode or bursting states are labeled by the nomenclature  $L^S$ . Mixed-mode oscillations (MMOs) were first observed in chemical reaction systems such as the Belousov-Zhabotinsky (BZ) [10, 11, 12] and the peroxidase-oxidase (PO) reaction system [13, 14, 15], while bursting dynamics was predominantly reported for biological processes such as nerve signal conduction [16, 17], signal transduction dynamics in the cell involving calcium ions as second messengers [18, 19] and the secretion of insulin by pancreatic  $\beta$ -cells [20, 21, 22]. Thus, the distinction between mixed-mode and bursting oscillations is somewhat arbitrary and seems to reflect the context in which they were found experimentally.

Bursting behavior can be alternatively classified by a slow-fast analysis following Rinzel and Ermentrout [23]. Systems exhibiting bursting oscillations typically involve a fast oscillatory subsystem which is coupled to a slowly evolving variable which acts as a quasi-static bifurcation parameter for the fast subsystem. Accordingly, one can classify the bursting behavior by the type of bifurcations occurring in the fast subsystem, that lead to the emergence and disappearance of the bursting state [24]. MMOs are frequently encountered in the transition region from simple periodic or quasi-periodic to chaotic behavior where they either appear in periodic-chaotic or as (incomplete) Farey sequences (cf. Table 1.1). The latter often arise from phase-locked states on an invariant 2-torus as, for example, in the BZ [11, 25, 26] and in the PO system [14, 15, 27]. However, Hauser and Olsen [13] found MMOs in the PO system which were associated with a saddle-focus homoclinic orbit instead of a 2-torus. Similarly, Koper [28] observed MMOs in a three-variable extension of the Boissonade-DeKepper model [29] which emerge from a neutrally twisted homoclinic orbit in a codimension two bifurcation.

Another possible scenario was put forward by Ringland et. al. [30] who showed that a one-parameter family of two-extremum maps may (in a certain limit) equally account for the ordering of MMOs into Farey sequences without the necessity of involving a 2-torus. Goryachev et. al. [31] found a concrete realization of this map in terms of a Poincaré map associated with the 3-dimensional flow of another three-variable exten-

$F_n$	Elements in $F_n$
$F_1$	$\{\frac{0}{1}, \frac{1}{1}\}$
$F_2$	$\{\frac{0}{1}, \frac{1}{2}, \frac{1}{1}\}$
$F_3$	$\{\frac{0}{1}, \frac{1}{3}, \frac{1}{2}, \frac{2}{3}, \frac{1}{1}\}$
$F_4$	$\{\frac{0}{1}, \frac{1}{4}, \frac{1}{3}, \frac{1}{2}, \frac{2}{3}, \frac{3}{4}, \frac{1}{1}\}$

Table 1.1.: The general Farey sequence  $F_n$  is defined for any positive integer number  $n$ . It contains the set of irreducible rational numbers  $a/b$  with  $0 \leq a \leq b \leq n$  arranged in increasing order. Each three successive terms in a Farey sequence obey Farey arithmetic, i.e. the middle term in the sequence  $p/q, p'/q', p''/q''$  is the ‘sum’ of the neighbors according to  $\frac{p'}{q'} = \frac{p}{q} \oplus \frac{p''}{q''} \equiv \frac{p+p''}{q+q''}$ .

sion of the Boissonade-DeKepper model which accounts for a qualitative description of transient MMOs in the BZ reaction. They reported that the MMOs are embedded into a horseshoetype attractor.

In the present thesis, we investigate the bursting oscillations in the hemin – hydrogen peroxide – sulfite system (hemin system) [32, 33, 34] which represents a so-called pH oscillator (Fig. 1.2) since it induces periodic changes in the proton concentration of the reaction medium. Thus, the production and consumption of  $H^+$  ions are essential steps in the reaction mechanism of a pH oscillator. A large family of pH oscillators is based on the autocatalytic oxidation of  $HSO_3^-$  by  $H_2O_2$  [35] while they differ in the  $H^+$ -consuming species that provides for a negative feedback to allow for an oscillatory dynamics [35, 36, 37, 38, 39]. One of the main motivations to study pH oscillators is their potential relevance for biological systems since changes in the pH value affect many physiological parameters in the environment of the system, e.g. in the permeability of membranes or the activity of enzymes.

So far, most of the known pH oscillators involve only inorganic substances which clearly limits their biological relevance. Therefore, Hauser et. al. [32] developed a new pH oscillator based on the well-known pH-dependent oxidation of  $HSO_3^-$  by  $H_2O_2$  [35] which involves hemin as an enzyme model compound that provides for the required negative feedback step in order to generate oscillatory dynamics. Since hemin is considered as a biocompatible mimick of heme-containing enzymes [40, 41, 42], the hemin reaction system represents a first step towards a biologically more realistic pH oscillator.

The dynamical properties observed in the family of pH oscillators is very rich. Experimental and numerical investigations revealed a period doubling route to chaos [36, 37] as well as complex oscillatory patterns such as bursting oscillations [43, 44]. However, a detailed bifurcation analysis revealing the nature of the complex oscillatory patterns in pH oscillator systems has, to our knowledge, not yet been performed. Therefore, we devote one part of the present thesis to a detailed study of bursting oscillations in the

## 1. Introduction

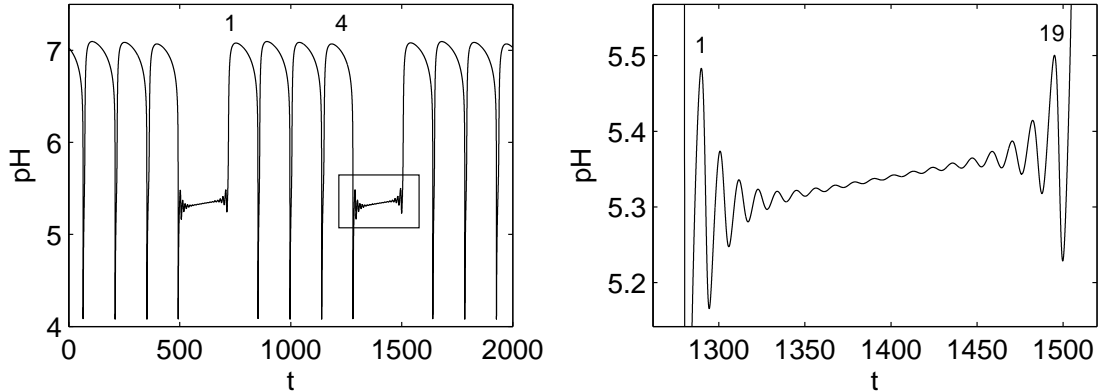


Figure 1.2.: Time series obtained from a numerical simulation of the bursting pH oscillations in the hemin system (left image): 4 large amplitude oscillations alternate with 19 small ones. The rectangular region is magnified in the right image showing the small amplitude oscillations.

hemin system where we are particularly interested in the bifurcations involved in the transition from simple periodic to bursting oscillations as well as in the elucidation of the underlying bursting mechanism. A thorough understanding of the nonlinear behavior exhibited by simple reaction schemes, such as that of the hemin system, which only consists of reactions involving the enzyme species hemin and its substrates, may essentially facilitate the comprehension of the dynamics in more complex reaction networks.

A second major issue, that will be addressed in the course of the thesis, is how complex reaction networks, such as those describing metabolism [45, 46], atmospheric chemistry [47, 48], and combustion reactions [49, 50], can be simplified while keeping their essential dynamical properties. For example, the realistic modeling of large scale systems, such as a detailed description of combustion reactions [50] or the Belousov-Zhabotinsky reaction [51], usually requires the integration of large systems of ordinary differential equations (ODE systems). Moreover, one is usually interested in the system's behavior as one or more externally tunable parameters are continuously varied. Thus, it is highly desirable from a practical point of view to be able to identify the essential dynamical degrees of freedom in a given reaction network in order to obtain reduced systems which are much easier to investigate, but still show the relevant dynamics of the original system.

A reduction of complex reaction mechanisms may also be useful for other, more theoretical reasons: For example, one would like to know those reaction steps and chemical species in a given mechanism that are necessary to generate a certain type of dynamics. This information could then be used to design dynamical systems with desired properties. While a general answer to this problem is still missing, there are promising results about bistable [52], oscillatory [53, 54] and a certain class of chaotic systems [55]. The main tools of investigation in this field are stoichiometric network analysis [56] and

sensitivity analysis [57]. Both theoretical approaches have been successfully combined with principal component analysis to identify essential reaction steps in diverse systems such as the metabolism of red blood cells [58] and the well-known Belousov-Zhabotinsky reaction [59].

There are basically two reasons why chemical reaction networks often show redundancies, which can be used for an effective model reduction: First, chemical reactions occur in fixed stoichiometries. This results in mass conservation relations for certain atoms and thus, not all chemical species in a given network act as independent degrees of freedom. Second and more importantly, chemical reactions naturally evolve on different time scales. Accordingly, their temporal evolution can be decomposed into a fast transient relaxation to lower dimensional invariant slow manifolds and a subsequent evolution on the union of these manifolds, which often still captures the interesting type of dynamics on experimentally accessible time scales. The mathematical description of such reaction networks leads to singularly perturbed systems for which a well developed theory [60, 61] exists. As a result, one obtains a lower dimensional approximation on the slow manifold of the original system.

In the course of the years, several methods exploiting singular perturbation techniques have been proposed to simplify complex chemical reaction networks such as lumping schemes [62] or the approximation of the invariant manifold based on a functional equation [63]. However, before these techniques may successfully be applied, one still needs to identify the different time scales in the system which is often the hardest task. The presence of different time scales is usually indicated by small dimensionless parameters in front of time derivatives of some of the phase space variables which indicates that these variables vary significantly only on very short time scales and thereafter follow instantaneously (algebraically) the dynamics of the slow degrees of freedom.

The conventional strategy to search for small parameters in a system is to introduce new dimensionless variables such that some combination of intrinsic parameters becomes sufficiently small and subsequently may be used as a singular perturbation parameter. Clearly, this procedure becomes a formidable task in more complex reaction networks and other methods are required; as for example the method of computational singular perturbation proposed by Lam [64]. Furthermore, the rescaling procedure is not free of ambiguity in choosing the 'right' scales [65] and if the rescaled variables are not bounded from above and below, then the rescaled kinetic parameters do not provide any indication, whether the corresponding reaction step is slow or fast. Thus, one is often guided by chemical intuition or experimental expertise to group the individual reactions according to slow and fast steps. Once the different time scales of a system are known, it is more or less straight forward to apply singular perturbation techniques in order to reduce the dimensionality of the original system.

In view of the above mentioned problems to identify the relevant time scales in a system, we shall introduce a new method that allows to systematically find slow manifolds in a certain class of reaction networks (including those following a mass-action kinetics) which neither relies on a priori knowledge about the time scales nor requires a sophisticated rescaling procedure to identify small parameters in a system. Instead, we directly use the solution curves from a numerical integration routine to check whether

## 1. Introduction

certain nonlinear functions of the phase space variables, which we call *quasi-integrals*, are approximately constant along the numerically obtained solution curves. Quasi-integrals define nonlinear algebraic constraints among some of the phase space variables and thus, may be used to eliminate dynamical degrees of freedom in the reaction network; for example, by a quasi-steady-state approximation (QSSA) [66, 67]. In this sense, the method of quasi-integrals may serve as a supplement to existing methods which rely on a priori knowledge of time scales.

In the next Section, we introduce the hemin system in some detail since it represents the main object of study in this thesis. Afterwards, we give a detailed outline of the thesis and thereby conclude the introduction.

### 1.1. The hemin – hydrogen peroxide – sulfite system

The hemin – hydrogen peroxide – sulfite system belongs to a family of pH oscillators which are based on the pH-dependent oxidation of  $\text{HSO}_3^-$  by  $\text{H}_2\text{O}_2$  since this reaction produces  $\text{H}^+$  ions in an autocatalytic fashion [35, 36, 37, 38, 39]. In order to prevent the unbounded production of protons,  $\text{H}^+$ -consuming reactions are required, which play the role of a negative feedback step and thus, open the possibility for an oscillatory dynamics of the pH value in the reaction medium. In earlier studies of pH oscillators, inorganic compounds such as hexacyanoferrate [36, 35], thiosulfate [43], sulfide [68], or hydrogen carbonate [37] have been used to accomplish the negative feedback. However, due to the use of purely inorganic substances, the corresponding pH oscillator systems are not necessarily physiologically compatible. To this purpose, Hauser et. al. [32] developed a pH oscillator where hemin provides for the  $\text{H}^+$ -consuming reaction steps and thus, represents a first step towards a biologically more realistic pH oscillator.

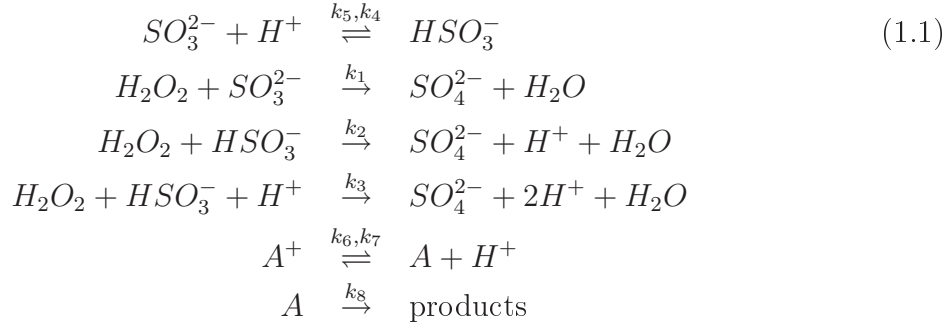
The hemin system was studied experimentally under open conditions in a continuous-flow stirred tank reactor to which the necessary reactants are continuously supplied at a certain rate  $k_0$  and from which all products are continuously removed at the same rate. Thus, there is a constant matter flow through the system keeping it away from thermodynamical equilibrium.

With increasing flow rate  $k_0$ , the following sequence of nonequilibrium states was observed: acidic (pH $\sim$  6.5) stationary state  $\rightarrow$  relaxational oscillations  $\rightarrow$  bursting oscillations  $\rightarrow$  alkaline (pH $\sim$  7.6) stationary state. The bursting oscillations consist of one large amplitude oscillation and a certain number of small amplitude oscillations per period.

A first reaction mechanism was proposed in [32, 33] based on the well established oxidation of  $\text{HSO}_3^-$  by  $\text{H}_2\text{O}_2$  which involves the autocatalytic reaction step. In addition, two pH-dependent equilibria between different forms of hemin were considered as sources for the negative feedback step. However, we showed in a recent publication [34] that one of these two equilibria, the pH-dependent dimerisation of hemin, provides only a minor contribution to the onset of oscillations and may therefore be neglected, since we are aiming at a minimal reaction mechanism which only contains the essential reaction steps in order to reproduce the observed dynamics.

### 1.1. The hemin – hydrogen peroxide – sulfite system

Instead, it became necessary to take the degradation of hemin by  $H_2O_2$  into account which is known to occur at high  $H_2O_2$  concentrations exceeding  $8 \times 10^{-3} \text{ mol l}^{-1}$  [69]. In this degradation process, the porphyrin ring of hemin is oxidatively cleaved by a yet unknown agent. This reaction was found to be of first order with respect to hemin [70]. Due to the uncertainty concerning the oxidising agent and in order to keep the mechanistic model as simple as possible, we proposed the following reaction scheme for the hemin system [34]



where the degradation process is taken into account by an unspecific decomposition of hemin according to  $A \xrightarrow{k_8} \text{products}$ . The products are assumed not to take part in any further reaction of the system.

The first four reaction steps in (1.1) represent the well established oxidation of  $HSO_3^-$  by  $H_2O_2$  [35, 36, 37, 38]. The autocatalytic step is contained in the fourth reaction where  $H^+$  produces  $2H^+$ . The rate constants  $k_1, \dots, k_5$  were measured in dependence on the temperature in [38]. The fifth reaction step in (1.1) denotes the pH-dependent

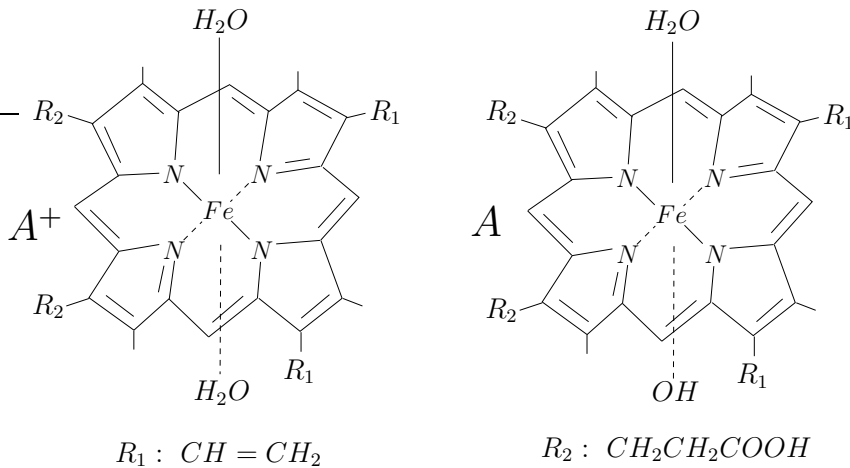


Figure 1.3.: The hemin molecule consists of a central iron atom  $Fe^{III}$  and a porphyrin ring which may either coordinate with two aquo ligands ( $A^+$ ) or to one hydroxy and one aquo ligand ( $A$ ).

## 1. Introduction

equilibrium between two forms of hemin whose porphyrin ring may either coordinate with two aquo ligands in which case it is denoted as  $\text{Hm}^{2+}$  or to one hydroxy and one aquo ligand abbreviated as  $\text{Hm}^+$  (Fig. 1.3). The corresponding rate constants  $k_6, k_7$  have been measured in [71].

The only rate constant whose value has not been precisely determined yet is that of the hemin decay, i.e.  $k_8$ . Consequently, we shall regard it, in addition to the flow rate  $k_0$ , as a second variable parameter in our model.

In order to model the dynamical behavior of the reaction system (1.1) we assume the individual reaction steps to follow a mass-action kinetics, i.e. we assume that the frequency of collisions leading to a reaction between two chemical species is proportional to their concentration. This is a valid assumption if [65, 72] (i) the concentrations of the involved atoms/molecules are not too high such that a doubling of the initial concentration for one species results in a doubling of effective collisions leading to a chemical reaction, (ii) the reaction medium is homogeneous which is assured by stirring and (iii) the temperature is held constant during the experiment such that the parameters  $k_i$  are truly constant (the experiments for the hemin system were carried out at 25°C).

We derived a 6-dimensional ODE system from the reaction mechanism (1.1) to model the bursting behavior of the hemin system [34]:

$$\begin{aligned}
 \dot{x}_1 &= -k_1x_1x_2 + k_4x_3 - k_5x_1x_4 + k_0(x_1^0 - x_1) \\
 \dot{x}_2 &= -k_1x_1x_2 - k_2x_2x_3 - k_3x_2x_3x_4 + k_0(x_2^0 - x_2) \\
 \dot{x}_3 &= -k_2x_2x_3 - k_3x_2x_3x_4 - k_4x_3 + k_5x_1x_4 - k_0x_3 \\
 \dot{x}_4 &= k_2x_2x_3 + k_3x_2x_3x_4 + k_4x_3 - k_5x_1x_4 + k_6x_6 - k_7x_4x_5 + k_0(x_4^0 - x_4) \\
 \dot{x}_5 &= k_6x_6 - k_7x_4x_5 - k_8x_5 + k_0(x_5^0 - x_5) \\
 \dot{x}_6 &= -k_6x_6 + k_7x_4x_5 - k_0x_6
 \end{aligned} \tag{1.2}$$

where the pH value is given as the negative decadic logarithm of the proton concentration  $\text{H}^+$  ( $x_4$ ) and the ‘dot’ denotes derivatives with respect to time  $t$ . To simplify notation, we assigned the following abbreviations to the chemical species:

$$\begin{aligned}
 x_1 &\leftrightarrow \text{SO}_3^{2-} \\
 x_2 &\leftrightarrow \text{H}_2\text{O}_2 \\
 x_3 &\leftrightarrow \text{HSO}_3^- \\
 x_4 &\leftrightarrow \text{H}^+ \\
 x_5 &\leftrightarrow \text{Hm}^{2+} \\
 x_6 &\leftrightarrow \text{Hm}^+.
 \end{aligned} \tag{1.3}$$

The terms proportional to  $k_0$  in (1.2) describe the matter flow through the continuous-flow stirred tank reactor to which the four species  $\text{SO}_3^{2-}(x_1^0)$ ,  $\text{H}_2\text{O}_2(x_2^0)$ ,  $\text{H}^+(x_4^0)$  and  $\text{Hm}^{2+}(x_5^0)$  are supplied at the variable rate  $k_0$  while all six chemical species are removed from the reactor at the same rate. The numerical values of the rate constants  $k_1, \dots, k_8$  and the concentrations in the external reservoirs  $x_i^0$  that were used in the numerical simulations, are compiled in Table B.1 of the appendix B.2. According to the experimental

### 1.1. *The hemin – hydrogen peroxide – sulfite system*

situation, the flow rate  $k_0$  is used as the principal bifurcation parameter ranging in the interval  $k_0 \in [1 \cdot 10^{-4} s^{-1}, 4.5 \cdot 10^{-4} s^{-1}]$ .

## 1.2. Outline of the thesis

The thesis consists of two main Parts and an Appendix. In the main Parts, we investigate two thematically distinct aspects of the dynamical properties of the hemin – hydrogen peroxide – sulfite system: In the first Part, the method of quasi-integrals is developed as a general procedure to identify the essential dynamical degrees of freedom in a given reaction network. In particular, this method will be used to derive a 3-dimensional ODE system as an approximation to the 6-dimensional hemin system (1.2). In the second Part, we exploit the slow-fast structure of the hemin system to analyze the origin of its bursting behavior by a suitable (slow-fast) bifurcation analysis. As a result, we identify the bursting mechanism of the hemin system as a subHopf/fold-cycle burster according to a classification scheme that has been introduced by Izhikevich [24] to classify the bursting behavior of neural systems. A systematic two-parameter bifurcation analysis reveals a transition in the bursting behavior of the hemin system from subHopf/fold-cycle to fold/subHopf type. In addition, the slow-fast analysis provides an explanation for the origin of quasi-periodic behavior in the hemin system, even though the underlying mechanism might be of more general importance.

### Part I

**Chapter 2** gives a short introduction into the theory of singularly perturbed systems.

It begins with a simple motivating example using a singularly perturbed algebraic equation. Afterwards, we introduce the main ideas of the geometrical approach to singular perturbation theory for ODE systems due to Fenichel [60], since this theory serves as the mathematical basis for the method of quasi-integrals.

**Chapter 3** introduces the concept of quasi-integrals and reveals its relation to the theory of singularly perturbed systems. First, we exemplarily show how to find quasi-integrals in the hemin system and further, how they can be used to reduce the number of dynamical degrees of freedom in that system. In particular, we derive a 3-dimensional approximation to the 6-dimensional ODE system (1.2). In a second step, we outline how the method of quasi-integrals can be extended to a large class of reaction networks. The results of this Chapter have been published in [73].

**Chapter 4** compares the dynamical properties of the 6-dimensional hemin system (1.2) with those of its 3-dimensional approximation. To this purpose, local one- and two-parameter bifurcation diagrams are calculated which demonstrate that both systems are virtually identical.

**Chapter 5** summarizes the results of the first Part and gives a short outlook.

### Part II

**Chapter 6** describes how the bursting oscillations arise in the 3-dimensional hemin system subsequent to a period doubling cascade and the formation of a chaotic attractor. We list some of the bursting states that were found by direct numerical

integration and discuss their bifurcation sequences in terms of Farey progressions. In addition, we introduce the total concentration of hemin species as a new variable since it evolves on a slower time scale than the remaining variables; an observation that will be essential when we analyze the bursting oscillations in Chapter 8.

**Chapter 7** exemplifies the slow-fast analysis introduced by Rinzel and Ermentrout [23] with a cartoon of the slow-fast structure of the 3-dimensional hemin system. In particular, we demonstrate how a slow variable may act as a quasi-static bifurcation parameter for the remaining 2-dimensional fast subsystem. In addition, we mention a classification scheme for bursting mechanisms that has been introduced by Izhikevich [24] to classify the bursting behavior of neural systems.

**Chapter 8** is devoted to a detailed study of the slow-fast structure of the hemin system. First, we show that at a fixed value of the flow rate  $k_0$ , the bursting oscillations are caused by a saddle-node bifurcation of periodic orbits in conjunction with a subcritical Hopf bifurcation, both of which occur in the fast subsystem for nearby values of the slow variable that was introduced in Chapter 6. By a systematic two-parameter continuation in the flow rate and the slow variable, we identify a transition in the bursting behavior from subHopf/fold-cycle to fold/subHopf type which can be attributed to a homoclinic bifurcation in the fast subsystem. Finally, we perform a slow-fast analysis of the hemin system in a parameter region where a 2-torus is stable. This analysis shows that the rather unusual phase flow on the torus is due to a coupling of an oscillator in the fast subsystem with the slow variable and thus, is a result of the slow-fast structure of the hemin system.

**Chapter 9** summarizes and discusses the results of the second Part.

The Appendix consists of three Chapters:

**Chapter A** provides the basic notions of dynamical systems theory and gives an introduction to bifurcation theory as far as it appears necessary to understand the ideas and arguments in the remainder of the thesis. Therefore, this Chapter should be used as a reference. In particular, Sections A.3 and A.4 should be consulted for details about local codimension one and two bifurcations, respectively, which will be frequently referred to throughout the work. Global (homoclinic) bifurcations are discussed in Section A.5.

**Chapter B** gives an introduction to numerical continuation procedures and strategies. Furthermore, it provides the parameter settings for the hemin and the peroxidase-oxidase system which are necessary to setup the numerical simulations.

**Chapter C** contains a second example for the application of the method of quasi-integrals developed in Chapter 3. The reaction mechanism of the peroxidase-oxidase reaction is investigated which exclusively contains irreversible reaction steps and therefore, poses a nontrivial application of the method of quasi-integrals. Nevertheless, we identify three possible quasi-integrals two of which lead to reduced systems that quantitatively agree quite well with the original 10-dimensional one.



Part I.

# Quasi-Integrals and Slow Manifolds in Reaction Networks



## 2. Singular Perturbation Theory

The method of quasi-integrals is mainly inspired by the singular perturbation theory for ODE systems. Therefore, we give a brief outline of that theory in the present Chapter and thereby lay the mathematical foundation for the reduction method using quasi-integrals in Chapter 3.

In perturbation theory, one studies how small disturbances of a system affect its behavior which is assumed to be known under isolated conditions, i.e. without the disturbances. For concreteness, consider a perturbed system  $S_\varepsilon$  which is, for example, described by algebraic, differential, or integral equations, or combinations thereof. Then a natural, though by no means necessary assumption (otherwise there was no singular perturbation theory), is that the solution  $x_\varepsilon$  of the perturbed system is in some sense ‘close’<sup>1</sup> to the solution  $x_0$  of the unperturbed problem  $S_0$  provided the perturbation parameter  $\varepsilon$  is sufficiently small. If this assumption holds over the entire domain of definition, the according perturbation problem is called *regular* and one can find a solution of the perturbed problem in terms of a (asymptotic) power series expansion in  $\varepsilon$ . However, it may happen that the unperturbed problem  $S_0$  (i) has no solution or (ii) has a solution that is not uniformly valid in the domain of definition or (iii) has many solutions. In these cases, the perturbation problem  $S_\varepsilon$  is called *singular*.

### 2.1. A motivating example

A hallmark of singularly perturbed systems is that they model processes which occur on at least two different scales such that a solution of the unperturbed problem is usually only valid at one of the two scales.

To illustrate this statement, consider the solutions of the algebraic equations

$$\begin{aligned} f(x, \varepsilon) &\equiv x^2 - 2x + \varepsilon = 0, & 0 < \varepsilon \ll 1 & \quad (2.1) \\ f(x, 0) = \lim_{\varepsilon \rightarrow 0} f(x, \varepsilon) &= x^2 - 2x = 0 \end{aligned}$$

which are given by

$$\begin{aligned} x_\varepsilon^{1,2} &= 1 \pm \sqrt{1 - \varepsilon} & (2.2) \\ x_0^{1,2} = \lim_{\varepsilon \rightarrow 0} x_\varepsilon^{1,2} &= \{2, 0\}. \end{aligned}$$

Obviously, the solutions  $x_\varepsilon^{1,2}$  of the perturbed problem  $f(x, \varepsilon) = 0$  continuously deform into the solutions  $x_0^{1,2}$  of the unperturbed equation. In particular, the solutions  $x_\varepsilon^{1,2}$  have

---

<sup>1</sup>In order to compare two solutions, one can, for example, introduce an appropriate norm in the space where the system is defined.

## 2. Singular Perturbation Theory

power series expansions near  $\varepsilon = 0$  starting as

$$x_\varepsilon^1 = 2 - \frac{1}{2}\varepsilon - O(\varepsilon^2) \text{ and} \quad (2.3)$$

$$x_\varepsilon^2 = 0 + \frac{1}{2}\varepsilon + O(\varepsilon^2), \quad (2.4)$$

respectively, which shows that they are close to the unperturbed solutions  $x_0^{1,2}$  for  $\varepsilon$  sufficiently small. Thus,  $\varepsilon$  is a regular perturbation parameter for  $f(x, \varepsilon) = 0$ .

In a next step we shift the position of the small parameter such that it occurs in front of the monomial of highest degree and consider the following (singular) perturbation problem (cf. Chapter 9 in [65]):

$$g(z, \varepsilon) = \varepsilon z^2 - 2z + 1 = 0 \quad (2.5)$$

whose solutions are now given by

$$z_\varepsilon^{1,2} = \frac{1}{\varepsilon}(1 \pm \sqrt{1 - \varepsilon}). \quad (2.6)$$

Up to the scale factor  $1/\varepsilon$ , these are the same solutions as in (2.2). However, the scale factor has a huge impact on the power series expansions since we now have:

$$z_\varepsilon^1 = \frac{2}{\varepsilon} - \frac{1}{2} - O(\varepsilon) \text{ and} \quad (2.7)$$

$$z_\varepsilon^2 = \frac{1}{2} + O(\varepsilon). \quad (2.8)$$

Hence, in the limit  $\varepsilon \rightarrow 0$ ,  $z_\varepsilon^1$  becomes unbounded while  $z_\varepsilon^2$  remains finite.

If, on the other hand, one naively performs the limit  $\varepsilon \rightarrow 0$  in (2.5), one obtains the first order equation  $-2z + 1 = 0$  which has only one solution:  $z_0 = 1/2$ . Thus, from the unperturbed problem, one only gets the regular solution (2.8) of the perturbed problem:

$$\lim_{\varepsilon \rightarrow 0} z_\varepsilon^2 = 1/2 = z_0;$$

the singular solution (2.7) is missing.

The singular nature of the perturbation problem (2.5) may also be seen in a different way by exploiting the multi-scale structure of the system. To this purpose, we introduce a new variable according to

$$\xi := \varepsilon z, \quad 0 < \varepsilon \ll 1 \quad (2.9)$$

and look again at equation (2.5), but now on a smaller scale defined by (2.9). After performing the scale transformation (2.9) and multiplying the resulting equation by  $\varepsilon$ , (2.5) reads

$$\tilde{g}(\xi, \varepsilon) = \xi^2 - 2\xi + \varepsilon = 0, \quad (2.10)$$

i.e. on the small scale we again obtain a regular perturbation problem which, in this case, is identical with (2.1). Consequently, the solutions  $\xi_\varepsilon^{1,2}$  of (2.10) can also be obtained in terms of power series expansions identical to those in (2.3) and (2.4). Finally, one gets the two solutions  $z_\varepsilon^{1,2} = \frac{1}{\varepsilon}\xi_\varepsilon^{1,2}$  for the singularly perturbed system (2.5) which are, of course, identical with (2.7) and (2.8).

We summarize:

1. The appearance of a small parameter in front of the highest order term in an algebraic equation such as (2.5) usually indicates the existence of (some) singular solutions. This aspect has a natural translation to differential equations where singular behavior is indicated by small parameters in front of the highest order derivative term.
2. Looking at equation (2.10), it seems as if the singularity was transformed away since in this equation,  $\varepsilon$  is a regular perturbation parameter. This is, however, not the case since it is now the scale transformation (eq. 2.9) that becomes singular in the limit  $\varepsilon \rightarrow 0$ .
3. Finally, we again wish to point out the multi-scale structure of (2.5) and (2.10). If we look at a small scale (using  $\xi$  variables) the system (2.10) is well-behaved and has the two regular solutions  $\xi_\varepsilon^{1,2}$ . If, on the other hand, the scale is increased by performing the limit  $\varepsilon \rightarrow 0$ , only one of the solutions ( $z_\varepsilon^2$ ) remains regular while the other one ( $z_\varepsilon^1$ ) becomes singular.

In the next Section, we shall address the question under which conditions one may approximate a singularly perturbed problem by a regularly perturbed one for the case that the system is described by ordinary differential equations.

## 2.2. ODE systems with ‘small’ parameters

The geometrical singular perturbation theory for ordinary differential equations has been elaborated by Fenichel [60] in the 1970s. We shall present the main ideas of this approach as far as it is necessary to motivate the concept of quasi-integrals in Chapter 3.

In the following we consider  $n$ -dimensional ODE systems of the form

$$\begin{aligned}\dot{x}(t) &= f(x, y, \varepsilon) \\ \varepsilon \dot{y}(t) &= g(x, y, \varepsilon)\end{aligned}\tag{2.11}$$

where  $\varepsilon$  is again a positive, sufficiently small dimensionless parameter,  $(x, y) \in U \subset \mathbb{R}^{n-m} \times \mathbb{R}^m$ , and  $f$  and  $g$  are vector-valued functions of the form  $f : U \rightarrow \mathbb{R}^{n-m}$  and  $g : U \rightarrow \mathbb{R}^m$ , respectively. The ‘dot’ denotes derivatives with respect to the (time) parameter  $t$ .

The occurrence of the small parameter  $\varepsilon$  in front of  $\dot{y}$  in (2.11) indicates that these quantities vary significantly only on the fast time scale  $t/\varepsilon$  and thereafter instantaneously follow the slow dynamical degrees of freedom played by the  $x$  variables. Technically, this can be seen by taking the limit  $\varepsilon \rightarrow 0$  in which case the ODE system (2.11) reduces to the differential-algebraic system

$$\begin{aligned}\dot{x}(t) &= f(x, y, 0) \\ 0 &= g(x, y, 0).\end{aligned}\tag{2.12}$$

## 2. Singular Perturbation Theory

Similar to the case of the algebraic equation (2.5) in the previous Section where the limiting process led to a reduction in the order of the original equation, the same limiting procedure now leads to a reduction of the dynamical degrees of freedom from  $n$  in (2.11) to  $n-m$  in (2.12) where the  $y$ -components of the solution curve  $(x(t), y(t))$  are implicitly determined by the algebraic equation  $g(x, y, 0) = 0$  once the solution  $x(t)$  is known.

Again, the singular behavior of the  $y$ -components of the solution curve  $(x(t), y(t))$  on long time scales (comparable with  $t$ ) can be remedied by studying the ODE system (2.11) on a faster time scale  $\tau$  which is introduced as

$$\tau = \frac{t}{\varepsilon}. \quad (2.13)$$

On the time scale  $\tau$ , the ODE system (2.11) reads:

$$\begin{aligned} x'(\tau) &= \varepsilon f(x, y, \varepsilon) \\ y'(\tau) &= g(x, y, \varepsilon) \end{aligned} \quad (2.14)$$

for which  $\varepsilon$  is now a regular perturbation parameter since it does not appear anymore in front of derivatives with respect to  $\tau$  (which are abbreviated with a 'prime'). In the limit  $\varepsilon \rightarrow 0$ , the ODE system (2.14) reduces to the so-called fast subsystem

$$\begin{aligned} x'(\tau) &= 0 \\ y'(\tau) &= g(x, y, 0). \end{aligned} \quad (2.15)$$

Thus, on the fast time scale  $\tau$  only the  $y$ -components follow a dynamical evolution while the  $x$ -components are treated as constants since their derivative with respect to  $\tau$  is zero. As long as  $\varepsilon \neq 0$ , the two systems (2.11) and (2.14) are completely equivalent. In the limit  $\varepsilon \rightarrow 0$ , however, this equivalence is lost since the scale transformation (2.13) becomes singular.

It is now the aim of singular perturbation theory to investigate under which conditions the solutions of the reduced system (2.12) represent a good approximation to the solutions of the original (singular perturbation) problem (2.11).

The result is the following: Assume that the algebraic equation  $g(x, y, 0) = 0$  in (2.12) defines a smooth manifold  $y = \tilde{y}(x)$  which is normally attracting in the sense that the Jacobian matrix  $D_y g(x, y) |_{y=\tilde{y}(x)}$  of the linearized fast subsystem along  $y = \tilde{y}(x)$

$$(\delta y)' = D_y g(x, y) |_{y=\tilde{y}(x)} \delta y \quad (2.16)$$

has only negative eigenvalues for  $x$  belonging to a compact region in  $\mathbb{R}^{n-m}$ , then there exists a slow invariant manifold  $\psi(x, \varepsilon) = \tilde{y}(x) + O(\varepsilon)$  that can be used to approximate the dynamics of the  $n$ -dimensional ODE system (2.11) for sufficiently small  $\varepsilon$  by the  $n-m$ -dimensional ODE system

$$\dot{x} = f(x, \psi(x, \varepsilon), \varepsilon) \quad (2.17)$$

which is now a regular perturbation problem in  $\varepsilon$ .

Of great practical relevance is the limit  $\varepsilon \rightarrow 0$  corresponding to the *quasi-steady-state approximation* (QSSA)

$$\dot{x} = f(x, \tilde{y}(x), 0) \quad (2.18)$$

where the slow manifold  $\psi(x, \varepsilon)$  is approximated by the quasi-stationary manifold  $\tilde{y}(x)$ . Notice that in practical applications  $\varepsilon$  is usually given in terms of intrinsic system parameters and therefore cannot be made arbitrarily small. Nevertheless it is often sufficient to approximate the slow manifold of a system by the quasi-stationary manifold in order to obtain a reasonable description of the dynamics of the  $n$ -dimensional system even in the case that  $\varepsilon$  is different from zero.

We wish to stress again that the manifold  $y = \tilde{y}(x)$  is entirely composed of stationary points of the fast subsystem (2.15) which parametrically depend on the slow variables  $x \in \mathbb{R}^{n-m}$ . In particular, the approximation (2.18) is only valid in those compact regions of  $\mathbb{R}^{n-m}$  where the quasi-stationary manifold  $y = \tilde{y}(x)$  is attracting which may limit the range of allowed initial conditions for the  $x$  variables.

The property that the slow manifold  $\psi(x, \varepsilon)$  is invariant under the flow of the ODE system (2.11) is expressed by the equation:

$$\dot{\psi}(x, \varepsilon) = \psi_x(x, \varepsilon)\dot{x} = 0, \quad (2.19)$$

where  $\psi_x(x, \varepsilon)$  denotes partial differentiation with respect to  $x \in \mathbb{R}^{n-m}$ . Accordingly, the slow manifold can be obtained as a solution of the partial differential equation

$$\psi_x(x, \varepsilon)f(x, \psi(x, \varepsilon)) = \frac{1}{\varepsilon}g(x, \psi(x, \varepsilon), \varepsilon) \quad (2.20)$$

where we set  $y = \psi(x, \varepsilon)$  and used (2.11) to replace the time derivatives  $\dot{x}$  and  $\dot{\psi}$  in (2.19) with the corresponding vector-valued functions  $f$  and  $g$ , respectively. In general, it will be impossible to find explicit solutions of the nonlinear partial differential equation (2.20). However, in many cases one may find an approximation to the slow manifold in terms of a power series expansion in the small parameter  $\varepsilon$

$$\psi(x, \varepsilon) = \tilde{y}(x) + \varepsilon\psi_1(x) + O(\varepsilon^2) \quad (2.21)$$

where the quasi-stationary manifold  $\tilde{y}(x)$  reappears as the zeroth order term.

Finally, we mention that the approximation (2.18) has two desirable features which is the reason for the great practical importance of the QSSA: First, it is valid on the slow time scale  $t$ , i.e. it describes the long-time behavior of the system which is also accessible to experimental investigations. Second, the fast dynamical degrees of freedom are eliminated and thus, one is left with a problem of reduced (numerical) complexity.



## 3. Quasi-Integrals

The individual reaction steps in (bio-)chemical reaction networks often evolve on different time scales. The mathematical description of such networks naturally leads to singularly perturbed ODE systems. However, in large systems it is practically impossible to identify the small perturbation parameters in the system without any prior knowledge of the order of magnitude of the individual reaction steps. Therefore, we shall develop a method which does not require any a priori knowledge, but instead makes direct use of the solution curves which are obtained by numerical integration routines. The results of this Chapter and Appendix C are published in [73].

### 3.1. Quasi-integrals in the hemin system

In the following, we shall exemplify the method of quasi-integrals with the hemin system introduced in Section 1.1. In the first step, the ODE system (1.2) is rewritten in compact vector notation

$$\dot{x} = \mathbf{C} \cdot R(x, k) + k_0(x^0 - x)$$

where we introduced the matrix of stoichiometric coefficients  $\mathbf{C}$  (without the in- and outflow terms proportional to  $k_0$ ) and the vector of reaction rates  $R$  as:

$$\mathbf{C} = \begin{pmatrix} -1 & 0 & 0 & 1 & -1 & 0 & 0 & 0 \\ -1 & -1 & -1 & 0 & 0 & 0 & 0 & 0 \\ 0 & -1 & -1 & -1 & 1 & 0 & 0 & 0 \\ 0 & 1 & 1 & 1 & -1 & 1 & -1 & 0 \\ 0 & 0 & 0 & 0 & 0 & 1 & -1 & -1 \\ 0 & 0 & 0 & 0 & 0 & -1 & 1 & 0 \end{pmatrix} \quad \mathbf{R} = \begin{pmatrix} k_1 x_1 x_2 \\ k_2 x_2 x_3 \\ k_3 x_2 x_3 x_4 \\ k_4 x_3 \\ k_5 x_1 x_4 \\ k_6 x_6 \\ k_7 x_4 x_5 \\ k_8 x_5 \end{pmatrix}. \quad (3.1)$$

Accordingly, the reaction mechanism of the hemin system comprises 6 chemical species and 8 elementary reaction steps. The latter are arranged into the components of the reaction rate vector  $R$ .

In the second step, we use the theory of singularly perturbed systems as it has been introduced in Section 2.2 to motivate the concept of quasi-integrals. To this purpose, let us pretend for a moment that there were two time scales in the hemin system (1.2) so that it can be transformed into the standard form of a singularly perturbed system (2.11) by identifying a suitable combination of intrinsic system parameter which can play the role of an epsilon in (2.11). Let us further assume that the small parameter

### 3. Quasi-Integrals

epsilon appears in the first rate equation of (1.2) which therefore admits a form similar to the second equation in (2.11):

$$\begin{aligned}\varepsilon \dot{x}_1 &= \underbrace{-k_1 x_1 x_2 + k_4 x_3}_{g_0(x_1, x_2, x_3)} + \varepsilon \underbrace{(-k_5 x_1 x_4 + k_0(x_1^0 - x_1))}_{\tilde{g}(x_1, x_4)} \\ &= \underbrace{g_0(x_1, x_2, x_3)}_{g(x, y, \varepsilon)} + \varepsilon \tilde{g}(x_1, x_4) \\ \varepsilon \dot{y} &= g(x, y, \varepsilon)\end{aligned}\tag{3.2}$$

where we identified  $x_1$  with the fast variable  $y$  and  $(x_2, \dots, x_6)$  with the slow variable  $x$  in (2.11). The motivation for this particular choice of the function  $g(x, y, \varepsilon)$  comes from the fact that if we were allowed to perform the limit  $\varepsilon \rightarrow 0$  in (3.2), we would have found a quasi-stationary manifold given by the algebraic equation

$$g_0(x_1, x_2, x_3) = 0 = -k_1 x_1 x_2 + k_4 x_3\tag{3.3}$$

provided it is normally attracting in the sense of Section 2.2.

The crucial point is now the following: Instead of explicitly searching for a small parameter in the ODE system (1.2), which would facilitate the transformation (3.2), we simply test whether the ratio

$$I_{14} = \frac{k_1 x_1 x_2}{k_4 x_3} \equiv \frac{R_1}{R_4} \stackrel{?}{\sim} 1\tag{3.4}$$

approaches the constant (or at least nearly constant) value 1 along the numerically obtained solution curves  $x_i(t)$  in which case (3.3) is simultaneously fulfilled. Since  $I_{14}$  is a nonlinear function of the phase space variables, whose time derivative  $\dot{I}_{14} \sim 0$  is nearly zero along the solution curves, we call it a *quasi-integral*. Note that if the time derivative was exactly zero,  $I_{14}$  would be an exact integral for the nonlinear flow of the ODE system (1.2).

By reversing the order of the above argument, it is clear that each quasi-integral of the form (3.4) defines a quasi-stationary manifold (3.3) in the sense of Section 2.2 which, in turn, can be used to reduce the number of dynamical degrees of freedom in the originally 6-dimensional ODE system (1.2). On the other hand, since the partition of  $g$  into  $g_0$  and  $\tilde{g}$  in (3.2) was arbitrary, it is also clear how to proceed in order to search for other quasi-integrals. For example, in a next step one could test whether the condition

$$I_{45} = \frac{k_4 x_3}{k_5 x_1 x_4} \equiv \frac{R_4}{R_5} \stackrel{?}{\sim} 1\tag{3.5}$$

is fulfilled in which case the quasi-stationary manifold would be given by

$$g_0(x_1, x_3, x_4) = k_4 x_3 - k_5 x_1 x_4 = 0 = R_4 - R_5.\tag{3.6}$$

By continuing along this line of argument, one can systematically test all distinct combinations of the form (3.4) and (3.5) for being approximately constant. To this

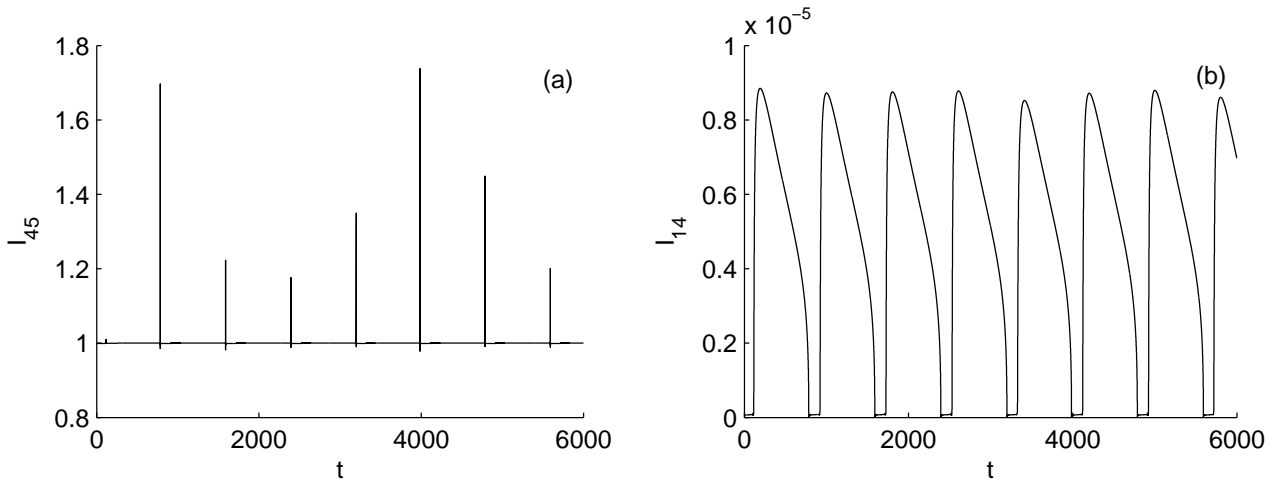


Figure 3.1.: Different ratios of components of the reaction rate vector  $R$  are shown: While  $I_{45} = R_4/R_5$  approaches a constant value and therefore defines a quasi-stationary manifold,  $I_{14} = R_1/R_4$  remains a heavily oscillating function bounded away from 1 and thus, does not fulfill the condition for a quasi-integral.

purpose, one has to consider only those reaction rates  $R_i$  in a given rate equation which appear with an opposite sign, since these are the only ones that can potentially balance each other. If this procedure is carried out for all six rate equations in (1.2), one has found all possible quasi-stationary manifolds which can be represented as ratios of certain components of the reaction rate vector  $R$ .

In the hemin system, we find precisely one quasi-integral (eq. 3.5). It is shown in Fig. 3.1 together with  $I_{14}$  which represents a counter example. Note that  $I_{45}$  always remains in the neighborhood of the constant value 1 except for short time intervals where spiking outliers occur (Fig. 3.1a). To the contrary,  $I_{14}$  remains a heavily oscillating function on the scale  $10^{-5}$  which is far away from the constant value 1 (Fig. 3.1b). Thus,  $I_{45}$  defines a quasi-stationary manifold while  $I_{14}$  does not.

We conclude with some general remarks concerning the method of quasi-integrals. First of all, the method is applicable without any prior knowledge about the different time scales which might be present in a given reaction network. This property makes it particularly suitable for a straightforward reduction of high dimensional systems. On the other hand, we have not yet specified what we mean when we require that a quasi-integral is *approximately* constant, since the distinction between different ratios such as  $I_{14}$  and  $I_{45}$  might not be as clear cut as in Fig. 3.1. However, even in those cases, the method is applicable if one uses ratios that are approximately constant for a formal reduction of the original ODE system and subsequently compares it with the reduced version, for example, based on a local bifurcation diagram. This is, in fact, the strategy that we shall follow in Section 4.1 and in the appendix C where the method of quasi-integrals

### 3. Quasi-Integrals

is applied to the 10-dimensional PO system.

## 3.2. Using quasi-integrals for model reduction

Having identified the quasi-integral (3.5), which possibly defines a quasi-stationary manifold, we wish to use it now to eliminate one dynamical degree of freedom in the hemin system (1.2). To this purpose, we rewrite the 6-dimensional hemin system in the standard form of a singularly perturbed system (eq. 2.11)

$$\begin{aligned}
 \dot{x}_2 &= -R_1 - R_2 - R_3 + k_0(x_2^0 - x_2) \\
 \dot{x}_5 &= R_6 - R_7 - R_8x_5 + k_0(x_5^0 - x_5) \\
 \dot{x}_6 &= -R_6 + R_7 - k_0x_6. \\
 \varepsilon\dot{x}_1 &= R_4 - R_5 + \varepsilon(-R_1 + k_0(x_1^0 - x_1)) \\
 \varepsilon\dot{x}_3 &= -(R_4 - R_5) + \varepsilon(-R_2 - R_3 - k_0x_3) \\
 \varepsilon\dot{x}_4 &= R_4 - R_5 + \varepsilon(R_2 + R_3 + R_6 - R_7 + k_0(x_4^0 - x_4))
 \end{aligned} \tag{3.7}$$

where we have already used the knowledge about the existence of the quasi-stationary manifold  $g_0(x_1, x_3, x_4) = R_4 - R_5$  in order to place the small parameter  $\varepsilon$  at the correct positions. For clarity, the components of the reaction rate vector  $R$  were used to denote the individual reaction steps in (3.7).

We notice that a naive reduction, following the procedure in Section 2.2, is damned to fail, since the term  $R_4 - R_5$  appears in *three* different rate equations in the ODE system (3.7). This (misleadingly) suggests that the fast subsystem is of the form:

$$\begin{aligned}
 x_1' &= R_4 - R_5 \equiv g_0 \\
 x_3' &= -(R_4 - R_5) \equiv -g_0 \\
 x_4' &= R_4 - R_5 \equiv g_0
 \end{aligned} \tag{3.8}$$

which is obtained after rescaling according to  $\tau = t/\varepsilon$  and performing the limit  $\varepsilon \rightarrow 0$  in (3.7) ( the ‘prime’ again denotes derivatives with respect to the fast time scale  $\tau$ ). On the other hand, there is only *one* equation (eq. 3.6) defining the quasi-stationary manifold and thus, the determinant of the Jacobian matrix

$$\frac{\partial(g_0, -g_0, g_0)}{\partial(x_1, x_3, x_4)} \tag{3.9}$$

of the fast subsystem (3.8) is two-fold degenerate, i.e. it has two zero eigenvalues. Consequently, the quasi-steady-state approximation (2.18) must not be applied to the ODE system (3.7).

The reason for the degeneracy of the fast subsystem is the presence of (mass) conservation relations in the reaction mechanism of the hemin system which have not been considered so far. Such kind of conservation relations are frequently encountered in chemical reaction systems. They simply express the fact that atoms of a certain kind

can not be destroyed during a chemical reaction. Instead they aggregate and dissociate in fixed stoichiometric relations.

In general, the existence of mass conservation relations is expressed by a non-maximal rank of the stoichiometric matrix  $\mathbf{C}$  (eq. 3.1) which in our case has rank 4. Thus, there are two left eigenvectors of  $\mathbf{C}$  with eigenvalue zero. They can be chosen as

$$\begin{aligned} v_1^T &= (1, -1, 1, 0, 0, 0) \\ v_2^T &= (0, 0, 1, 1, 0, 1) \end{aligned} \quad (3.10)$$

which satisfy the eigenvalue equations

$$v_{1,2}^T \cdot \mathbf{C} = 0 \cdot v_{1,2}^T.$$

In the following, we use these eigenvectors as the last two rows of the linear coordinate transformation

$$\begin{pmatrix} y_1 \\ y_2 \\ y_3 \\ y_4 \\ y_5 \\ y_6 \end{pmatrix} = \begin{pmatrix} 0 & 1 & 0 & 0 & 0 & 0 \\ 0 & 0 & 0 & 0 & 0 & 1 \\ 0 & 0 & 0 & 0 & 1 & 0 \\ 1 & 0 & 0 & 0 & 0 & 0 \\ 1 & -1 & 1 & 0 & 0 & 0 \\ 0 & 0 & 1 & 1 & 0 & 1 \end{pmatrix} \cdot \begin{pmatrix} x_1 \\ x_2 \\ x_3 \\ x_4 \\ x_5 \\ x_6 \end{pmatrix} \quad (3.11)$$

which brings the ODE system (1.2) into a form

$$\begin{aligned} \dot{y}_1 &= k_0 x_2^0 - y_1 \left\{ k_0 + k_1 y_4 + (k_2 + k_3 (y_6 - y_5 - y_1 - y_2 + y_4)) (y_5 - y_4 + y_1) \right\} \\ \dot{y}_2 &= -k_6 y_2 + k_7 y_3 (y_6 - y_5 - y_1 - y_2 + y_4) - k_0 y_2 \\ \dot{y}_3 &= -k_8 y_3 + k_6 y_2 - k_7 y_3 (y_6 - y_5 - y_1 - y_2 + y_4) + k_0 (x_5^0 - y_3) \\ \dot{y}_4 &= k_4 (y_5 - y_4 + y_1) - k_5 y_4 (y_6 - y_5 - y_1 - y_2 + y_4) - k_1 y_1 y_4 + k_0 (x_1^0 - y_4) \\ \dot{y}_5 &= k_0 (x_1^0 - x_2^0 - y_5) \\ \dot{y}_6 &= k_0 (x_4^0 - y_6) \end{aligned} \quad (3.12)$$

where the last two equations for  $y_5$  and  $y_6$  become decoupled from the 4-dimensional subsystem corresponding to the  $(y_1, y_2, y_3, y_4)$  variables. Note that the latter four variables are just relabeled versions of four of the original variables, i.e. we have  $y_1 = x_2$ ,  $y_2 = x_6$ ,  $y_3 = x_5$  and  $y_4 = x_1$ .

The last two equations in (3.12) describe the mass conservation relations. They can be integrated separately and yield the following solution for zero initial condition:

$$\begin{aligned} y_5(t) &= (x_1^0 - x_2^0)(1 - \exp(-k_0 t)) \\ y_6(t) &= (x_4^0)(1 - \exp(-k_0 t)). \end{aligned}$$

This means that after a transient time of order  $t \sim 1/k_0$ , the trajectories of the ODE system (3.12) (and equally that of (1.2)) approach an attracting 4-dimensional manifold which is formally defined in the limit  $t \rightarrow \infty$  as

$$\begin{aligned} \lim_{t \rightarrow \infty} y_5(t) &= \lim_{t \rightarrow \infty} (x_1(t) - x_2(t) + x_3(t)) = x_1^0 - x_2^0 =: y_5^\infty \\ \lim_{t \rightarrow \infty} y_6(t) &= \lim_{t \rightarrow \infty} (x_3(t) + x_4(t) + x_6(t)) = x_4^0 =: y_6^\infty. \end{aligned} \quad (3.13)$$

### 3. Quasi-Integrals

In chemical terms, these two relations express the conservation of S atoms and H<sup>+</sup> ions, respectively:

$$\begin{aligned} [SO_3^{2-}] - [H_2O_2] + [HSO_3^-] &= [SO_3^{2-}]^0 - [H_2O_2]^0 \\ [HSO_3^-] + [H^+] + [AH] &= [H^+]^0 \end{aligned} \quad (3.14)$$

which is obtained using the correspondence between the chemical species and the phase space variables (1.3). Since the last two equations in (3.12) do not contain any essential dynamical information, but merely express the stoichiometric constraints in the reaction mechanism (1.1), the transient approach to the 4-dimensional manifold (3.13) can be neglected by replacing the variables  $y_5$  and  $y_6$  in (3.12) with their asymptotic values according to (3.13)

$$y_5 = y_5^\infty, \quad y_6 = y_6^\infty. \quad (3.15)$$

as a result, we obtain a 4-dimensional ODE system

$$\begin{aligned} \dot{y}_1 &= k_0 x_2^0 - y_1 \left\{ k_0 + k_1 y_4 + \left( k_2 + k_3 (y_6^\infty - y_5^\infty - y_1 - y_2 + y_4) \right) (y_5^\infty - y_4 + y_1) \right\} \\ \dot{y}_2 &= -k_6 y_2 + k_7 y_3 (y_6^\infty - y_5^\infty - y_1 - y_2 + y_4) - k_0 y_2 \\ \dot{y}_3 &= -k_8 y_3 + k_6 y_2 - k_7 y_3 (y_6^\infty - y_5^\infty - y_1 - y_2 + y_4) + k_0 (x_5^0 - y_3) \\ \varepsilon \dot{y}_4 &= k_4 (y_5^\infty - y_4 + y_1) - k_5 y_4 (y_6^\infty - y_5^\infty - y_1 - y_2 + y_4) + \varepsilon (-k_1 y_1 y_4 + k_0 (x_1^0 - y_4)) \end{aligned} \quad (3.16)$$

where the stoichiometric constraints (3.13, 3.14) are properly taken into account. Moreover, the quasi-stationary manifold (3.6) now appears in only *one* rate equation which, due to our choice of the linear coordinate transformation (3.11), is that of  $y_4 \equiv x_1$ . The fast subsystem is now given by

$$\begin{aligned} \frac{d}{d\tau} y_4 &= \underbrace{k_4 (y_5^\infty - y_4 + y_1)}_{R_4} - \underbrace{k_5 y_4 (y_6^\infty - y_5^\infty - y_1 - y_2 + y_4)}_{R_5}. \\ &= R_4 - R_5 \end{aligned} \quad (3.17)$$

Its stationary points

$$k_4 \underbrace{(y_5^\infty - y_4 + y_1)}_{x_3} - k_5 \underbrace{y_4}_{x_1} \underbrace{(y_6^\infty - y_5^\infty - y_1 - y_2 + y_4)}_{x_4} = 0 \quad (3.18)$$

define the quasi-stationary manifold for the 4-dimensional version of the hemin system (eq. 3.16). Due to the proper consideration of the chemical constraints (3.14), this is now a quadratic equation for  $y_4 \equiv x_1$  whose solution is given by

$$y_4 = \frac{1}{2} (y_5^\infty - y_6^\infty + y_1 + y_2 - \frac{k_4}{k_5}) \pm \frac{1}{2} \sqrt{(y_5^\infty - y_6^\infty + y_1 + y_2 - \frac{k_4}{k_5})^2 + 4 \frac{k_4}{k_5} (y_5^\infty + y_1)}. \quad (3.19)$$

Here, we must consider only the positive square root, since  $y_4$  represents a concentration and therefore  $y_4 \geq 0$  must hold. direct computation of the (1-dimensional) Jacobian

matrix along the manifold (3.19) shows that it is globally attracting since we have:

$$\begin{aligned} \frac{\partial}{\partial y_4}(R_4 - R_5)|_{y_4=y_4(y_1, y_2)} &= -k_4 - k_5(y_6^\infty - y_5^\infty - y_1 - y_2 + 2y_4)|_{y_4=y_4(y_1, y_2)} \\ &= -k_5 \sqrt{(y_5^\infty - y_6^\infty + y_1 + y_2 - \frac{k_4}{k_5})^2 + 4\frac{k_4}{k_5}(y_5^\infty + y_1)} \end{aligned}$$

which is negative for all  $(y_1, y_2) \in \mathbb{R}_+^2$ . This shows in particular, that the fast subsystem (3.17) is no longer degenerate. On the other hand, it is known [74] that if the fast subsystem is entirely composed of reversible reactions, as it is in our case ( $R_4$  and  $R_5$  correspond to the first reversible reaction step in (1.1)), then its stationary points automatically define an attracting manifold for the original flow.

Finally, we perform the QSSA using the procedure outlined in Section 2.2 and arrive at the following 3-dimensional ODE system:

$$\begin{aligned} \dot{y}_1 &= k_0 x_2^0 - y_1 \left\{ k_0 + k_1 y_4 + \left( k_2 + k_3(y_6^\infty - y_5^\infty - y_1 - y_2 + y_4) \right) (y_5^\infty - y_4 + y_1) \right\} \\ \dot{y}_2 &= -k_6 y_2 + k_7 y_3 (y_6^\infty - y_5^\infty - y_1 - y_2 + y_4) - k_0 y_2 \\ \dot{y}_3 &= -k_8 y_3 + k_6 y_2 - k_7 y_3 (y_6^\infty - y_5^\infty - y_1 - y_2 + y_4) + k_0 (x_5^0 - y_3), \end{aligned} \quad (3.20)$$

where  $y_4 = y_4(y_1, y_2)$  is now a function of  $y_1$  and  $y_2$  according to the expression for the quasi-stationary manifold (3.19). That the 3-dimensional ODE system (3.20) truly represents a very good (even quantitative) approximation to the long-time behavior of the hemin system (1.2) will be shown in Chapter 4, in particular in Section 4.1, where we compare the local one- and two-parameter bifurcation diagrams for both systems.

We remark that the defining equation for the quasi-stationary manifold (3.18) represents a so-called *quadric* [75] which is the 3-dimensional analog of a *conic section*. Quadrics can be thought of as smooth embedded surfaces in  $\mathbb{R}^3$ . In the case of equation (3.18), we find after performing appropriate linear transformations (translation, rotation) a *hyperbolic paraboloid* (Fig. 3.2) whose normal form is given by

$$\frac{y^2}{b^2} - \frac{x^2}{a^2} = z \quad (x, y, z) \in \mathbb{R}^3.$$

The parameters  $a$  and  $b$  are given as functions of the constants  $k_4, k_5, y_5^\infty$ , and  $y_6^\infty$ . They determine the particular shape of the surface.

### 3.3. Quasi-integrals in general reaction networks

We briefly describe how to generalize the method of quasi-integrals to reaction networks of the form:

$$\dot{x} = f(x, k) \equiv \mathbf{C} \cdot R(x, k) \quad (3.21)$$

where the components of the vector field  $f$  can be written as linear combinations of components of the reaction rate vector  $R$ :

$$\dot{x}_l = f_l(x, k) = \sum_{i=1}^r C_{li} R_i(x, k) \quad l = 1 \dots n. \quad (3.22)$$

### 3. Quasi-Integrals

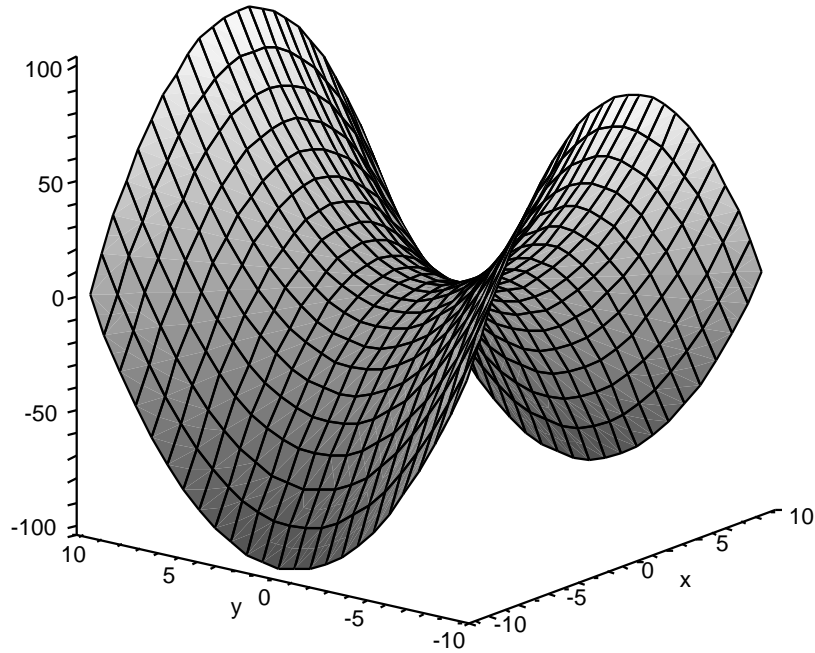


Figure 3.2.: The slow manifold for the hemin system is a so-called hyperbolic paraboloid whose representation in standard coordinates is given by  $\frac{y^2}{b^2} - \frac{x^2}{a^2} = z$ .

Here,  $x \in \mathbb{R}^n$  denotes the time-dependent state,  $k \in \mathbb{R}^r$  stands collectively for all parameters in the system and the constant matrix  $\mathbf{C}$  represents the stoichiometric matrix. In the following, we shall not assume a particular shape of the reaction rate vector  $R$ . However, since a large class of (bio-)chemical reaction systems (such as the hemin and the PO system studied in this thesis) is modeled by mass-action type reaction networks, we note that in this case, the components of the reaction rate vector are given by

$$R_i(x, k) = k_i \prod_j x_j^{\kappa_j^{ji}} \quad i = 1 \dots r, \quad j = 1 \dots n. \quad (3.23)$$

Thus, the general form (3.21) admits mass-action type kinetics as a special case, but also leaves the possibility to use other kinetic schemes. The constant matrix  $\kappa$  in (3.23) contains the kinetic information of each individual reaction step. Both of the above mentioned matrices,  $\mathbf{C}$  and  $\kappa$ , have as many rows as there are chemical species ( $n$ ) and as many columns as there are individual reaction steps ( $r$ ) and thus, completely specify the topology of a network following a mass-action kinetics.

Recall that in Section 3.2 we searched in each rate equation for reaction steps that balance each other along the numerically obtained trajectories. To this purpose, we partitioned the function  $g(x, y, \varepsilon)$  in (3.2) into a dominating part  $g_0(x, y)$  which was supposed to describe the quasi-stationary manifold in the limit  $\varepsilon \rightarrow 0$  and a negligible part  $\tilde{g}(x, y, \varepsilon)$ . In general, the dominating part will be of the form:

$$(g_0)_{ij}^l = C_{li}R_i(x(t), k) + C_{lj}R_j(x(t), k) \sim 0, \quad (3.24)$$

where the index  $l = 1, \dots, n$  runs over all rate equations in (3.22) while  $i, j = 1, \dots, r$  denote the individual reaction steps occurring in a particular rate equation.

Quasi-integrals are defined as those ratios

$$I_{ij}^l = \frac{C_{li}R_i(x(t), k)}{C_{lj}R_j(x(t), k)} \sim -1 \quad (3.25)$$

that approach an almost constant value along the trajectories  $x_l(t)$  of (3.22) for a certain combination of indices  $l \in \{1 \dots n\}, i, j \in \{1 \dots r\}$ . The occurrence of the ‘ $-1$ ’ on the right-hand side in (3.25) is due to the fact that in (3.24) we must consider only those reaction steps  $R_i, R_j$  for which  $\text{sign}(C_{lj}) = -\text{sign}(C_{li})$  holds because otherwise (3.24) can not be fulfilled. This condition reduces the number of index combinations  $(l, i, j)$  that must be taken into account during the search for quasi-integrals. On the other hand, it may also happen that the same combination of reaction steps occurs in different rate equations in which case they can be omitted.

In a next step, one can easily extend the definition for a quasi-integral (3.25) and try to balance more than two reaction steps in which case the dominant part  $g_0$  of  $g(x, y, \varepsilon)$  could be, for example, of the form:

$$(g_0)_{ijk}^l = C_{li}R_i(x(t), k) + C_{lj}R_j(x(t), k) + C_{lk}R_k(x(t), k) \sim 0. \quad (3.26)$$

In this case, quasi-integrals would be given by:

$$I_{ijk}^l = \frac{C_{li}R_i(x(t), k) + C_{lk}R_k(x(t), k)}{C_{lj}R_j(x(t), k)} \sim -1 \quad (3.27)$$

provided that e.g.  $\text{sign}(C_{li}) = \text{sign}(C_{lk}) = -\text{sign}(C_{lj})$  holds. Indeed, for the PO system, which will be discussed in appendix C, we find two quasi-integrals of this type.

From the above description it is clear that the search for quasi-integrals is an algorithmic procedure which can be summarized in the following three steps:

1. First, integrate the ODE system (3.21) over a sufficiently long time interval to obtain the trajectories for parameter values, where the interesting asymptotic kind of dynamics is observed.
2. Second, check whether quasi-integrals of the form (3.25) (or equally (3.27)) exist.
3. Third, apply singular perturbation techniques (for example the QSS (eq. 2.18)) to reduce the number of dynamical degrees of freedom in the system.

### 3. *Quasi-Integrals*

In the end, it is a good idea to check the quality of the approximation due to the loose definition of a quasi-integral as being ‘almost constant’. This can be done, for example, by comparing the local bifurcation diagrams for the original and the reduced system which, at least, reveals whether both systems belong to the same topological class.

second reason for the necessity to compare the dynamics of the original with that of the reduced system is that quasi-integrals are usually determined for one particular set of parameters and therefore, the reduction procedure is technically valid for only one point in parameter space. Thus, by systematically comparing the local bifurcations in dependence on relevant system parameters, one can ensure that the reduced system has truly inherited the dynamical properties of the original system in a whole parameter range.

In this thesis, we always compare the original and the reduced systems based on their local bifurcation diagrams.

## 4. Local Bifurcations in the Hemin System

This Chapter is devoted to a comparison between the 6-dimensional hemin system (eq. 1.2) and its 3-dimensional approximation (eq. 3.20) that was derived in Section 3.2 using the method of quasi-integrals. We begin with a presentation of a two-parameter bifurcation diagram which shows the global bifurcation structure of the 3-dimensional hemin system. In the next step, we take a section along a one-parameter path in the two-parameter plane in order to study some of the codimension one bifurcation sequences in detail. Finally, we show that the 6-dimensional hemin system (eq. 1.2) and its 3-dimensional approximation (eq. 3.20) are indistinguishable based on their local bifurcation structure.

Notice that for the presentation of the results, we shall use rescaled dimensionless variables and parameters according to Appendix B.2. In addition, we will find several codimension one and codimension two bifurcations in the course of the investigation. All of them are described in Appendix A.3 and A.4 in some detail which, therefore, should be consulted for reference.

### 4.1. Two-parameter continuation in $k_0$ and $k_8$

During the experimental investigations of the hemin system [32, 33], the flow rate  $k_0$  was taken as the principal bifurcation parameter (cf. Sec. 1.1) controlling the matter flow through the reaction system. In order to perform a two-parameter continuation, we chose the decay rate of hemin  $k_8$  as a second bifurcation parameter for two reasons: First, its experimental value has not been precisely determined so far and second, the mechanistic role of hemin is to prevent the unbounded production of  $H^+$  ions and, thus, the hemin decay rate should be a sensible parameter. In fact, if  $k_8$  is identically zero, the ODE systems (1.2) and (3.20) become essentially 2-dimensional and no complex dynamics is possible anymore.

Generically, as two parameters of an ODE system are varied, several codimension two bifurcations may be encountered along branches of codimension one bifurcations. Those bifurcations, that are relevant for the hemin system, are summarized in Appendix A.4 which should be consulted for details.

Figure 4.1 shows the two-parameter bifurcation diagram for the 3-dimensional ODE system (3.20) where the flow rate  $k_0$  and the hemin decay rate  $k_8$  have been used as continuation parameters. It basically consists of five regions: In regions 1 and 5, there is only one stable stationary state. Coming from region 1, the stationary state loses

#### 4. Local Bifurcations in the Hemin System

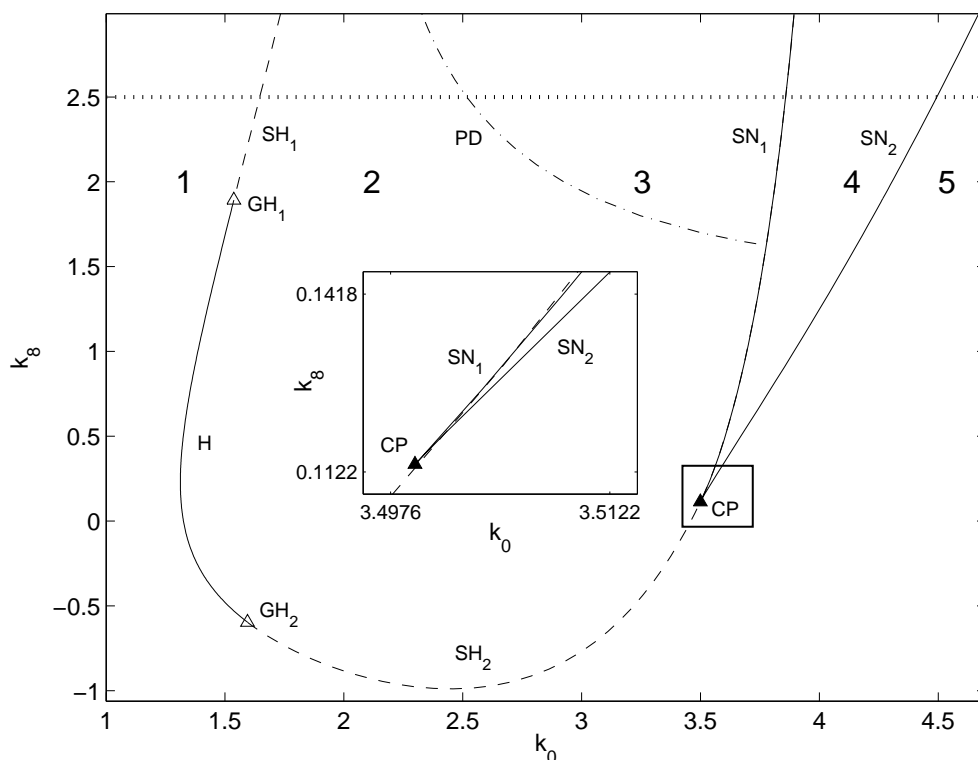


Figure 4.1.: Two-parameter bifurcation diagram in the flow rate  $k_0$  and the hemin decay rate  $k_8$ . Bursting oscillations are stable in region 3 which is bounded by the period doubling curve (PD) and the saddle-node curve  $SN_1$ . The dotted line at  $k_8 = 2.5$  marks the parameter path along which the codimension one bifurcation diagram in Fig. 4.2 has been calculated. Symbols denote:  $SH_i$  - curves of subcritical Hopf bifurcations (dashed),  $H$  - curve of supercritical Hopf bifurcations (solid),  $SN_i$  - curves of saddle-node bifurcations of fixed points (solid),  $PD$  - curve of period doubling bifurcations (dash-dot), codimension two points:  $GH_i$  - generalized Hopf bifurcations (open triangle),  $CP$  - cusp (filled triangle, see also the inset).

stability via a subcritical ( $SH_1$ , dashed line) or a supercritical Hopf bifurcation ( $H$ , solid line). In the latter case this leads immediately to the emergence of stable oscillations which remain of simple periodicity throughout region 2 while in the subcritical case simple periodic oscillations also arise, but in a series of secondary bifurcations that will be discussed in Section 4.2. The two branches of Hopf bifurcations meet in a codimension two bifurcation point, the generalized Hopf bifurcation  $GH_1$  at  $k_8 = 1.892$  where the first Liapunov coefficient vanishes.

As the curve of supercritical Hopf bifurcations ( $H$ ) is traced towards lower values of  $k_8$ , the curve again becomes subcritical ( $SH_2$ ) at  $GH_2$  where  $k_8$  is negative. Notice that the

region where  $k_8$  is negative does not have a physical significance; it is merely included for a consistent description of the bifurcation scenario. Finally, the subcritical Hopf bifurcation turns into a neutral saddle (where the eigenvalues fulfill  $\lambda_1 + \lambda_2 = 0$  with  $\lambda_1, \lambda_2 \in \mathbb{R}$ ) close to the cusp singularity (CP, solid triangle). However, this does not correspond to a bifurcation. The region in the vicinity of the cusp point is magnified in the inset of Fig. 4.1 which shows that two branches of saddle-node points ( $\text{SN}_1$  and  $\text{SN}_2$ ) emanate from CP.

Bursting oscillations are stable in region 3. This region is entered through a curve of period doubling bifurcations (PD) while it is terminated by a branch of the saddle-node points  $\text{SN}_1$ . In region 4 two saddle points coexist with one stable equilibrium which remains the only fixed point in region 5 where it is stable. Accordingly, all trajectories settle down to a stationary state in the regions 4 and 5.

The partition into five regions, however, only gives a first impression of the expected dynamics of the ODE system (1.2). For example, there is a narrow band to the right of the period doubling curve PD where a whole cascade of period doubling bifurcations occurs as the flow rate  $k_0$  is increased for a fixed value of  $k_8$ . Subsequently, a folded chaotic attractor emerges before the first periodic bursting oscillations appear in region 3. The bifurcations occurring beyond the period doubling bifurcation PD are discussed in Sections 6.2 and 6.3. Furthermore, it is known from the normal form theory of codimension two bifurcations [76] that there is an additional curve bifurcating from the generalized Hopf point  $\text{GH}_1$  in Fig. 4.1 (in our case towards higher values of  $k_8$ ) along which a saddle-node bifurcation of periodic orbits takes place. This bifurcation is involved in the emergence of stable simple periodic oscillations above the generalized Hopf point  $\text{GH}_1$  where the Hopf bifurcation is subcritical. The details will be discussed in the next Section.

## 4.2. Bifurcations along a one-parameter path

In order to obtain a full picture of the bifurcation sequences, we take a section along the one-parameter path  $k_8 = 2.5$  in the  $k_0$ - $k_8$  plane (dotted line, Fig. 4.1) where the stationary state disappears via a subcritical Hopf bifurcation. As in the case of the two-parameter continuation, there are now several codimension one bifurcations of stationary points and periodic solutions that may be encountered upon varying one parameter in the ODE system (3.20). The relevant bifurcations are summarized in the Appendix A.3 which should be consulted for reference.

Coming from region 1 of the two-parameter plane above the generalized Hopf bifurcation point (cf. Fig. 4.1), the simple periodic oscillations arise in the following scenario (inset Fig. 4.2): The stable stationary state (solid line) loses stability at  $k_0 = 1.6461$  via a subcritical Hopf bifurcation (SH) giving rise to an unstable limit cycle with one unstable dimension (one of the two Floquet multipliers is outside the unit circle). The subcritical Hopf is followed by a saddle-node bifurcation of periodic orbits (SNP) at  $k_0 = 1.6438$  where the second multiplier also leaves the unit circle and the limit cycle gains a second unstable dimension. In the narrow parameter interval between the SNP

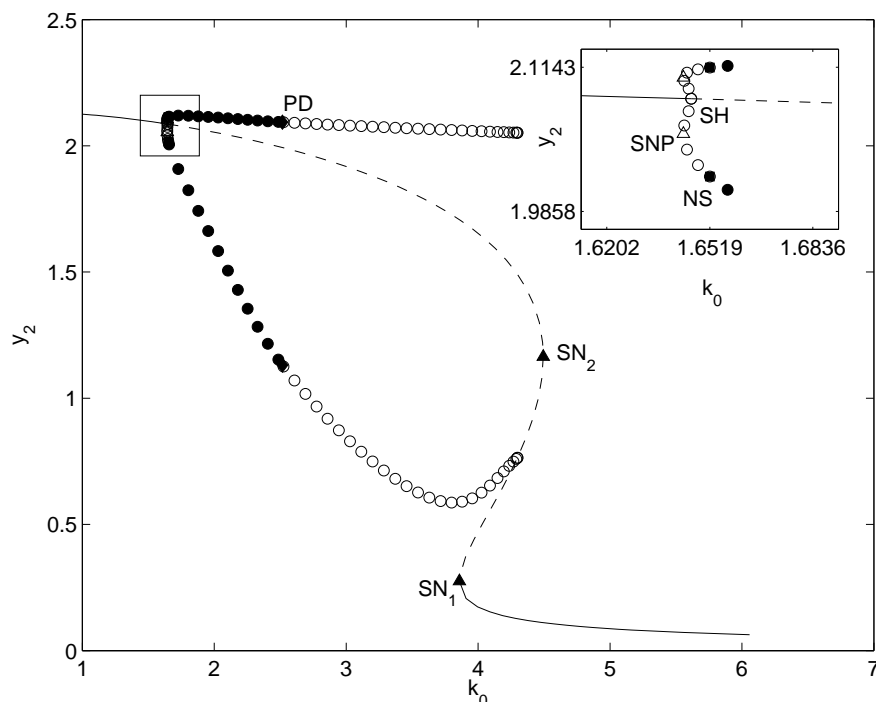


Figure 4.2.: One-parameter bifurcation diagram along the line  $k_8 = 2.5$  (cf. Fig. 4.1).

The inset shows a magnification of the rectangular region where the simple periodic oscillations (solid circles) emerge via a subcritical Hopf (inset, SH) followed by a saddle-node bifurcation of periodic orbits (inset, open triangle, SNP) and an (inverse) Neimark-Sacker bifurcation (inset, filled square, NS). Between SNP and SH, the only stable attractor is a fixed point while a torus is stable between SH and NS. Mixed-mode oscillations are observed beyond the period doubling (PD) where the primary limit cycle (open circles) is unstable (see text for details). The oscillatory region extends until the saddle-node bifurcation  $SN_1$  where a homoclinic bifurcation occurs (see also Section 6.3). For the oscillatory states, the minimum and the maximum amplitude of the oscillation are plotted.

and the SH bifurcation point, the stationary state is the only attractor since the coexisting limit cycle is unstable. Stable oscillations, however, arise at  $k_0 = 1.6519$  by an (inverse) Neimark-Sacker (NS) bifurcation where both multipliers simultaneously cross the unit circle inwards. Thus, there is a stable quasi-periodic solution bifurcating to the left of the Neimark-Sacker point (towards lower  $k_0$  values) where it coexists with a saddle point (corresponding to the dashed line in the inset of Fig. 4.2) in the parameter interval  $k_0 \in (1.6461, 1.6519)$ .

The properties of the torus solution are further discussed in Section 8.3 where we analyze the phase flow on the torus using the slow-fast structure of the hemin system.

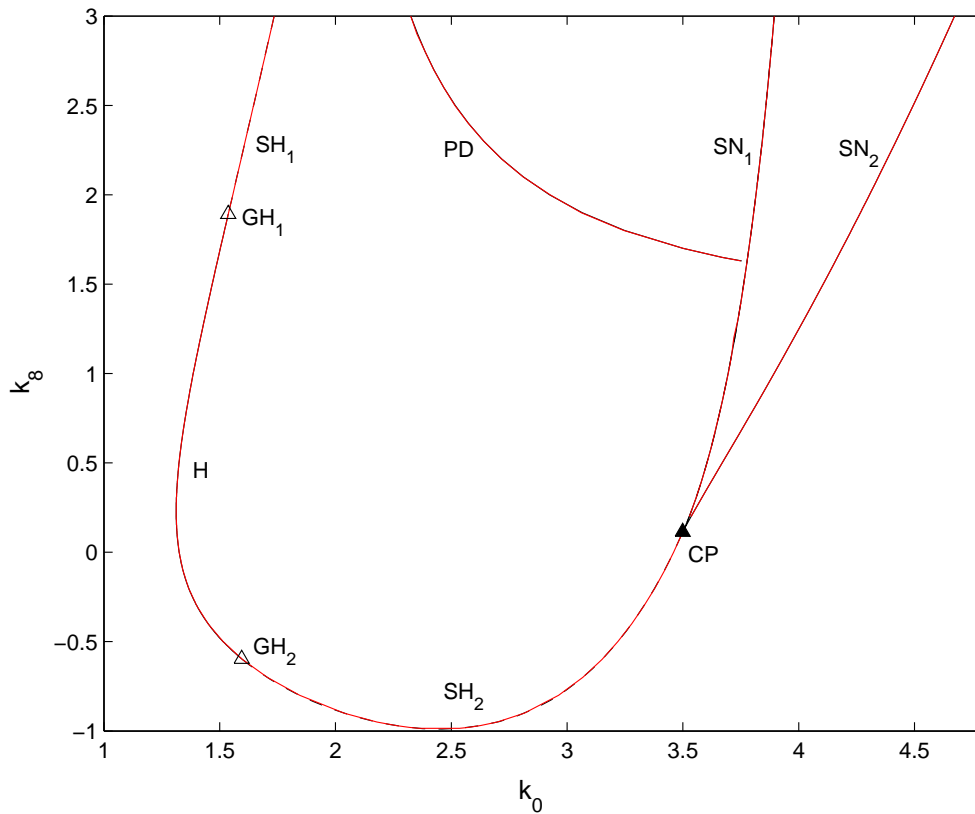


Figure 4.3.: Overlay of the two-parameter bifurcation diagrams of the 3-dimensional ODE system (3.20) (black lines) and the original 6-dimensional ODE system (1.2) (red lines).

### 4.3. Comparison between the 6-d system and its 3-d approximation

As Fig. 4.3 reveals, there is virtually no difference between the two-parameter bifurcation diagrams of the 3-dimensional (black lines) and the original 6-dimensional hemin system (red lines). Accordingly, the local bifurcation structure of the 6-dimensional ODE system (1.2) is perfectly preserved by the 3-dimensional ODE system (3.20). Thus, the latter yields a very good quantitative approximation to the original dynamics which, therefore, will be used for a further investigation of the bursting oscillations in the second Part of the thesis.

The two-parameter bifurcation diagram for the 6-dimensional system (1.2) was reconstructed from 1-dimensional bifurcation diagrams taken along equally spaced sections in the two-parameter plane where  $k_8$  was varied with a stepsize of 0.1.



## 5. Summary and Discussion

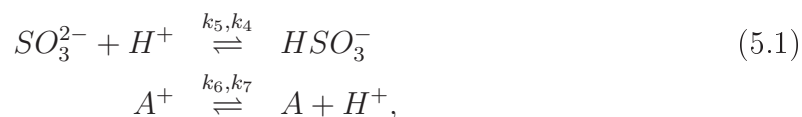
The first Part of the thesis is concerned with the reduction of complex (bio-)chemical reaction networks of the form (3.22) while keeping their essential dynamical properties. We have introduced the concept of quasi-integrals as a numerical method for systematically finding a particular class of quasi-stationary manifolds in such networks. Subsequently, the slow manifolds can be used to eliminate as many dynamical degrees of freedom as there are quasi-integrals in a given reaction network. As a result, one obtains a system of reduced dimensionality which contains only the essential dynamical degrees of freedom.

It was shown that quasi-integrals of the type (3.25) and (3.27) may arise from ratios between certain components of the reaction rate vector  $R$ . In general, the components of the reaction rate vector are nonlinear functions of the phase space variables describing the kinetics of the individual reaction steps. Thus, the class of slow manifolds, that can be detected, not only includes linear relationships among the phase space variables, but generically also contains those which are defined by nonlinear equations.

The method of quasi-integrals is inspired by the geometrical singular perturbation theory of Fenichel [60] (cf. Sec. 3.1) which sets the suitable mathematical framework for the description of chemical reaction systems evolving on different time scales. In this approach, the existence of quasi-integrals such as (3.25) and (3.27) is a sufficient condition for the existence of a slow manifold. The major advantages of the proposed method are that

- it does not require a priori knowledge about the relevant time scales in a system. To the contrary, it identifies them.
- it does not rely on a sophisticated rescaling procedure in order to identify small parameters in the system.
- it is an algorithmic procedure and therefore, it is especially suited for a straightforward reduction of higher dimensional networks.

In Section 3.2, we have exemplarily introduced the method of quasi-integrals using the 6-dimensional hemin system (1.2). The reaction mechanism (1.1) of the hemin system comprises the two equilibria



and it is not too surprising that the quasi-integral, that we have found, corresponds to one of them, namely the first equilibrium reaction in (5.1). However, this observation is

## 5. Summary and Discussion

not trivial since the second equilibrium reaction in (5.1) does not define a quasi-integral. In order to demonstrate that the method of quasi-integrals does not only detect quasi-stationary manifolds associated with equilibrium reactions, we also applied the method to the 10-dimensional peroxidase–oxidase reaction system (cf. Appendix B.3) which, in contrast to the hemin system, is entirely composed of irreversible reaction steps. Remarkably, we identified three possible quasi-integrals in the reaction mechanism of the PO system, two of which lead to reduced systems that even quantitatively agree quite well with the original one.

In Section 4.3, we compared the 6-dimensional ODE system (1.2) with its 3-dimensional approximation (3.20) based on their local codimension two bifurcation diagrams. The 3-dimensional system has been obtained in Section 3.2 as a result of a QSS using the quasi-integral (3.5). The fact that the bifurcation diagrams for both systems are virtually identical demonstrates that the 3-dimensional ODE system has the same dynamical properties as the original 6-dimensional ODE system (1.2) and thus, the former may be used for a further analysis of the bursting oscillations in the second Part of the thesis.

The crucial step in identifying a quasi-integral was to define, under which conditions the graph of a quasi-integral is to be regarded as ‘almost constant’. As we have already noticed, there is some ambiguity in this definition and especially for higher dimensional ODE systems, it would be of great value to have a numerical measure that allows for a more systematic or even automatic detection of quasi-integrals. Based on some common properties shown by all of the detected quasi-integrals, we suggest the following working definition: a quasi-integral is a non-constant function of the phase space variables that remains bounded almost everywhere in a stripe of adjustable thickness  $\mu$  around 1. This means that outliers are only allowed in time intervals of adjustable length  $\delta$  which should be small as compared to typical time scales in the system such as the period of the oscillations.

However, when deciding whether a certain ratio  $I_{ij}$  is to be regarded as almost constant, our method is quite similar to other semi-objective methods such as principal component analysis or even singular perturbation theory. In the case of principal component analysis, one usually has to decide how many modes to keep in order to reconstruct the original data based on the eigenvalue spectrum of a suitable covariance matrix. But since there is no a priori interpretation of the principal components of a given data set, a rigorous measure, indicating how many modes to retain, is equally missing. On the other hand, for singular perturbation theory to be valid, the singular perturbation parameter  $\varepsilon$  is required to be sufficiently small. However, as we have already pointed out, in practical applications  $\varepsilon$  is given in terms of intrinsic system parameters and thus, has some fixed constant value. Moreover, it may even become of order unity for some systems without leaving the range of applicability of singular perturbation theory. Thus, for a particular system one usually relies on numerical simulations in order to test the validity of the approximation. Indeed, this is exactly what we have done when we compared the original and the reduced systems based on their local bifurcations.

Future efforts should comprise tests of the method of quasi-integrals in higher dimensional reaction networks in conjunction with a suitable extension and/or implementation of our working definition of a quasi-integral.

## Part II.

# The Origin of Bursting Behavior in the Hemin System



# 6. Dynamics and Bursting Oscillations in the Hemin System

In this Chapter, we investigate the bifurcations leading to the emergence of bursting oscillations in the hemin system (1.1) and subsequently, discuss their bifurcation sequences in terms of Farey progressions. Thereby, we continue the description of the bifurcation diagram of the hemin system in its 3-dimensional approximation (3.20) where the simple periodic oscillations arose via a series of codimension one bifurcations involving a subcritical Hopf bifurcation, a saddle-node bifurcation of periodic orbits and an inverse Neimark-Sacker bifurcation (Fig. 4.2).

In the next Section, we shall introduce a coordinate system that will be more suitable for the investigation of the bursting oscillations, since it is well adapted to the slow-fast structure of the hemin system. In Section 6.2, we describe the formation of a chaotic attractor that emerges subsequent to the period doubling bifurcation PD shown in the one-parameter bifurcation diagram of Fig. 4.2. This suggests that the bursting oscillations arising beyond the period doubling cascade are not associated with phase-locked states on a 2-torus. Instead, we observe periodic-chaotic progressions of mixed-mode states in Section 6.3 which are organized in pruned Farey sequences.

## 6.1. Change of coordinates

For convenience, we will change the notation of the variables  $(y_1, y_2, y_3, y_4)$  used in (3.20) to  $(x, y, z, s)$  and abbreviate the constant  $x_4^0 - x_1^0 + x_2^0$  as  $c$ . In the new coordinates, the 3-dimensional hemin system (3.20) reads

$$\begin{aligned}\dot{x} &= k_0 x_2^0 - x \left\{ k_0 + k_1 s(x, y) + \left( k_2 + k_3 (c - x - y + s(x, y)) \right) \right\} (x_1^0 - x_2^0 + x - s(x, y)) \\ \dot{y} &= -k_0 y - k_6 y + k_7 z (c - x - y + s(x, y)) \\ \dot{z} &= k_0 (x_5^0 - z) - k_8 z + k_6 y - k_7 z (c - x - y + s(x, y))\end{aligned}\tag{6.1}$$

where  $s(x, y)$  stands for the slow manifold (3.19) of the 6-dimensional system (1.2) given by

$$s = \frac{1}{2} \left( x + y - c - \frac{k_4}{k_5} \right) + \frac{1}{2} \sqrt{\left( x + y - c + \frac{k_4}{k_5} \right)^2 + 4 \frac{k_4}{k_5} (x_1^0 - x_2^0 + x)}.\tag{6.2}$$

However, numerical simulations suggest to investigate the bursting oscillations in the hemin system in a different coordinate system where the slow-fast structure of the ODE

## 6. Dynamics and Bursting Oscillations in the Hemin System

system (6.1) becomes more apparent. To this purpose, we introduce the sum of  $y$  and  $z$  as a new coordinate according to

$$p = y + z. \quad (6.3)$$

This linear coordinate transformation has the effect that one of the three equations in (6.1) becomes linear in the new coordinate system. On the other hand, numerical simulations show that  $y$  and  $z$  are basically anticorrelated (cf. Fig. 6.1 in the next Section) such that the sum of them evolves on a much slower time scale than the 2-dimensional  $x$ - $y$  subsystem. This observation will be crucial to analyze the origin of bursting and quasi-periodic behavior in the hemin system. In chemical terms, the sum of  $y$  and  $z$  is nothing but the total concentration of hemin species in the system which, therefore, might also be of physiological relevance.

Using  $(x, y, p)$  coordinates, the ODE system (6.1) is transformed into

$$\begin{aligned} \dot{x} &= k_0 x_2^0 - x \left\{ k_0 + k_1 s(x, y) + \left( k_2 + k_3 (c - x - y + s(x, y)) \right) \right\} (x_1^0 - x_2^0 + x - s(x, y)) \\ \dot{y} &= -(k_6 + k_0)y + k_7(p - y)(c - x - y + s(x, y)) \\ \dot{p} &= k_0(x_5^0 - p) - k_8(p - y) \end{aligned} \quad (6.4)$$

which will be the starting point for the slow-fast analysis of the hemin system in Chapter 8.

## 6.2. A period doubling route to chaos

In the following, we shall describe the formation of a chaotic attractor which emerges subsequent to the period doubling bifurcation PD in Fig. 4.2, but prior to the bursting oscillations. Recall that the simple periodic oscillations (full circles in Fig. 4.2) were generated by an inverse Neimark-Sacker bifurcation at  $k_0 = 1.6519$ . They remain stable up to  $k_0 = 2.5169$  where the first of a series of period doubling bifurcations renders the simple oscillations unstable and creates a stable period-2 cycle (Fig. 6.1a). The next two period doublings occur at  $k_0 = 2.5241$  (Fig. 6.1b) and 2.5253 (not shown).

During the period doubling cascade, the two multipliers of the primary unstable limit cycle (open circles in Fig. 4.2) rapidly diverge until they are separated by approximately 12 orders of magnitude, i.e.  $\mu_1 \sim 10^6$  and  $\mu_2 \sim 10^{-6}$ . Thus, the associated Poincaré map exhibits a strong contraction in one and a fast expansion in the other direction indicating the creation of a folded attractor for the subsequent chaotic states.

Figure 6.1c shows one of these states together with its Poincaré map (cf. inset). For the Poincaré map, we plot the value of the  $x$  variable each time the  $y$  variable passes a local minimum against the value of  $x$  at the preceding minimum of  $y$ . As a result, the Poincaré map exhibits a typical (asymmetric) tent map shape indicating chaotic behavior. Indeed, the largest Liapunov exponent, characterizing the local divergence of initially close trajectories, is found to be 0.84 at  $k_0 = 2.529$ . Figure 6.1d shows a nearby chaotic state at  $k_0 = 2.53$  with a Liapunov exponent of 1.12. This state differs from the former one in that the trajectory now performs small amplitude excursions to the

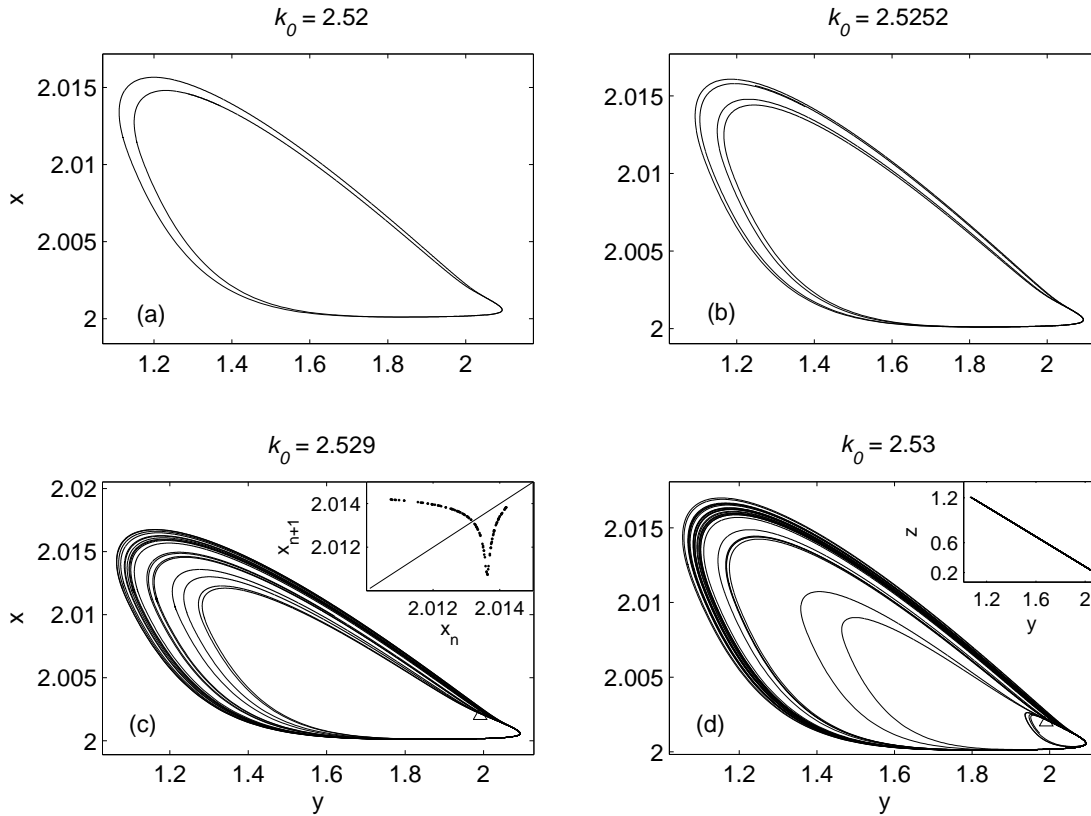


Figure 6.1.: Period doubling cascade leading to a chaotic attractor: Phase space projections of period-2 (a), period-4 (b) and two subsequent chaotic states (c),(d) are shown. The chaotic trajectory in (c) performs only large amplitude oscillations while the chaotic trajectory in (d) makes irregular excursions to the neighborhood of the saddle point (open triangle). The associated Poincaré map of the chaotic state in (c) is shown in the inset. It exhibits the shape of an inverse tent map with a cuspid tip (see text for details). The inset in (d) shows the same chaotic state as in (d) but in a  $y$ - $z$  projection of (6.1) where it becomes apparent that the chaotic attractor is contained in a thin layer in phase space.

neighborhood of the saddle point (open triangle) in an irregular fashion indicating the upcoming bursting oscillations. The inset in Fig. 6.1d shows the same chaotic trajectory at  $k_0 = 2.53$  but in a  $y$ - $z$  projection where it becomes self-evident that  $y$  and  $z$  are basically anticorrelated which causes the chaotic attractor to be contained in a thin layer in phase space; a property that also holds for the subsequent bursting oscillations. Due to the anti-correlation between  $y$  and  $z$ , their sum  $y + z$  changes only slowly in time which again suggests to introduce the sum of  $y$  and  $z$  as a new variable as we have done in equation (6.3).

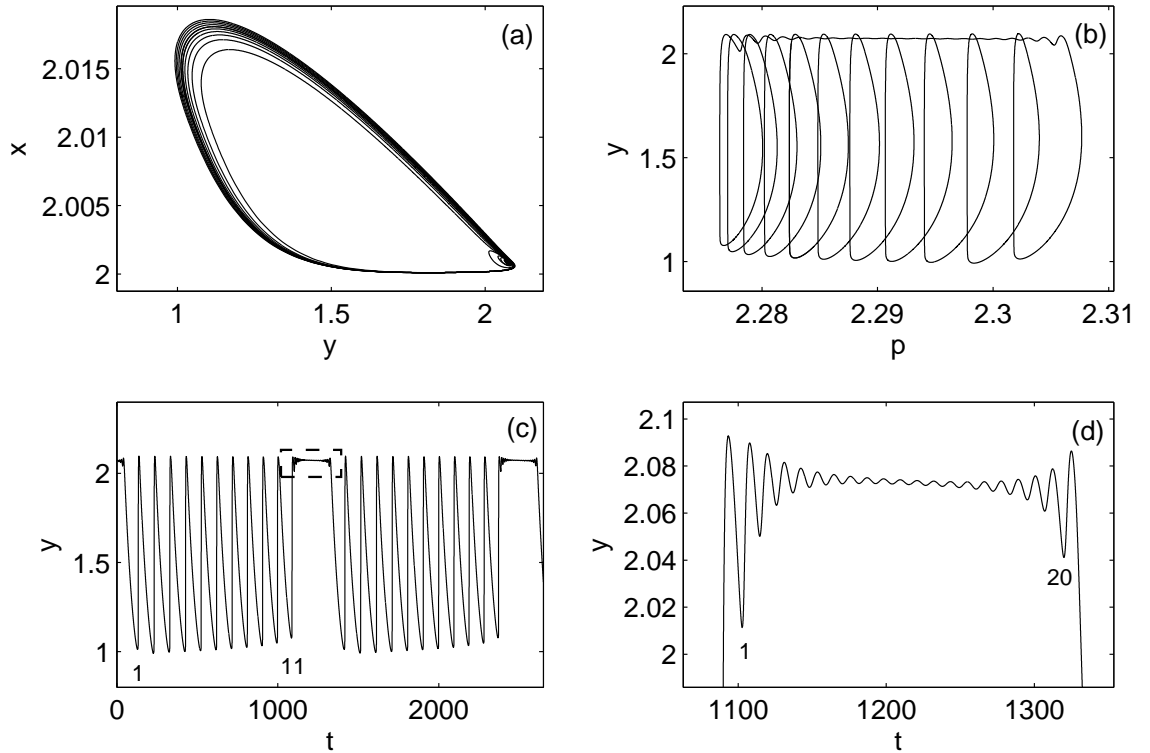


Figure 6.2.: The  $11^{20}$  bursting state (MMO) at  $k_0 = 2.545$  is shown in a  $y$ - $x$  projection (a) and in a  $p$ - $y$  projection (b) from which the unfolding of the bursting state along the  $p$  direction becomes apparent. The corresponding time series is presented in (c) while the dashed rectangular region in (c) is magnified in (d) showing the small amplitude oscillations.

### 6.3. Bursting oscillations

Subsequent to the formation of the chaotic attractor, we observe periodic-chaotic progressions of bursting oscillations (or MMOs) which are organized into pruned Farey sequences as described below. Note that the bursting states are not shown in the one-parameter bifurcation diagram of Fig. 4.2 since they do not bifurcate from the primary periodic orbit. Instead, they emerge beyond the chaotic window that follows the period doubling bifurcation  $PD$ . This suggests that they belong to isolated bifurcation curves. Therefore, we present some of the bursting states that were found by direct numerical integration at the corresponding parameter values.

The first periodic bursting state is observed at  $k_0 = 2.545$  where 11 large amplitude oscillations alternate with 20 small excursions (Fig. 6.2). According to the mixed-mode nomenclature  $L^S$ , this state is denoted as  $11^{20}$ . Figure 6.2a shows a projection onto the  $x$ - $y$  plane (similar to that in Fig. 6.1). If we regard, however, the same state in the  $p$ - $y$

projection (Fig. 6.2b) using the newly introduced  $(x, y, p)$  coordinate system (cf. Sec. 6.1), the ‘unfolding’ of the bursting oscillations along the  $p$  direction becomes apparent: In the  $x$ - $y$  projection (Fig. 6.2a) the small amplitude oscillations are located in the right lower corner while in Fig. 6.2b they occur along a line-like manifold at  $y \sim 2.1$ . In Fig. 6.2c we present the time series corresponding to the phase portraits of Figs. 6.2(a,b). The dashed rectangular region is magnified in Fig. 6.2d showing the small amplitude oscillations.

As the flow rate  $k_0$  increases from 2.545, where a  $11^{20}$  state is observed, to  $k_0 = 3.778$ , narrow chaotic windows alternate with further periodic windows which contain bursting states with a gradually decreasing number  $L$  of large amplitude oscillations. This periodic-chaotic sequence approaches the window corresponding to  $L = 1$  at  $k_0 = 3.31$  where a  $1^{16}$  state is stable. Within each periodic window of fixed  $L$ , we find pruned Farey sequences of bursting states with a different number  $S$  of small amplitude oscillations. For example, in the periodic window corresponding to the  $4^S$  states, the following progression was numerically resolved:  $4^{17}$  ( $k_0 = 2.768$ )  $\rightarrow$   $4^{18}$  ( $k_0 = 2.780$ )  $\rightarrow$   $4^{19}$  ( $k_0 = 2.800$ )  $\rightarrow$   $4^{20}$  ( $k_0 = 2.830$ ). A complete Farey sequence would also contain the intermediate states which are obtained by Farey arithmetic (cf. Table 1.1), e.g.  $8^{35} = 4^{17} \oplus 4^{18}$ , etc.

In the transition region between two states  $L^S$  and  $L^{S+1}$  with the same number of large amplitude oscillations, narrow chaotic windows as well as concatenated states of the form  $L^S L^{S+1}$  are found. The latter are periodic patterns that repeat after two revolutions while their number of small amplitude oscillations differs by one. For the example above, the  $4^{17}4^{18}$  state is observed at  $k_0 = 2.775$  (Fig. 6.3) while the other two states  $4^{18}4^{19}$ ,  $4^{19}4^{20}$  occur at  $k_0 = 2.795$ , 2.817, respectively.

The parameter window where  $L^S$  states are stable becomes larger as  $L$  gets smaller. Consequently, we also observed progressions starting with a lower number of small amplitude oscillations, e.g.  $1^{13}$  at  $k_0 = 3.235$ . At  $k_0 = 3.390$ , the number of small amplitude oscillations for the  $1^S$  progression already exceeds 20, but their amplitudes are too small to be counted. As the sequence of  $1^S$  states approaches  $k_0 = 3.778$ , the number of small amplitude oscillations steadily increases while the chaotic region between two such states becomes broader. Thus, one may suspect that within each periodic window of a fixed number of large amplitude oscillations,  $L^S$  states with arbitrary integer number  $S$  exist though most of them occur in too narrow parameter intervals to be observed in numerical simulations.

Subsequent to the periodic-chaotic progression of bursting oscillations, there is a further periodic window where we observe simple periodic oscillations which are now of relaxational type and have long periods (Fig. 6.4a). In Section 8.2 we shall show that the hemin system undergoes a transition in the bursting mechanism at  $k_0 = 3.778$  which causes the relaxational character of the oscillations beyond the periodic-chaotic progression of bursting states. The relaxational oscillations terminate at  $k_0 = 3.858$  by a saddle-node homoclinic bifurcation (cf. Appendix A.5) where the saddle-node bifurcation  $SN_1$  (cf. Figs. 4.1 and 4.2) occurs on the formerly periodic solution (Fig. 6.4b).

This completes the discussion of the bifurcation diagram in Fig. 4.2 along the one-parameter path at  $k_8 = 2.5$  in Fig. 4.1.

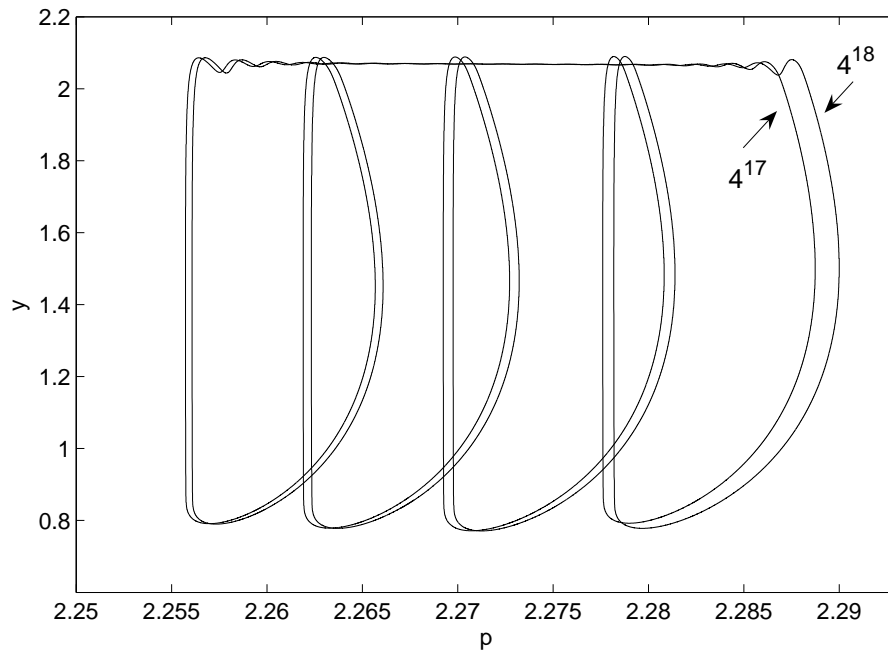


Figure 6.3.: The concatenated bursting state  $4^{17}4^{18}$  at  $k_0 = 2.775$  in a  $p$ - $y$  projection: The trajectory ‘closes’ after two revolutions; one consists of 4 large and 17 small, the other one of 4 large and 18 small amplitude oscillations.

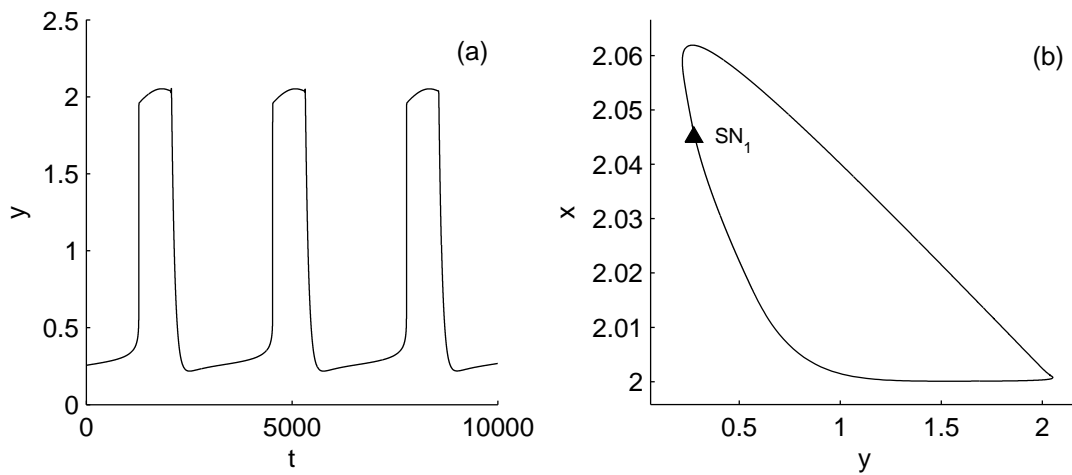


Figure 6.4.: Large relaxational oscillations at  $k_0 = 3.8$  close to a homoclinic orbit (a). The corresponding trajectory in phase space is shown in (b).  $SN_1$  marks the location where a saddle-node bifurcation (the same as in Fig. 4.2) is to occur at  $k_0 = 3.858$  on the formerly periodic solution. This yields a saddle-node homoclinic bifurcation causing the oscillations to vanish.



# 7. Slow-Fast Analysis – The Method

Before the slow-fast structure of the hemin system will be analyzed in detail, we present the basic ideas underlying a slow-fast analysis as it has been introduced by Rinzel and Ermentrout [23] to describe the bursting behavior of neural systems. In such systems, the dynamical variables evolve on different time scales similar to the reaction networks that have been investigated in the first Part of the thesis. However, the crucial difference is now that the time scale separation between the slow and the fast processes is not infinite anymore.

As a consequence, one can not simply assume that the fast processes relax to a slow manifold and henceforth instantaneously follow the slow dynamical degrees of freedom. Instead, the fast dynamical variables must not be neglected in the dynamical description. In fact, it is the dynamics of the slow processes that trigger certain bifurcations in the fast subsystem. As a result, there are several attracting states in different regions of phase space. One may then arrive at a geometrical comprehension of the dynamics since the flow of a system exhibiting a slow-fast structure is mostly confined to the neighborhood of the attracting states of the fast subsystem.

We shall use a cartoon of the hemin system in order to exemplarily describe its slow-fast structure in phase space. This example should facilitate the understanding of the bifurcation diagrams that will be presented in Chapter 8 where we analyze the slow-fast structure of the hemin system in detail.

## 7.1. Cartoon of the slow-fast structure of the hemin system

Consider Fig. 7.1 where the slow-fast structure of the 3-dimensional hemin system (6.4) is illustrated in a cartoon using the  $(x, y, p)$  coordinate system. Here we assume that the dynamics of the hemin system can be decomposed into a fast motion in the  $x$  and  $y$  directions and a slow motion along the  $p$  direction. Accordingly, the dynamics of the system should be describable in terms of an ODE system of the form

$$\begin{aligned}\dot{x} &= f(x, y, p) \\ \dot{y} &= g(x, y, p) \\ \dot{p} &= \varepsilon h(x, y, p)\end{aligned}\tag{7.1}$$



For example, as  $p$  moves to the left, the stable and the unstable limit cycle merge in a saddle-node bifurcation (SNP) and disappear leaving the stable stationary (thin black line) state as the only invariant set. On the other hand, as  $p$  moves to the right, the unstable limit cycle shrinks and vanishes in a subcritical Hopf bifurcation (SH). Henceforth, a large amplitude limit cycle coexists with a saddle point. Eventually, a saddle-node bifurcation ( $\text{SN}_1$ ) takes place on the large amplitude limit cycle to form a saddle-node homoclinic orbit (cf. Appendix A.5) by which the periodic solution of the fast subsystem ceases to exist.

Now the basic assumption underlying the slow-fast analysis is that the finite time scale separation between the fast  $x$ - $y$  subsystem and the slow  $p$  dynamics is such that the stationary and oscillatory states, that exist in the fast subsystem at a particular value of  $p$ , extend along the  $p$  direction to quasi-stationary manifolds in the 3-dimensional phase space (cf. Fig. 7.1), i.e. the stationary states become a line-like quasi-stationary manifold ( $\mathcal{L}$ ) while the oscillatory states form a (finite) cylinder-like manifold ( $\mathcal{C}$ ) which is terminated at one side by a saddle-node bifurcation (SNP) and at the other side by a saddle-node homoclinic orbit.

Here the term ‘quasi-stationary’ is used in a somewhat different meaning as compared to the first Part of the thesis where it denoted the zeroth order approximation to a slow manifold to which the flow is confined due to an infinite time scale separation between the fast and slow processes (see Section 2.2). Here and in the following, we shall use the term ‘quasi-stationary manifold’ in the sense that the flow of the 3-dimensional ODE system (7.1) is only confined to the neighborhood of the quasi-stationary manifolds. For example, to the left of the saddle-node bifurcation (SNP),  $\mathcal{L}$  is the only attracting set. Consequently, a trajectory would evolve close to  $\mathcal{L}$  in an oscillatory or straight manner depending whether the eigenvalues along  $\mathcal{L}$  are complex or real, respectively. Similarly, between the subcritical Hopf (SH) and the saddle-node bifurcation ( $\text{SN}_1$ ), the cylinder-like manifold  $\mathcal{C}$  is the only attracting set such that in this region of the phase space a trajectory would perform large amplitude oscillations in the neighborhood of  $\mathcal{C}$ .

## 7.2. A classification scheme for bursting behavior

We have explained how the qualitative behavior of the 3-dimensional flow (7.1) can be understood in terms of the invariant sets of the fast  $x$ - $y$  subsystem and their bifurcations leading to different attracting states in the corresponding regions of the phase space. Note, however, that the dynamics of a particular trajectory is essentially determined by the third equation in (7.1) which describes the slow dynamics of the quasi-static bifurcation parameter.

A systematic approach to classify the bursting behavior of systems exhibiting a slow-fast structure has been developed by Izhikevich [24]. By taking into account all possible combinations of codimension one bifurcations that may occur in the fast subsystem, different bursting mechanisms are distinguished by the kind of bifurcations that lead to the bursting behavior. According to this classification scheme, the hemin system, as it is shown in Fig. 7.1, is a subHopf/fold-cycle burster, since the two bifurcations, SH and

## 7. *Slow-Fast Analysis – The Method*

SNP, essentially determine the bursting behavior of this system (cf. Chapter 8).

## 8. The Slow-Fast Structure of the Hemin System

This Chapter is devoted to a detailed study of the slow-fast structure of the hemin system by which the origin of its bursting as well as its quasi-periodic behavior will be elucidated. The basis for the slow-fast analysis will be the 3-dimensional hemin system in the representation of (6.4) that has been introduced in Section 6.1 using  $(x, y, p)$  coordinates. In this coordinate system, the slow-fast structure of the hemin system becomes manifest since  $p$  evolves on a slower time scale than the 2-dimensional  $x$ - $y$  subsystem. Furthermore, numerical simulations have shown that the bursting oscillations ‘unfold’ along the  $p$  direction (cf. Fig. 6.2b) indicating that the  $(x, y, p)$  coordinate system is especially suited for a slow-fast analysis. Notice that while in the hemin system, the slow variable is simply given by the linear combination  $p = y + z$ , it may be difficult to find such a suitable variable in general.

The slow-fast analysis is performed by treating the slow variable  $p$  as a (quasi-static) bifurcation parameter for the 2-dimensional fast subsystem

$$\begin{aligned}\dot{x} &= k_0 x_2^0 - x \left\{ k_0 + k_1 s(x, y) + \left( k_2 + k_3 (c - x - y + s(x, y)) \right) \right\} (x_1^0 - x_2^0 + x - s(x, y)) \\ \dot{y} &= -(k_6 + k_0)y + k_7(p - y)(c - x - y + s(x, y))\end{aligned}\quad (8.1)$$

which is simply obtained by omitting the third equation in the 3-dimensional hemin system (6.4)

$$\dot{p} = -(k_0 + k_8)p - k_8 y + k_0 x_5^0 \quad (8.2)$$

that describes the slow  $p$  dynamics since both,  $k_0$  and  $k_8$ , vary on the scale  $10^{-4} s^{-1}$ .

In the following, we will analyze the bifurcation structure of the ODE system (8.1) in two steps: In Section 8.1, we fix the flow rate  $k_0$  at an arbitrary value and describe the bifurcations in the fast subsystem (8.1) leading to the bursting oscillations at this particular value of  $k_0$ . Depending on the current value of the slow variable  $p$ , we will find different attracting states in the fast subsystem. These states extend to quasi-stationary manifolds along the  $p$  direction and confine the trajectories of the full 3-dimensional system (6.4) to their neighborhood.

In Section 8.2, we investigate how the quasi-stationary manifolds that exist at a particular value of  $k_0$  change in dependence on  $k_0$ . Therefore,  $k_0$  may be regarded as an external bifurcation parameter for the 2-dimensional subsystem (8.1). To the contrary, the actual value of the slow variable  $p$  can not be prescribed arbitrarily. Instead it evolves dynamically – although within a narrow range of values – according to equation (8.2) and thus,  $p$  can be called an internal bifurcation parameter.

## 8. The Slow-Fast Structure of the Hemin System

Note that the truncated ODE system (8.1) no longer depends on the hemin decay rate  $k_8$  which was used as a second bifurcation parameter in the two-parameter bifurcation diagram in Fig. 4.1. Thus, for each fixed value of the external bifurcation parameter  $k_0$ , we obtain certain quasi-stationary manifolds in the 3-dimensional system that exist independently of  $k_8$ . However,  $k_8$  determines (together with  $k_0$ ) the slow dynamics of the  $p$  variable according to equation (8.2) and consequently, it influences the dynamics of the trajectories of the full 3-dimensional system.

The last Section is devoted to a detailed study of the torus solution that has been encountered close to the subcritical Hopf bifurcation in Fig. 4.2. We show that the rather unusual phase flow along the torus is a result of the slow-fast structure of the hemin system which can be analyzed in the same way as the bursting oscillations.

### 8.1. Slow-fast analysis at a fixed value of $k_0$

In the following, we analyze the codimension one bifurcations of the fast subsystem (8.1) at a fixed value of the flow rate  $k_0$  which we arbitrarily chose as 2.8. At this particular value of the flow rate, we will find that the bifurcation structure of the fast subsystem (8.1) is similar to the one described in Section 7.1 where we used a cartoon of the hemin system to illustrate its slow-fast structure.

Figure 8.1a shows the bifurcation diagram of the fast subsystem where  $p$  has been used as a bifurcation parameter whose range has been limited due to minimum and maximum values obtained from prior numerical simulations. Stationary states are plotted as thin lines while the maxima and minima of the oscillatory states are plotted as bold lines. The stability of the states is indicated by color and line style: black solid lines denote stable states while red dashed lines encode unstable states.

There are two branches of stable stationary states in the fast subsystem, one at  $y \sim 2.07$  and the other at  $y$  close to 1. Both of these branches become unstable via subcritical Hopf bifurcations ( $\text{SH}_1$  and  $\text{SH}_2$ ) while the stable oscillations emerge via saddle-node bifurcations ( $\text{SNP}_1$  and  $\text{SNP}_2$ ) where a stable limit cycle merges with an unstable one.

The dashed rectangular region in Fig. 8.1a is magnified in Fig. 8.1b. It shows the bifurcations in the fast subsystem together with the  $4^{19}$  bursting state (blue) at  $k_8 = 2.5$  which is confined to the region in phase space where the subcritical Hopf  $\text{SH}_1$  and the saddle-node bifurcation  $\text{SNP}_1$  occur in the fast subsystem. Notice that in this region of the phase space the bifurcation structure is exactly the same as in Fig. 7.1.

The dotted line  $\dot{p} = 0$  denotes the nullcline of (8.2), i.e. it indicates in which region of the phase space the trajectory (blue line) moves to the left ( $\dot{p} < 0$ , below the nullcline) and to the right ( $\dot{p} > 0$ , above the nullcline). Note that the orbit is always confined to the neighborhood of the invariant sets of the fast subsystem. At the present value of  $k_8 = 2.5$ , it makes 4 loops close to the cylinder-like manifold (bold black solid line) before it ‘jumps’ to the line-like manifold (black thin line) where it performs 19 small oscillations. This can be seen in Fig. 8.1c which shows a magnification of the dashed rectangular region in Fig. 8.1b. In general, a  $L^S$  state wraps  $L$  times around the cylinder-like manifold and oscillates  $S$  times along the line-like manifold. In Fig. 8.1d a 3-dimensional view of the

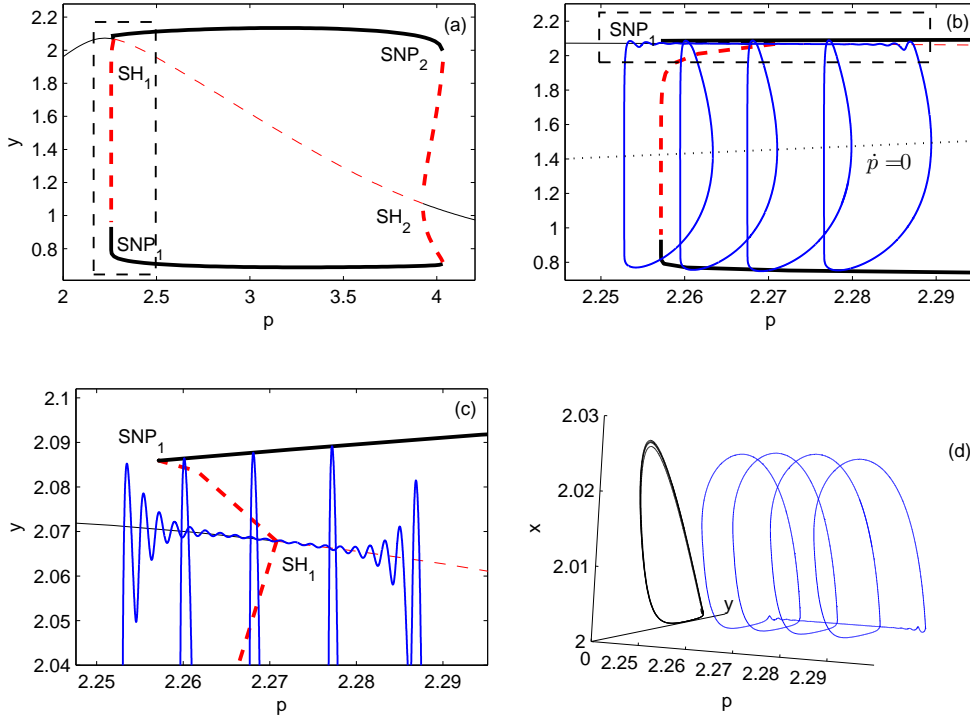


Figure 8.1.: Slow-fast analysis at a fixed value of the flow rate  $k_0 = 2.8$ : The bifurcation diagram of the fast subsystem (8.1) (a). The dashed rectangular region is magnified in (b) together with the trajectory (blue line) of a  $4^{19}$  state at  $k_8 = 2.5$ . The dashed rectangular region in (b) is magnified in (c). In (d) a 3-dimensional view of the  $4^{19}$  state is shown together with a projection onto the  $x$ - $y$  plane. Solid and dashed bold lines denote maxima and minima of a stable (black) and an unstable (red) limit cycle while solid and dashed thin lines denote stable (black) and unstable (red) fixed points of the fast subsystem.

$4^{19}$  state in the  $(x, y, p)$  coordinate system is visualized together with a projection onto the  $x$ - $y$  plane which again demonstrates the unfolding of the bursting state along the  $p$  direction.

In order to clarify how the bifurcations in the fast subsystem lead to the emergence and disappearance of the bursting oscillations, we describe one revolution of the trajectory in detail: To the left of the  $\text{SNP}_1$  point in Figs. 8.1(b,c) the line-like quasi-stationary manifold is the only attractor. Since it is entirely composed of stable stationary states of the fast subsystem (8.1) which are foci, the trajectory performs damped oscillations along this manifold (Fig. 8.1c). Subsequent to the subcritical Hopf point  $\text{SH}_1$ , the foci change stability and hence, the quasi-stationary manifold becomes unstable. Accord-

ingly, the amplitude of the oscillations increases again while the trajectory gets more and more attracted by the invariant cylinder-like manifold that is composed of stable limit cycle solutions of the fast subsystem. In the following the trajectory wraps around the cylinder-like manifold while it performs large amplitude oscillations. During that period, it spends some time above and some time below the plane defined by the nullcline  $\dot{p} = 0$  (Fig. 8.1b). In total, however, there is an effective movement of the trajectory towards lower  $p$  values until it passes the saddle-node bifurcation point  $\text{SNP}_1$  where the trajectory jumps back to the line-like quasi-stationary manifold to complete one cycle. The reason for the net movement towards lower  $p$  values is the slowing down effect that the line-like quasi-stationary manifold exerts on the part of the trajectory above the nullcline plane. In other words, the trajectory ‘feels’ the presence of the stationary points of the fast subsystem.

According to the classification of bursting mechanisms given in [24] (cf. Sec. 7.2), the hemin system is a subHopf/fold-cycle burster at  $k_0 = 2.8$  since the large amplitude oscillations terminate by a fold-cycle bifurcation ( $\text{SNP}_1$ ) while the small oscillations disappear via a subcritical Hopf bifurcation ( $\text{SH}_1$ ). As we shall show in the next Section, there is a transition in the bursting behavior at higher values of the flow rate  $k_0$ .

## 8.2. Two-parameter continuation in $p$ and $k_0$

So far we have analyzed the bifurcations in the fast subsystem (8.1) at one particular value of the external bifurcation parameter, namely at  $k_0 = 2.8$ . Now we investigate how the quasi-stationary states of the fast subsystem change as  $k_0$  is varied. To this purpose, we again proceed in two steps: First, we monitor the deformation of the line-like quasi-stationary manifold corresponding to the branch of stationary solutions of the fast subsystem. In the second step, we also include the oscillatory states and present a complete two-parameter bifurcation diagram of the fast subsystem using the slow variable  $p$  and the flow rate  $k_0$  as parameters.

Figure 8.2 shows how the line-like quasi-stationary manifold (blue lines) deforms as the flow rate  $k_0$  is increased from the value 2.8 (I) used in Section 8.1 via  $k_0 = 3.6$  (II) to  $k_0 = 3.8$  (III). Along these curves, we find certain codimension one bifurcations which are connected by curves obtained from a two-parameter continuation using  $p$  and  $k_0$  as parameters. For example, the curve I intersects the branches  $\text{SH}_1$  and  $\text{SH}_2$  (dashed red lines) in two points where subcritical Hopf bifurcations occur. These Hopf bifurcations are the same as those in Fig. 8.1a.

At a higher value of the flow rate ( $k_0 = 3.495$ ) there is a Bogdanov-Takens bifurcation (BT) occurring in the fast subsystem where the second branch of subcritical Hopf bifurcations  $\text{SH}_2$  terminates. As a consequence, the other two branches of stationary states (II and III) still intersect the first subcritical Hopf bifurcation curve  $\text{SH}_1$ , but no longer  $\text{SH}_2$ . Instead, the two branches II and III cross the two saddle-node bifurcation curves  $\text{SN}_1$  and  $\text{SN}_2$  that emerge at CP from a cusp singularity. Note that the location of the first saddle-node bifurcation  $\text{SN}_1$  moves towards lower  $p$  values as the flow rate  $k_0$  increases which may lead to interactions of  $\text{SN}_1$  with the oscillatory states generated in

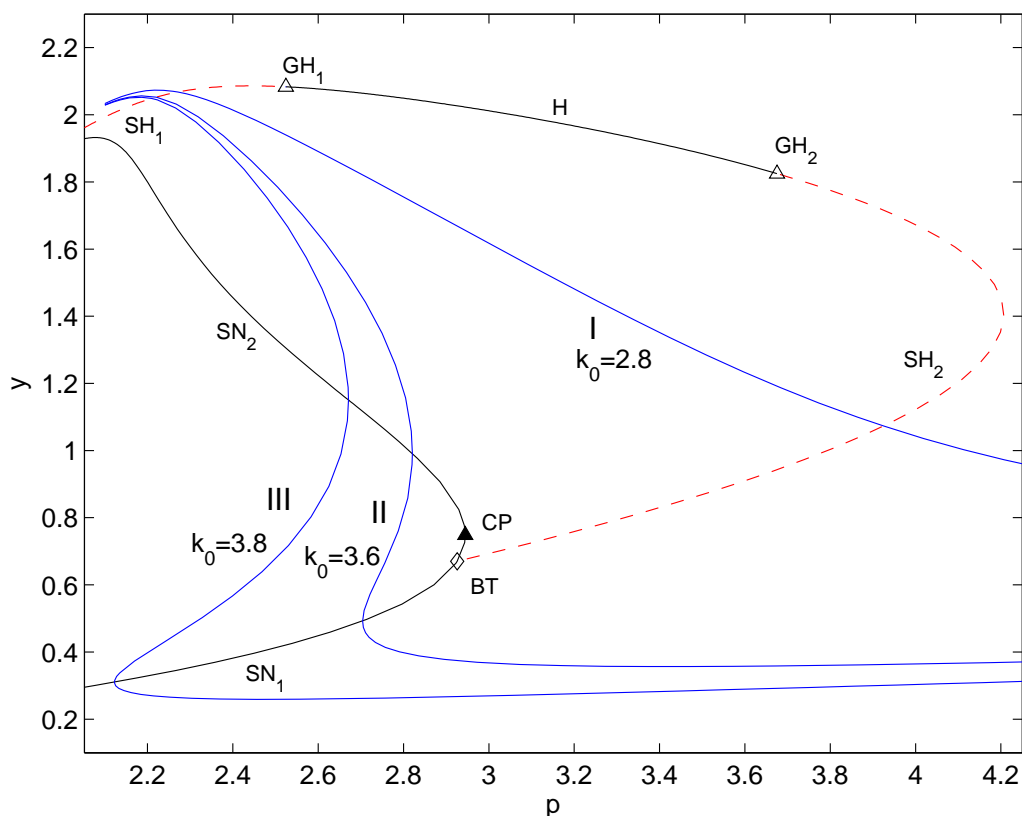


Figure 8.2.: The curves I, II, III show how the branch of stationary states (blue lines) of the fast subsystem (8.1) changes as the flow rate  $k_0$  is increased from 2.8 to 3.6 and 3.8. The codimension one bifurcations occurring along the curves I, II, III are found at the intersection points of these curves with the two-parameter continuation curves  $SH_i$  and  $SN_i$ . Symbols denote:  $SH_i$  - curves of subcritical Hopf bifurcations (dashed, red),  $H$  - curve of supercritical Hopf bifurcations (solid, black),  $SN_i$  - curves of saddle-node bifurcations of fixed points (solid, black), codimension two points:  $GH_i$  - generalized Hopf bifurcations (open triangle), BT - Bogdanov-Takens (diamond), CP - cusp (filled triangle).

the subcritical Hopf bifurcation  $SH_1$ , but which have been omitted in Fig. 8.2 for clarity.

The complete two-parameter bifurcation structure of the fast subsystem including the oscillatory states is summarized in Fig. 8.3 where  $p$  and  $k_0$  were used as parameters. The bifurcation lines  $SH_1$ ,  $SN_1$ , etc. are the same as those in Fig. 8.2. In addition, a branch of saddle-node bifurcations of periodic orbits ( $SNP_1$ ) is shown which bifurcates from the generalized Hopf bifurcation point  $GH_1$  (cf. inset Fig. 8.3a). This codimension

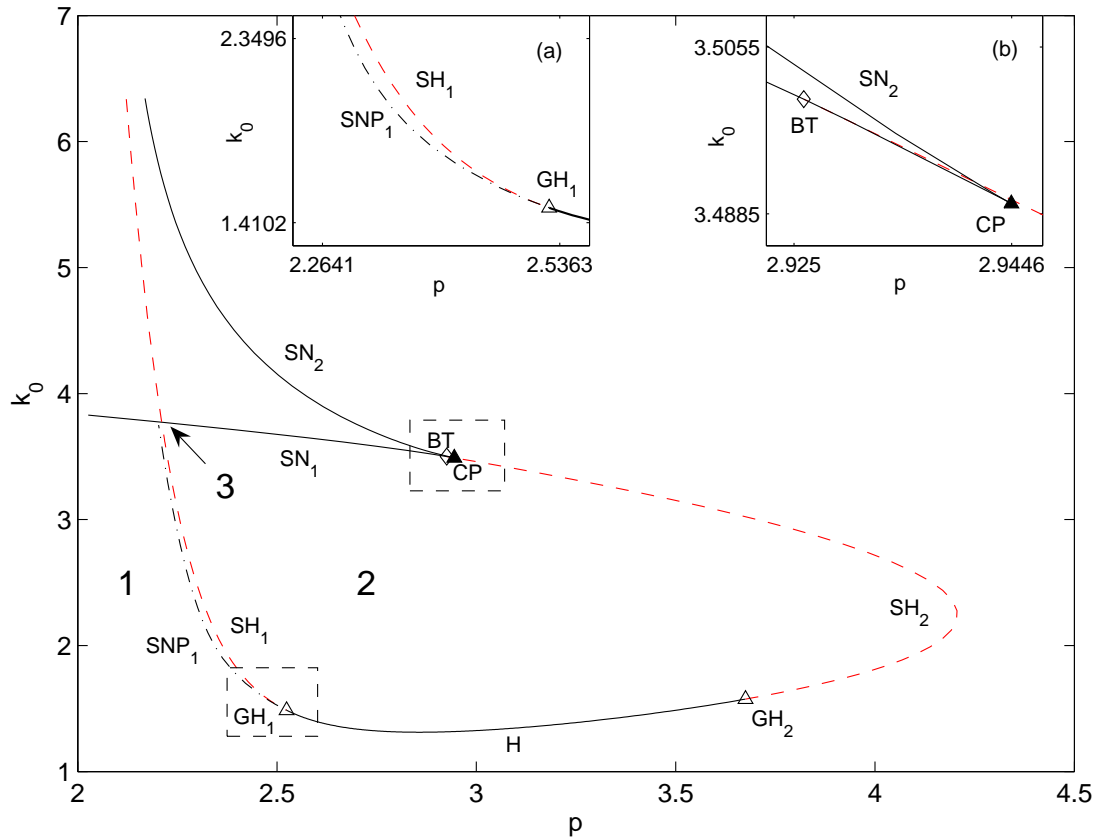


Figure 8.3.: Two-parameter bifurcation diagram of the fast subsystem(8.1) using the slow variable  $p$  and the flow rate  $k_0$  as parameters. If  $p$  sweeps back and forth between region 1 and 2 crossing the  $SNP_1$  curve, the dynamics of the whole system exhibits bursting behavior. In the neighborhood of the intersection point 3 a transition in the bursting mechanism occurs (see text and Fig. 8.4 for details). Symbols denote:  $SH_i$  - curves of subcritical Hopf bifurcations (dashed red),  $H$  - curve of supercritical Hopf bifurcations (solid),  $SN_i$  - curves of saddle-node bifurcations of fixed points (solid),  $SNP_1$  - curve of saddle-node bifurcations of periodic orbits (dash-dot), codimension two points:  $GH_i$  - generalized Hopf bifurcations (open triangle),  $BT$  - Bogdanov-Takens (diamond),  $CP$  - cusp (filled triangle).

two bifurcation point separates two branches of Hopf bifurcations, a supercritical ( $H$ , solid black line) and a subcritical one ( $SH_1$ , dashed red line). The second inset Fig. 8.3b shows a magnification of the region close to the cusp bifurcation point  $CP$  where the two branches of saddle-node bifurcations originate.

In the two-parameter bifurcation diagram Fig. 8.3, one can identify the invariant sets

of the fast subsystem at a given value of the slow variable  $p$  which, in turn, determine the potential dynamical properties of the system. For example, region 1 corresponds to the upper stationary state at  $y \sim 2.07$  while in region 2 we find the cylinder-like manifold that is composed of stable limit cycle solutions. In addition, there is a small bistable region bounded by the two curves  $\text{SNP}_1$  and  $\text{SH}_1$  where a limit cycle coexists with a stationary state (cf. Fig. 8.1c). Thus, we deduce that whenever the slow  $p$  dynamics is such that  $p$  sweeps back and forth between region 1 and 2 in phase space while crossing the  $\text{SNP}_1$  curve, the hemin system exhibits bursting behavior as described in Section 8.1.

### 8.2.1. A transition in the bursting behavior

The two-parameter bifurcation diagram shown in Fig. 8.3 can also be used to identify transitions in the bursting behavior of the hemin system. To this purpose, consider the intersection point  $(p, k_0) = (2.211, 3.773)$  marked as 3. Here, the subcritical Hopf bifurcation  $\text{SH}_1$  and the saddle-node bifurcation  $\text{SN}_1$  occur at the same value of  $p$  in phase space. Thus, it becomes possible that in a neighborhood of the intersection point the (unstable) oscillatory states emanating from the subcritical Hopf bifurcation may interact with the branch of (unstable) states that originate in the saddle-node bifurcation. In order to show that this truly leads to a transition in the bursting behavior of the hemin system, we compare the bifurcation diagrams of the fast subsystem for two neighboring values of the flow rate  $k_0$ .

Figure 8.4 shows the codimension one bifurcation diagrams of the fast subsystem for  $k_0 = 3.6$  (Fig. 8.4a) and  $k_0 = 3.8$  (Fig. 8.4c), respectively. Again, the trajectories (blue lines, calculated for  $k_8 = 2.5$ ) are superimposed on the bifurcation diagrams. The waveform of the oscillations is displayed in the corresponding time series (Figs. 8.4(b,d)). The branches of stationary states (thin lines) in Figs. 8.4(a,c) are the same as the curves II and III in Fig. 8.2, but now they are supplemented by the oscillatory states (bold lines) arising from the subcritical Hopf bifurcation  $\text{SH}_1$ . At  $k_0 = 3.6$ , the finite cylinder-like manifold is bounded by the saddle-node bifurcation  $\text{SNP}_1$  at the left side and the saddle-node homoclinic orbit  $\text{SNHC}$  at the right side (at  $p \sim 2.7$ ) where the saddle-node bifurcation  $\text{SN}_1$  occurs on the large amplitude limit cycle.

As the flow rate  $k_0$  increases from 3.6 to 3.8, the saddle-node homoclinic orbit moves together with the two saddle-node bifurcation points  $\text{SN}_1$  and  $\text{SN}_2$  towards lower  $p$  values until the first of them ( $\text{SN}_1$ ) collides with the unstable limit cycle (bold dashed red line) at approximately  $k_0 \sim 3.778$  (not shown), i.e. slightly above the intersection point 3 of Fig. 8.3. Subsequent to this bifurcation, the saddle-node homoclinic orbit has turned into a saddle homoclinic orbit (SHC) (cf. Appendix A.5 for the difference between the two types of homoclinic orbits) while the saddle-node bifurcation  $\text{SNP}_1$  has disappeared (Fig. 8.4c). Thus, the cylinder-like manifold (Fig. 8.4a, bold black solid lines) does not appear anymore for  $k_0 > 3.778$  and the fast subsystem becomes bistable. Henceforth, the bursting behavior of the hemin system is of fold/subHopf type since the upper stationary state disappears via the subcritical Hopf bifurcation  $\text{SH}_1$  while the lower stationary state undergoes a fold bifurcation at  $\text{SN}_1$ . A typical trajectory basically jumps back and forth between the two quasi-stationary states (Fig. 8.4c) causing the

## 8. *The Slow-Fast Structure of the Hemin System*

strong relaxational character of the oscillations (Fig. 8.4d).

## 8.3. The origin of quasi-periodic behavior in the hemin system

In the preceding Sections, we have shown that the origin of the bursting behavior of the hemin system may be well understood in terms of the invariant states of the fast subsystem (8.1) which the trajectories closely follow during their temporal evolution. It is the goal of the following investigation to show that the quasi-periodic behavior of the hemin system has a similar origin that can be equally analyzed by a slow-fast analysis.

To this purpose, we investigate the phase flow on the 2-torus that has been observed close to the subcritical Hopf bifurcation in Fig. 4.2 (cf. Sec. 4.2). Figure 8.5 again shows the inset of Fig. 4.2 where the Neimark-Sacker bifurcation NS appears in conjunction with the saddle-node bifurcation SNP and the subcritical Hopf bifurcation SH. By analyzing the slow-fast structure of the hemin system (6.4) in the vicinity of the Neimark-Sacker bifurcation point, we shall show that the rather unusual phase flow on the torus is a result of the finite time scale separation in the hemin system.

### 8.3.1. A torus with unusual phase flow

Figure 8.6 shows how the torus deforms as the flow rate  $k_0$  is decreased. In the projections on the  $p$ - $y$  plane (Figs. 8.6(a,b)), the numerical integration was stopped before the trajectory made a full revolution on the torus in order to reveal a portion of the flow along the ‘inner part’ of the torus. We observe a sharp transition from a smooth torus shown in Fig. 8.6a at  $k_0 = 1.65189$  close to the Neimark-Sacker bifurcation point in Fig. 8.5 to a highly distorted one at  $k_0 = 1.65180$  (Fig. 8.6b). The arrows indicate the direction of phase flow along the torus.

The saddle point  $S$  that emerges after the subcritical Hopf bifurcation SH (corresponding to the dashed line in Fig. 8.5) acts as an organizing center for the torus as can be seen in Fig. 8.6b: The flow approaches the ‘outer part’ of the torus along the 2-dimensional unstable manifold of the saddle point. Then it moves to the left (i.e. towards lower  $p$  values) until it changes direction and returns along the 1-dimensional stable manifold of the saddle. The reason for the trajectory to change its direction can be grasped from the slow-fast analysis of (6.4) and will be given below.

The phase flow on the 2-torus can be described as follows: If we consider a 2-torus as a direct product of two circles with a different radius (Fig. 8.7), then the angular velocity  $\omega_L$  along the circle with the larger radius is much higher than that of the circle with the smaller radius (Fig. 8.7a). However, close to the onset of quasi-periodic behavior, the opposite situation  $\omega_S > \omega_L$  is usually encountered [9] (Fig. 8.7b). In other words, the ‘unusual’ phase flow in Fig. 8.6 is a result of the time scale separation in the ODE system (6.4) since the trajectory moves much faster in the  $x$ - $y$  directions than along the  $p$  direction.

As the flow rate  $k_0$  is further decreased, the overall shape of the torus in Fig. 8.6b does not change significantly anymore. However, the time spent by the trajectory along the stable manifold of the saddle point  $S$  gradually increases until the torus and the saddle

point have eventually disappeared to the left of the subcritical Hopf point (SH) where only a stable fixed point exists (cf. Fig. 8.5).

### 8.3.2. Slow-fast analysis of the phase flow on the torus

Figure 8.8 shows the same projections of the phase flow on the torus as Figs. 8.6(a,c), but this time the bifurcation diagrams of the fast subsystem (8.1) are superimposed. The arrows indicate the direction of the flow on the torus while  $\text{SNP}_1$  and  $\text{SH}_1$  mark the locations where a saddle-node bifurcation of periodic orbits and a subcritical Hopf bifurcation occur in the fast subsystem. Thus, the bifurcation scenario in the fast subsystem is similar to that shown in Fig. 8.1 where we have analyzed the bursting oscillations at  $k_0 = 2.8$ .

Notice how the flow closely follows the quasi-stationary states of the fast subsystem. For example, at  $k_0 = 1.65189$ , the trajectory (blue line) basically sweeps back and forth the saddle-node bifurcation point  $\text{SNP}_1$  while it performs large amplitude oscillations in the vicinity of the cylinder-like manifold (bold black line), thereby creating quasi-periodic behavior (Fig. 8.8a). As long as the amplitude of the oscillations along the ‘inner part’ of the cylinder-like manifold is sufficiently large, the trajectory does not ‘feel’ the attractive line-like quasi-stationary manifold (thin black line) and therefore, remains in the neighborhood of the cylinder-like manifold.

However, as the flow rate  $k_0$  is decreased, the flow on the torus changes (Fig. 8.8b): As soon as the saddle-node point  $\text{SNP}_1$  is passed to the left, the trajectory is attracted by the line-like quasi-stationary manifold. Thus, it is the saddle-node point that causes the trajectory to change its direction. Then the orbit returns to the saddle point S along the stable manifold of S which, apparently, is confined to a neighborhood of the line-like quasi-stationary manifold. Subsequently, the trajectory moves along the 2-dimensional unstable manifold of the saddle point S to approach the cylinder-like manifold where it performs large amplitude oscillations while slowly moving to the left until the saddle-node point  $\text{SNP}_1$  is passed again and the next revolution begins.

The results shown in Fig. 8.8 suggest that the quasi-periodic behavior in the hemin system is caused by the particular constellation of the saddle-node ( $\text{SNP}_1$ ) and the subcritical Hopf bifurcation ( $\text{SH}_1$ ) occurring in the fast subsystem (8.1). Indeed, the two-parameter bifurcation diagram Fig. 8.3 shows that the fast subsystem is close to a Bautin bifurcation (cf. Appendix A.4) in Fig. 8.8. Since the curve of subcritical Hopf bifurcations  $\text{SH}_1$  always remains in the neighborhood of the curve of saddle-node bifurcations  $\text{SNP}_1$ , the two bifurcations always occur in the same region of phase space and thus, they may potentially trap a trajectory in the quasi-periodic way as described above for Fig. 8.8.

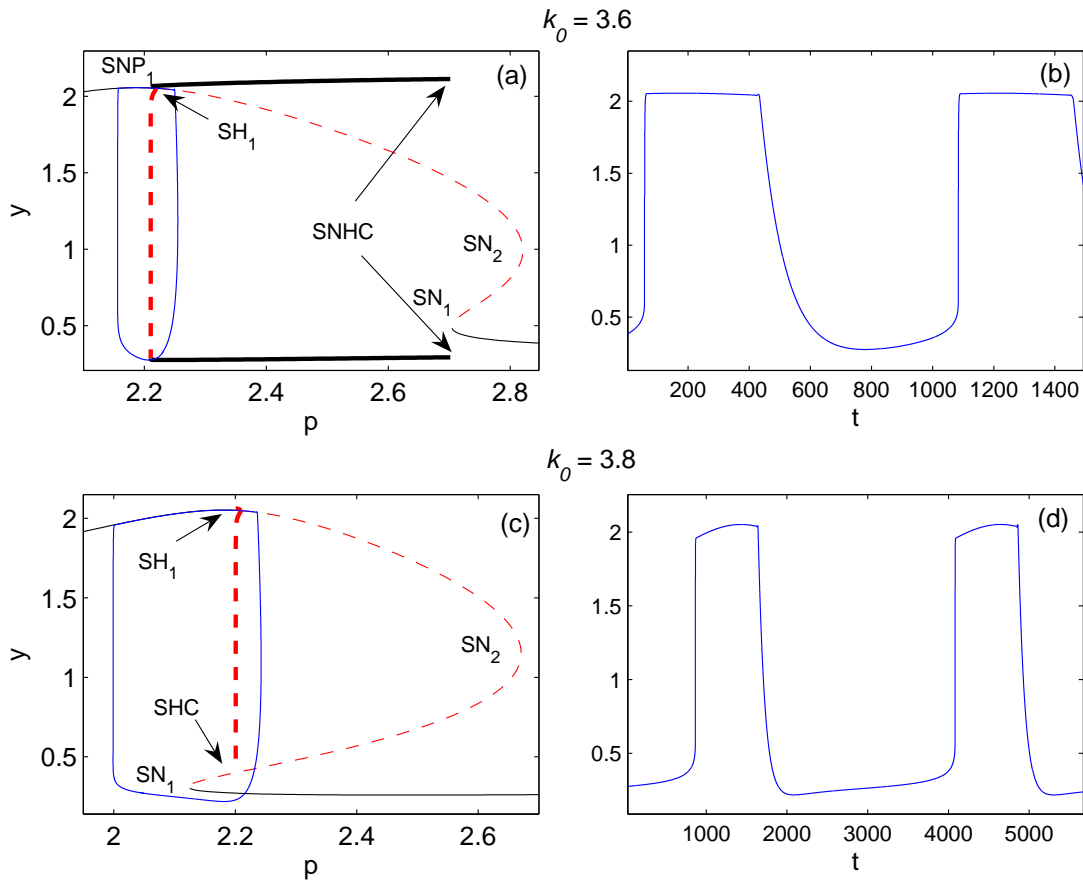


Figure 8.4.: Transition in the bursting behavior from subHopf/fold-cycle at  $k_0 = 3.6$  (a,b) to fold/subHopf type at  $k_0 = 3.8$  (c,d). (a),(c) show codimension one bifurcation diagrams of the fast subsystem together with trajectories (blue lines) calculated for  $k_8 = 2.5$  while (b),(d) depict the corresponding time series. As the flow rate  $k_0$  increases, the invariant cylinder-like manifold (formed by stable limit cycles of the fast subsystem) is destroyed as the location of the saddle-node bifurcation  $SN_1$  approaches the unstable limit cycle that is created in the subcritical Hopf bifurcation  $SH_1$  (a,c). Henceforth, the fast subsystem is bistable (c) and only relaxational oscillations are observed (d). Symbols denote:  $SH_1$  - subcritical Hopf bifurcation,  $SNP_1$  - saddle-node bifurcation of periodic orbits,  $SN_i$  - saddle-node bifurcation of fixed points,  $SHC$  - saddle homoclinic orbit,  $SNHC$  - saddle-node homoclinic orbit. Solid and dashed bold lines denote maxima and minima of a stable (black) and an unstable (red) limit cycle while solid and dashed thin lines denote stable (black) and unstable (red) fixed points of the fast subsystem, respectively.

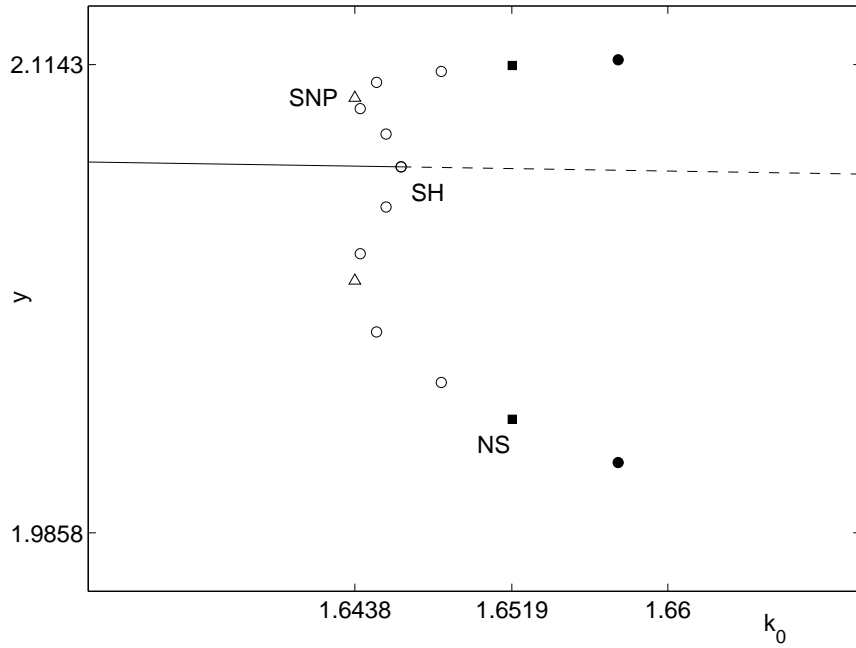


Figure 8.5.: Inset of Fig. 4.2: A torus solution bifurcates at  $k_0 = 1.6519$  from the Neimark-Sacker Point NS (black square) towards lower values of  $k_0$ . It exists in a narrow interval up to the subcritical Hopf bifurcation SH at  $k_0 = 1.6461$ . Other symbols denote: SNP (open triangle) - saddle-node bifurcation of periodic orbits, solid line - stable fixed point, dashed line - saddle point, open/black circle - unstable/stable limit cycle.

8.3. The origin of quasi-periodic behavior in the hemin system

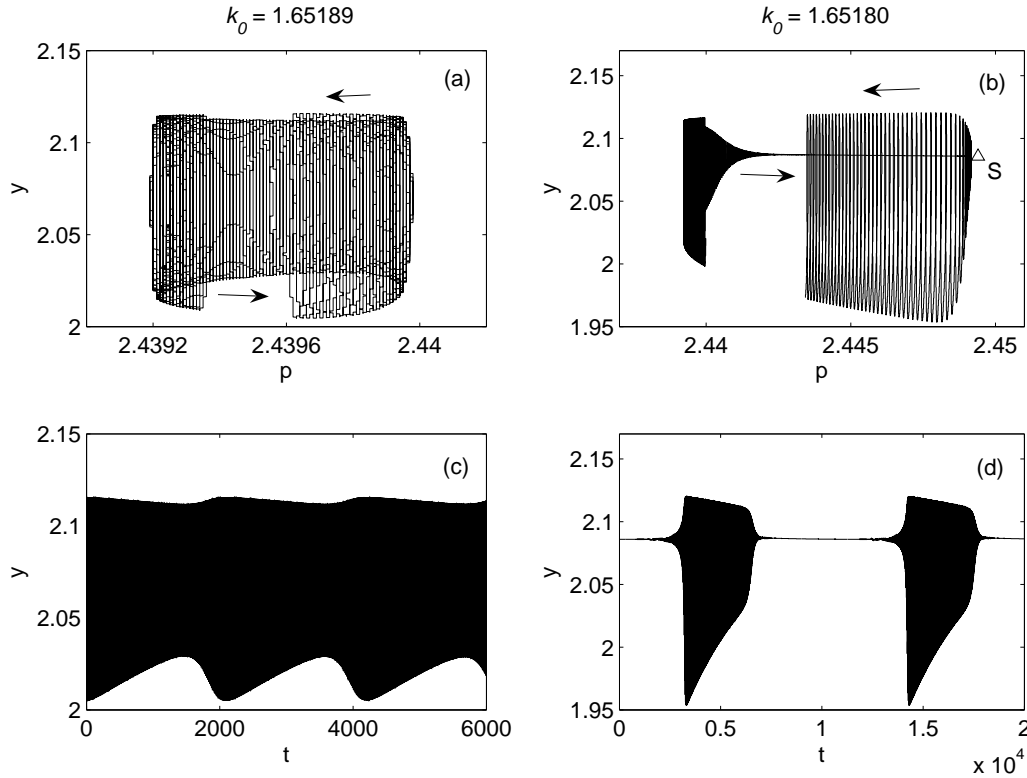


Figure 8.6.: Deformation of the 2-torus as the flow rate  $k_0$  is decreased: (a),(b) represent projections onto the  $p$ - $y$  plane while (c),(d) depict the corresponding time series. Close to the Neimark-Sacker point  $NS$  in Fig. 8.5, the torus looks smooth (a). At a slightly decreased value of the flow rate, the ‘inner part’ of the torus rapidly shrinks to a line-like manifold along which the trajectory approaches the stable manifold of the saddle point  $S$  (b).

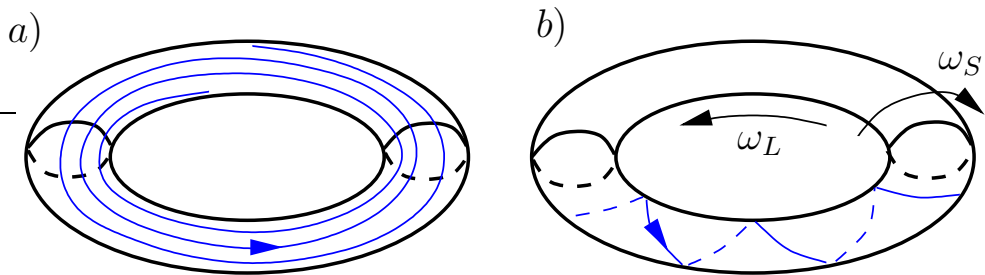


Figure 8.7.: Flow on a 2-torus with different ratios of angular velocities:  $\omega_L > \omega_S$  (‘unusual’) (a) and  $\omega_L < \omega_S$  (‘usual’) (b).

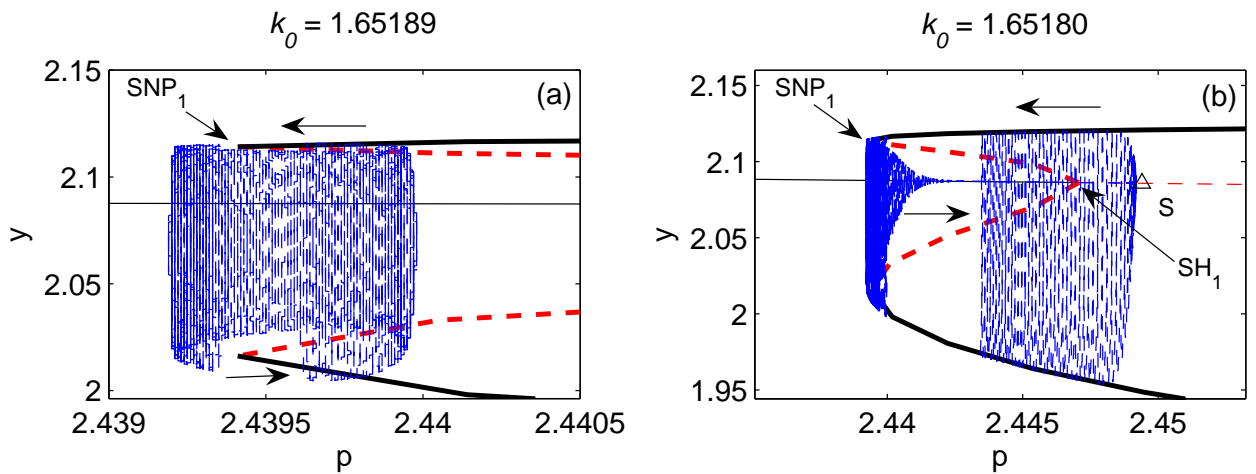


Figure 8.8.: Slow-fast analysis of the phase flow on the 2-torus close to the Neimark-Sacker bifurcation (a) and slightly below (b) (see text for details). The trajectories (blue) are superimposed on bifurcation diagrams of the fast subsystem (8.1). Invariant sets of the fast subsystem: Stable/unstable limit cycles are displayed in bold black/red lines while stable/unstable stationary states are drawn as thin black/red lines.

## 9. Summary and Discussion

In the second Part of the thesis, we have studied the bursting or mixed-mode oscillations in the 3-dimensional hemin system (6.4) where we have been particularly interested in the elucidation of the mechanism generating the bursting oscillations.

In Chapter 6, we showed that the bursting oscillations in the hemin system arise subsequent to the formation of a chaotic attractor that follows a period doubling cascade. This suggests that the bursting oscillations are not associated with phase-locked states on a 2-torus which is stable in another region of the parameter space. Instead, the MMOs come in periodic-chaotic sequences with different levels of organization. At the top level, the periodic windows are labeled by the number  $L$  of large amplitude oscillations which at the same time correspond to the levels of a Farey tree. Within each periodic window of fixed  $L$ , we observed pruned Farey sequences of  $L^S$  states with a different number  $S$  of small amplitude oscillations. Transitions between adjacent states  $L^S$  and  $L^{S+1}$  again occur via narrow chaotic windows where periodic concatenated states of the form  $L^S L^{S+1}$  are embedded. Similar bifurcation sequences were also observed by Hauser and Olsen [13] in the PO system and Koper [28] in a three variable model system.

The observation that mixed-mode states  $L^S$  of a gradually decreasing number  $L$  of large amplitude oscillations alternate with narrow chaotic windows together with the fact that a chaotic attractor was formed prior to the emergence of the first bursting state, suggests that the bursting oscillations might actually be embedded in a chaotic attractor similar to a scenario reported by Goryachev et. al. [31]. In this article it is argued that the mixed-mode states are embedded in a horseshoe-type attractor. The bifurcations of the MMOs are described on the basis of a detailed investigation of a suitable Poincaré map from which the transformation of the system's slow manifold into a horseshoe-type attractor could be derived as parameters are varied. During the transformation process, Poincaré maps are observed that are very similar to the one we calculated in Fig. 6.1c subsequent to the period doubling bifurcation. In particular, Goryachev et. al. also observe a tent map with almost cuspid tip (cf. Fig. 5e in [31]).

For the hemin system, however, it remains an open task to find a Poincaré section that is well-defined for the whole parameter range of  $k_0$  values, where the bursting oscillations are stable, which would facilitate to establish a closer link of the bursting dynamics in the hemin system to the mechanism proposed in [31].

In Chapter 7 we introduced the basics underlying a slow-fast analysis due to Rinzel and Ermentrout [23], and illustrated the slow-fast structure of the hemin system using the cartoon in Fig. 7.1. In addition, we mentioned a classification scheme for bursting mechanisms that has been elaborated by Izhikevich [24]. In this scheme, the bursting behavior is classified by the type of bifurcations that occur in the fast subsystem and lead to the bursting behavior.

## 9. Summary and Discussion

In Chapter 8, we decomposed the 3-dimensional ODE system (6.4) according to its slow-fast structure into the fast subsystem (8.1) and the slow dynamics for the quasi-static bifurcation parameter  $p$  (eq. 8.2). In the following, we analyzed the bifurcations occurring in the fast subsystem (8.1) in dependence on the slow variable  $p$ . In general, from such an analysis one can deduce the existence of quasi-stationary manifolds in phase space to whose neighborhood the trajectories of the ODE system (6.4) are confined and thus, one may arrive at a geometrical comprehension of the phase flow.

In a first step, we analyzed the slow-fast structure of the hemin system at a fixed value of the flow rate  $k_0$ . As a result, we found that certain codimension one bifurcations in the fast subsystem are responsible for the occurrence of bursting oscillations; in particular the constellation of the saddle-node bifurcation of periodic orbits  $\text{SNP}_1$  and the subcritical Hopf bifurcation  $\text{SH}_1$  turned out to be essential for the generation of the bursting oscillations (cf. Fig. 8.1). Accordingly, the bursting mechanism is of subHopf/fold-cycle type at the chosen parameter value for the flow rate and thus, it can be arranged into the classification scheme proposed by Izhikevich [24].

In a second step, we investigated how the stationary and oscillatory states of the fast subsystem change under variation of the flow rate  $k_0$ . To this purpose, we performed a systematic two-parameter continuation of the fast subsystem using the slow variable  $p$  and the flow rate  $k_0$  as parameters. From the resulting bifurcation diagram (Fig. 8.3), we identified a transition in the bursting behavior of the hemin system by which it becomes a fold/subHopf burster due to a change in the nature of the homoclinic orbit in the fast subsystem (Figs. 8.4(a,c)). At  $k_0 = 3.6$  (Fig. 8.4a), the fast subsystem has an orbit that is homoclinic to the nonhyperbolic equilibrium at  $p \sim 2.7$ . In contrast, at  $k_0 = 3.8$  (Fig. 8.4c), the saddle-node homoclinic orbit  $\text{SNHC}$  has turned into the saddle homoclinic orbit  $\text{SHC}$  which involves a hyperbolic equilibrium at  $p \sim 2.2$ .

The observation of a transition in the bursting behavior of the hemin system is a novel result at least from a theoretical point of view, since the slow-fast structure in other systems is, to our knowledge, mostly investigated at a particular parameter set in order to determine the type of bursting behavior according to the classification scheme of Izhikevich. However, such an approach prevents the detection of a transition in the bursting behavior although such a transition can be of physiological relevance.

Finally, we found that the same constellation of codimension one bifurcations of the fast subsystem ( $\text{SNP}_1$  in conjunction with  $\text{SH}_1$ ), that was already identified to allow for bursting oscillations, may equally account for quasi-periodic behavior in the hemin system, although in a different region of the parameter space. A detailed investigation of the phase flow on the 2-torus close to the Neimark-Sacker bifurcation in Fig. 8.5 revealed that the quasi-periodic behavior is due to the coupling of an oscillator in the fast subsystem (8.1) (which is represented by the stable limit cycle solution) with the  $p$  variable, but on a slow time scale. Indeed, a similar line of argument has been used by Koper [28] to explain the origin of quasi-periodicity in a different system although a slow-fast analysis has not been performed to support this statement. However, since tori with a phase flow similar to the one in Fig. 8.6 have been observed in several chemical systems [25, 26, 28], it is very likely that they share a common dynamical origin that can be analyzed by a suitable slow-fast analysis.

Part III.  
Appendix



# A. Dynamical Systems and Bifurcation Theory in a Nutshell

It is the aim of the present Chapter to provide the basic ideas and concepts underlying dynamical systems and bifurcation theory as they are necessary to understand the results in part I and II of this work. Therefore, it should be used as a reference. For convenience, the presentation will mostly be kept on an informal level.

We begin in Section A.1 with a brief introduction to the theory of finite dimensional dynamical systems where the basic notions and theorems are reviewed. In particular, the Hartman-Grobman and the stable manifold theorem will be presented as the basis for the local analysis of the nonlinear flow near fixed points and limit cycles.

Section A.2 is devoted to the foundations of bifurcation theory. Here we introduce the important notion of topological equivalence which defines an equivalence relation in the space of dynamical systems and thus, allows to compare the dynamical properties of two such systems. In addition, the center manifold theorem, parameter dependent dynamical systems and normal forms are discussed.

In Section A.3, we review the generic local bifurcations of fixed points and limit cycles, that can be observed as one parameter of a system is continuously varied. Section A.4 describes some of the generic local two-parameter bifurcations of fixed points that are frequently encountered in this work. We conclude this Chapter with Section A.5 where we briefly introduce two global bifurcations that involve a homoclinic orbit to a hyperbolic and a nonhyperbolic equilibrium, respectively.

Our presentation mainly follows the books of Guckenheimer & Holmes [9], Kuznetsov [76] and Jetschke [77] without particular reference.

## A.1. Dynamical systems

A (finite dimensional) dynamical system consists of a (finite dimensional) state space  $X$  and a one-parameter group of transformations  $(\varphi_t)_t$  on  $X$  where we have  $t \in \mathbb{R}$  for continuous-time and  $t \in \mathbb{Z}$  for discrete-time systems. For each  $t$ , the so-called flow map

$$\begin{aligned} \varphi_t : \quad X &\rightarrow X & (A.1) \\ x &\mapsto \varphi_t(x), \end{aligned}$$

is a diffeomorphism of the state space  $X$  transforming any initial state  $x$  into a final state  $\varphi_t(x) = \varphi(t, x)$  (cf. Fig. A.1a).

On the other hand, if we fix some initial point  $x_0 \in X$  then the map

$$\varphi(\cdot, x_0) : \mathbb{R} \rightarrow X \quad (A.2)$$

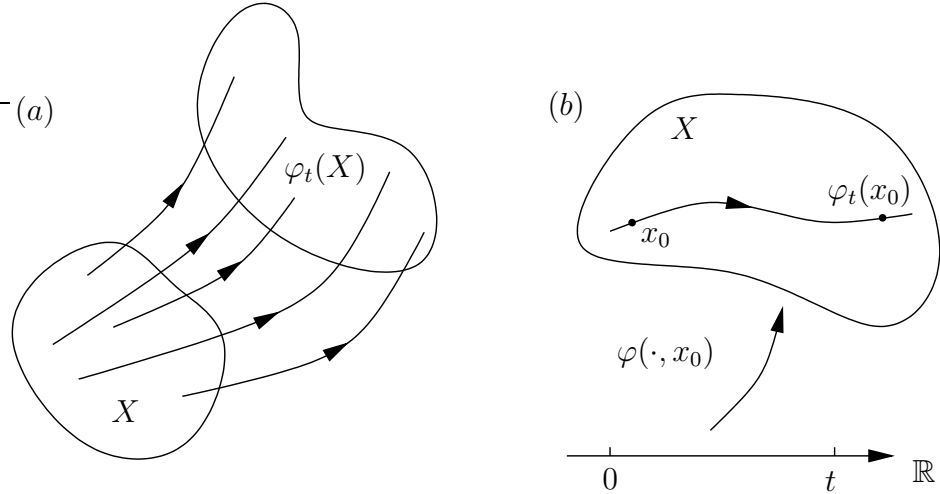


Figure A.1.: The flow of a dynamical system (a) and a particular trajectory passing through  $x_0$  (b).

describes a curve in  $X$ . The image  $\varphi(t, x_0)$  of the map in (A.2) is called orbit, solution curve or trajectory of the flow  $\varphi_t$  through the point  $x_0$  (Fig. A.1b). The flow satisfies the group properties:

$$\begin{aligned}\varphi_0 &= \text{id}_X \\ \varphi_t \circ \varphi_s &= \varphi_{t+s} = \varphi_s \circ \varphi_t,\end{aligned}$$

i.e. it yields an abelian action (in the group theoretical sense)  $\varphi_t : \mathbb{R}(\mathbb{Z}) \times X \rightarrow X$  of the real (integer) numbers on the phase space  $X$  defined by  $(t, x) \mapsto \varphi_t(x)$ .

In the following, we shall consider dynamical systems whose flow arises from a vector field in the sense that the flow satisfies for all  $x \in M \subseteq \mathbb{R}^n$  and all  $s$  out of an interval  $I = (a, b) \subseteq \mathbb{R}$ :

$$\frac{d}{dt}\varphi(t, x)|_{t=s} = f(\varphi(s, x)) \quad (\text{A.3})$$

where it is sufficient to think of a vector field as a map  $f : M \subset \mathbb{R}^n \rightarrow \mathbb{R}^n$ . If we use the  $n$ -dimensional Euclidean space  $\mathbb{R}^n$  equipped with coordinates  $x = (x_1, \dots, x_n)$  as the state space  $X$  and fix an initial condition  $\varphi(t, x_0)|_{t=0} = x(t, x_0)|_{t=0} = x_0$ , then (A.3) becomes a system of ordinary differential equations (ODE system):

$$\frac{d}{dt}x_i \equiv \dot{x}_i = f_i(x_1, \dots, x_n), \quad x_i(0) = (x_0)_i, \quad i = 1, \dots, n$$

or in short vector notation

$$\dot{x} = f(x), \quad x(0) = x_0. \quad (\text{A.4})$$

The (local) existence and uniqueness of a solution curve  $\varphi(\cdot, x_0) \equiv x(\cdot, x_0) : (a, b) \rightarrow M$  of the ODE system (A.4) is guaranteed provided  $f$  is, for example,  $C^1$ , i.e. once

differentiable and the derivative is continuous. However, exact solutions of the ODE system (A.4) can be found only if the components of the vector field are linear functions or  $f$  has certain continuous symmetries, i.e. it is equivariant with respect to a Lie group of transformations [78, 79]. Thus, the natural question arises: What can be said about the typical behavior of trajectories in the absence of such symmetries?

### A.1.1. The geometrical approach

In the qualitative theory of dynamical systems, a geometrical viewpoint is adopted where the properties of a dynamical system as a whole are more important than the fate of an individual trajectory. In particular, invariant manifolds are of paramount interest since they allow to classify the different types of long-time behavior that can be found in a dynamical system.

In the simplest case, a trajectory settles down to a stationary state which is associated with a singular point of the vector field  $f$ , i.e. it is a solution of the equation  $f(x) = 0$ . If the flow map satisfies  $\varphi_{t+T}(x) = \varphi_t(x)$  for some  $T \geq 0$  and for all  $t \geq 0$  and all  $x$  belonging to an orbit  $C$ , this orbit is called a limit cycle and corresponds to a periodic solution of the ODE system (A.4) with period  $T$ . These are the most simple examples of so-called invariant sets which represent the potential long-time behavior of a dynamical system. Thus, a good strategy for the investigation of any nonlinear dynamical system is to locate its invariant sets beginning with the fixed points and study subsequently the behavior of trajectories in the neighborhood of the invariant sets.

This approach is facilitated by the Hartman-Grobman and the stable manifold theorem for fixed points both of which come in two versions; one for continuous-time and one for discrete-time systems, i.e. iterated maps. They allow for a local reconstruction of the phase portrait (i.e. the collection of all orbits) near fixed points and limit cycles. In the case of a 2-dimensional system, the knowledge about the local behavior is often sufficient to reconstruct the global phase flow due to the topological restrictions in 2-dimensional space. In fact, fixed points and limit cycles are the only (generic) invariant sets for 2-dimensional continuous-time flows. To the contrary, in higher dimensional (continuous-time) systems, the long-time behavior of trajectories may become more complex and one usually relies on numerical simulations to obtain some global information about the corresponding phase flow. We remark that for discrete-time dynamical systems, there are no such topological restrictions and even 1-dimensional dynamical systems may become arbitrarily complex.

### A.1.2. Invariant sets, attractors, etc.

Before the main ideas of the Hartman-Grobman and the stable manifold theorem are discussed, we give some definitions of special sets in phase space that are relevant for the discussion of limiting behavior.

A subset  $S \subset \mathbb{R}^n$  is called *invariant* with respect to the flow  $\varphi_t$  if  $x \in S$  implies  $\varphi_t(x) \in S$  for all  $t$ . Fixed points and limit cycles are simple examples of invariant sets. A closed invariant set  $A \subset \mathbb{R}^n$  is called *attracting* if trajectories being in some

neighborhood  $U$  of  $A$  at  $t = 0$ , remain there for  $t \geq 0$  and approach the attracting set in the limit  $t \rightarrow \infty$ . The domain of attraction of the set  $A$  consists of all orbits reaching the neighborhood  $U$  of  $A$  in finite time, i.e.  $\cup_{t \leq 0} \varphi_t(U)$ .

An attractor is an attracting set containing a dense orbit. This requirement ensures that a typical trajectory belonging to the attractor comes arbitrary close to every point of the attractor. Fixed points and limit cycles show rather simple limiting behavior in the case that they are attracting. However, in higher dimensional systems ( $n \geq 3$ ), one may also find bounded regions in phase space containing complicatedly folded attracting sets that exhibit a ‘strange’ limiting behavior in the sense that nearby trajectories belonging to the attractor deviate (locally) exponentially fast from each other. The term ‘locally’ is important here since the attractor resides in a bounded region in phase space and therefore, two locally diverging trajectories may again come close together after some time. The ‘strong dependence on the initial conditions’ is a hallmark of chaotic behavior which basically prevents any long-time forecasts in real world chaotic systems where initial conditions are only known with finite accuracy. On the other hand, it is usually very difficult to ‘prove’ the existence of a chaotic attractor in a given dynamical system, in particular the existence of a dense orbit.

### A.1.3. Hartman-Grobman and stable manifold theorem

In order to state the Hartman-Grobman Theorem, we assume that at least one solution  $x^0$  of the fixed point equation

$$f(x) = 0 \tag{A.5}$$

has been found. Note that even this task is basically impossible for higher dimensional systems since (A.5) is a coupled nonlinear algebraic equation system.

Next, we study the temporal evolution of small deviations from the fixed point and set  $x(t) = x^0 + \xi(t)$ . If the deviations  $|\xi|$  are sufficiently small, one may linearize the ODE system (A.4) for the nonlinear flow around the fixed point  $x^0$  by truncating the higher order terms in  $|\xi|$ . As a result, the linear ODE system

$$\dot{\xi} = f_x(x^0)\xi, \quad \xi \in \mathbb{R}^n \tag{A.6}$$

is obtained which describes the temporal evolution of small deviations from the fixed point.

The flow map  $\varphi_t^L$  of the linearized equation (A.6) can be explicitly constructed in terms of the eigenvalues and the (generalized) eigenvectors of the (constant) Jacobian matrix  $f_x(x^0)$  whose entries are the first partial derivatives of the vector field evaluated at the fixed point, i.e.  $(f_x(x^0))_{ij} \equiv \frac{\partial f_i}{\partial x_j}|_{x=x^0}$ . A formal solution is just given by the matrix exponential  $\varphi_t^L = \exp t f_x(x^0)$  which is a one-parameter group of transformations mapping any initial state  $\xi_0$  to the final state  $\xi(t, \xi_0) = \varphi_t^L \xi_0$ . Thus, the linearized flow is globally defined for all  $\xi \in \mathbb{R}^n$  and all  $t \in \mathbb{R}$  which is not necessarily the case for the flow of the nonlinear ODE system (A.4) whose existence is only guaranteed locally and usually depends on the initial condition. The standard example is provided by the

solution  $x(t) = x_0/(1 - tx_0)$  of the ODE  $\dot{x} = x^2$  with initial condition  $x(0) = x_0$  whose positive time solutions are only defined up to time  $t = 1/x_0$ .

The question is now: What information about the local behavior of trajectories of the nonlinear flow close to the fixed point  $x^0$  can be obtained from the linearized equations (A.6)?

The answer is given by the Hartman-Grobman theorem which asserts that it is sufficient to study the linearized flow near the fixed point provided the Jacobian matrix  $f_x(x^0)$  has no eigenvalues with zero real part there, i.e.  $x^0$  is a hyperbolic fixed point. In this case, one can show that there is a continuous change of coordinates taking the orbits of the nonlinear flow to that of the linearized one while the sense of the orbits is preserved. This property states that the nonlinear and the linear flow are topologically equivalent; a notion that we shall return to in the next Section when bifurcation theory will be discussed. Topological equivalence is of paramount importance in the classification of dynamical systems since it is used to define its ‘generic’ properties.

The explicit solution of the linearized ODE system A.6 can be used to classify the type of fixed point according to the eigenvalue spectrum of the Jacobian matrix. If all eigenvalues have a negative real part, the fixed point is asymptotically stable, i.e. all sufficiently small perturbations decay in time and asymptotically approach the stationary state which, in this case, is called a *sink*. If the Jacobian matrix possesses at least one eigenvalue with positive real part, it is called a *saddle* which is unstable. In the case that all eigenvalues have a positive real part, the fixed point is called a *source*. This means that trajectories which start in the neighborhood of the source will diverge from it exponentially fast. Note, however, that the linear stability analysis does not answer questions of the type: What happens to the trajectory if it escaped the neighborhood of a saddle point or a source. In order to answer such questions, one has to include sufficient higher order terms in the Taylor expansion of the vector field in (A.6).

We now turn to the stable manifold theorem. Let  $\lambda_1, \dots, \lambda_s$  and  $\lambda_{s+1}, \dots, \lambda_n$  be the eigenvalues with negative and positive real part, respectively, and denote by  $E^s = \text{span}\{v_1, \dots, v_s\}$  and  $E^u = \text{span}\{v_{s+1}, \dots, v_n\}$  the stable and unstable eigenspaces that are spanned by the corresponding eigenvectors. The linear spaces  $E^s$  and  $E^u$  are subspaces of  $\mathbf{R}^n$  which are invariant under the linearized flow  $\varphi_t^L$ . Moreover, according to the stable manifold theorem, there exist local stable and unstable manifolds  $W_{loc}^s, W_{loc}^u$  in a neighborhood  $U(x^0)$  of the fixed point which are locally invariant under the nonlinear flow map  $\varphi_t$ . One can think of these manifolds as the nonlinear extensions of the linear stable and unstable subspaces  $E^s$  and  $E^u$ , to which they are tangent at  $x^0$  (Fig. A.2). Using the nonlinear flow map, the local invariant manifolds are defined as:

$$W_{loc}^s(x^0) = \{x \in U(x^0) | \varphi_t(x) \in U(x^0) \forall t \geq 0, \varphi_t(x) \rightarrow x^0 \text{ as } t \rightarrow \infty\} \quad (\text{A.7})$$

$$W_{loc}^u(x^0) = \{x \in U(x^0) | \varphi_t(x) \in U(x^0) \forall t \leq 0, \varphi_t(x) \rightarrow x^0 \text{ as } t \rightarrow -\infty\}.$$

Thus, the local stable (unstable) manifold consists of all trajectories that, once belonging to the neighborhood  $U(x^0)$  of the fixed point, remain there for all future (past) time and approach it as time tends to infinity (minus infinity).

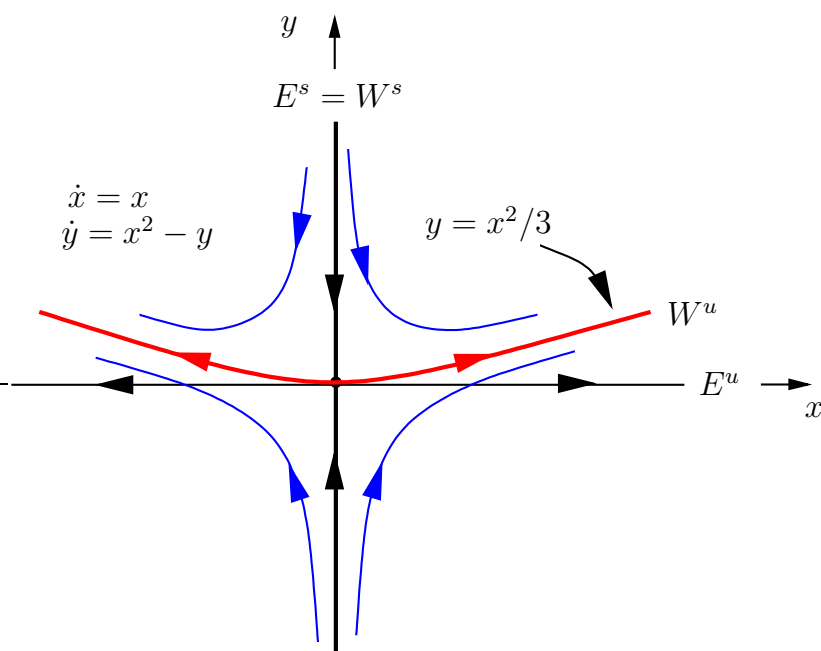


Figure A.2.: Stable (bold, black) and unstable manifolds (red) for a two-dimensional ODE system with fixed point  $(x^0, y^0) = (0, 0)$ .

By applying the nonlinear flow map backward (forward) in time to the local stable (unstable) manifold, one may define global stable and unstable manifolds (formally) as:

$$W^s(x^0) = \cup_{t \leq 0} \varphi_t(W_{loc}^s(x^0)), \quad W^u(x^0) = \cup_{t \geq 0} \varphi_t(W_{loc}^u(x^0)). \quad (\text{A.8})$$

Accordingly, the global stable (unstable) manifold consists of all points which (whose preimages) are mapped under the action of the nonlinear flow map to the local stable (unstable) manifold in finite time and thus, approach the fixed point as time tends to infinity (minus infinity). While the local manifolds can often be approximated by Taylor series, their global extensions can be computed explicitly only for very simple cases. However, the knowledge about their existence can facilitate the interpretation of numerical simulations.

#### A.1.4. Periodic orbits and Poincaré maps

Having analyzed the local phase flow near the singular points of the vector field  $f$ , the next step could be to find periodic solutions of the ODE system (A.4) and study the phase flow near those solutions. In the case of a continuous-time system, a periodic orbit is a closed invariant curve  $C$  composed of points  $x \in C$  all of which satisfy  $\varphi_{t+T}(x) = \varphi_t(x)$  for some  $T \geq 0$  and for all  $t \geq 0$ . The minimal  $T$  satisfying this condition is called the period of the orbit. As this definition shows, one actually needs an explicit representation of the nonlinear flow map in order to verify the periodicity condition. Thus, periodic solutions can, in general, be found only by numerical methods such as the continuation schemes discussed in Section B.1.

Nevertheless, much information of the local phase flow near a periodic orbit can be gained by a similar analysis to that of fixed points in Section A.1.3. To this purpose, one introduces the geometrical concept of a first return or Poincaré map (Fig.A.3) by taking a  $n - 1$  dimensional local cross section  $\Sigma \subset \mathbb{R}^n$  such that the periodic orbit as well as all nearby solution curves pierce the cross section transversally, i.e. the Euclidean scalar product  $(\nu(x), f(x)) \neq 0$  between the vector field  $f$  and the unit normal vector field  $\nu$  of the cross section vanishes nowhere on  $\Sigma$ . Denote the (unique) intersection point of the periodic orbit  $C$  with  $\Sigma$  by  $p$ . Then any point  $q \in U(p) \subset \Sigma$  out of a sufficiently small neighborhood  $U(p)$  will be mapped by the nonlinear flow map to another point  $P(q) = \varphi_\tau(q) \in \Sigma$  of the cross section where the first return time  $\tau = \tau(q)$ , in general, depends on the point  $q$ .

By this geometrical construction, the analysis of the local  $n$ -dimensional flow near the periodic orbit is effectively reduced to that of the  $n - 1$  dimensional Poincaré map  $P : U \rightarrow \Sigma$  which is accessible by the Hartman-Grobman and the stable manifold theorem for fixed points of iterated maps. In fact, the periodic orbit  $C$  will always intersect  $\Sigma$  at the same point  $p$  which therefore is a fixed point of the Poincaré map. Furthermore, solution curves starting sufficiently close to  $p$  will produce a sequence of points in  $\Sigma$  which corresponds to an orbit under the iterated application of the Poincaré map.

The Hartman-Grobman Theorem asserts that if the linearized Poincaré map  $P_q(q)|_{q=p}$  has no eigenvalues of unit modulus, the stability of the fixed point  $p$  and that of the cor-

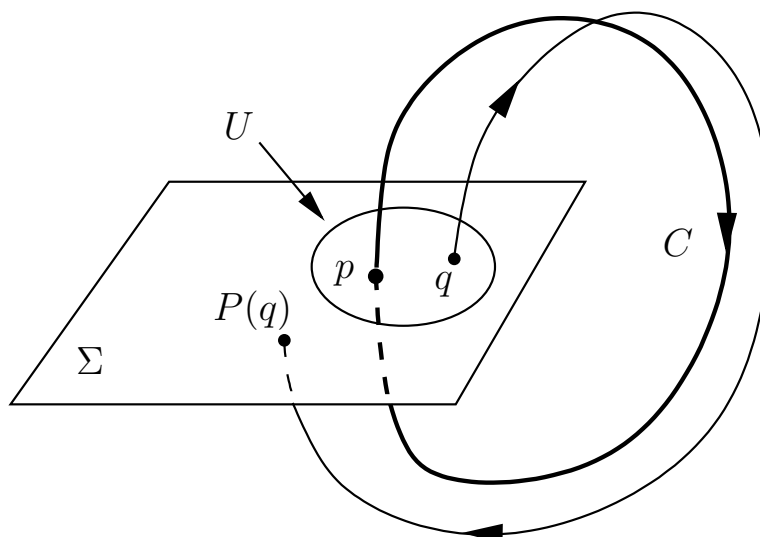


Figure A.3.: Orbits, which start in the neighborhood of a periodic solutions  $C$  of the nonlinear flow, induce an iterated map, the Poincaré map  $q \mapsto P(q)$ , on the transversal cross section  $\Sigma$ .

responding periodic orbit  $C$  is completely determined by the eigenvalues of the linearized Poincaré map. This is the equivalent condition for fixed points of iterated maps to be hyperbolic. The eigenvalues of an iterated map are also called *multipliers*. In the case that the  $n - 1$  multipliers are all of modulus less than one,  $p$  and  $C$  are asymptotically stable, otherwise  $p$  and  $C$  are unstable. Periodic solutions with at least one unstable direction are called saddle-cycles.

Finally, the stable manifold theorem guarantees the existence of local stable and unstable manifolds  $W_{loc}^s(p)$  and  $W_{loc}^u(p)$  which are tangent to the corresponding linear eigenspaces  $E^s(p)$  and  $E^u(p)$  of the linearized Poincaré map at  $p$ . These manifolds are composed of trajectories that remain in a neighborhood of the periodic orbit while they produce a sequence of intersection points on  $\Sigma$  which, in the case of solutions starting in  $W_{loc}^s(p)$ , converge to  $p$  as the number of iterations tends to infinity.

## A.2. Bifurcation theory

Bifurcation Theory is concerned with ‘generic’ properties of dynamical systems. While the qualitative theory of dynamical systems allows to characterize a particular system according to the local stability of its invariant sets, bifurcation theory deals with the problem whether the properties of a particular system persist under small perturbations in which case the system is called *structurally stable*. This issue is of high practical relevance since experimental systems are always subject to ‘external’ noise exerted by the environment which results in small random perturbations to the system under inves-

tigation. Thus, one can observe only those features of a system which are not affected by these perturbations, i.e. its generic features.

In order to tackle the problem of structural stability, one has to compare two dynamical systems and therefore one needs some notion of ‘closeness’ and the allowed class of ‘small perturbations’. These ideas are made precise when we regard two  $n$ -dimensional vector fields  $f$  and  $g$  as close (more precisely as  $\varepsilon - C^1$  close) if for all  $x \in K \subset \mathbb{R}^n$  out of some bounded region in phase space,  $\|f - g\| < \varepsilon$  and  $\|f_x - g_x\| < \varepsilon$  hold, where  $\|\cdot\|$  denotes any convenient norm in  $\mathbb{R}^n$ ,  $\mathbb{R}^{n^2}$  respectively. In addition, two  $n$ -dimensional ODE systems

$$\dot{x} = f(x), \quad \dot{x} = g(x)$$

are said to be *topologically equivalent* if there is a continuous change of coordinates  $h$  such that

$$h(\varphi_{t_f}^f(x)) = \varphi_{t_g}^g(h(x)),$$

i.e. orbits of the flow  $\varphi_{t_f}^f$  associated with  $f$  are continuously deformed into the corresponding orbits of  $\varphi_{t_g}^g$ .

Equipped with these definitions, we can now define a nonlinear ODE system  $\dot{x} = f(x)$  to be structurally stable if all sufficiently  $\varepsilon - C^1$  close systems  $\dot{x} = g(x)$  are topologically equivalent to  $\dot{x} = f(x)$ . In particular, the number and stability type of invariant sets of the flow  $\varphi_{t_f}^f$  are retained under small perturbations which implies that the phase portraits of topologically equivalent systems ‘look qualitatively the same’.

So far we have always assumed that the Jacobian matrix at a fixed point has no eigenvalue with zero real part in which case small perturbations to the system will produce topologically equivalent phase portraits. However, since the eigenvalues of the Jacobian matrix depend continuously on the system parameters, it may happen that one of the eigenvalues crosses the imaginary axis as a parameter is varied. In this case, one can expect topologically non-equivalent phase portraits for nearby parameter values.

As an example, consider the linear two-dimensional ODE system:

$$\begin{aligned} \dot{x}_1 &= a_{11}x_1 + a_{12}x_2 \\ \dot{x}_2 &= a_{21}x_1 + a_{22}x_2 \end{aligned} \tag{A.9}$$

which depends on four parameters given by the entries of the  $2 \times 2$  matrix  $A = (a_{ij})$ . The eigenvalues of this matrix are given by the roots of the characteristic polynomial:

$$\lambda^2 + \lambda \operatorname{tr}A + \det A = 0$$

where  $\operatorname{tr}A = a_{11} + a_{22}$  and  $\det A = a_{11}a_{22} - a_{12}a_{21}$ . The qualitative behavior of trajectories near the only fixed point  $(0, 0)$  is summarized in (Fig. A.4). Along the parabola  $(\operatorname{tr}A)^2 = 4\det A$  (bold black line), the eigenvalues change from real to complex while the topological nature of the fixed point is not altered, i.e. a sink remains a sink, whether solutions approach it in straight lines or in spirals.

The important point to note is that in the space of linear systems of the form (A.9), the stability type of the fixed point is completely determined by the two quantities  $\det A$

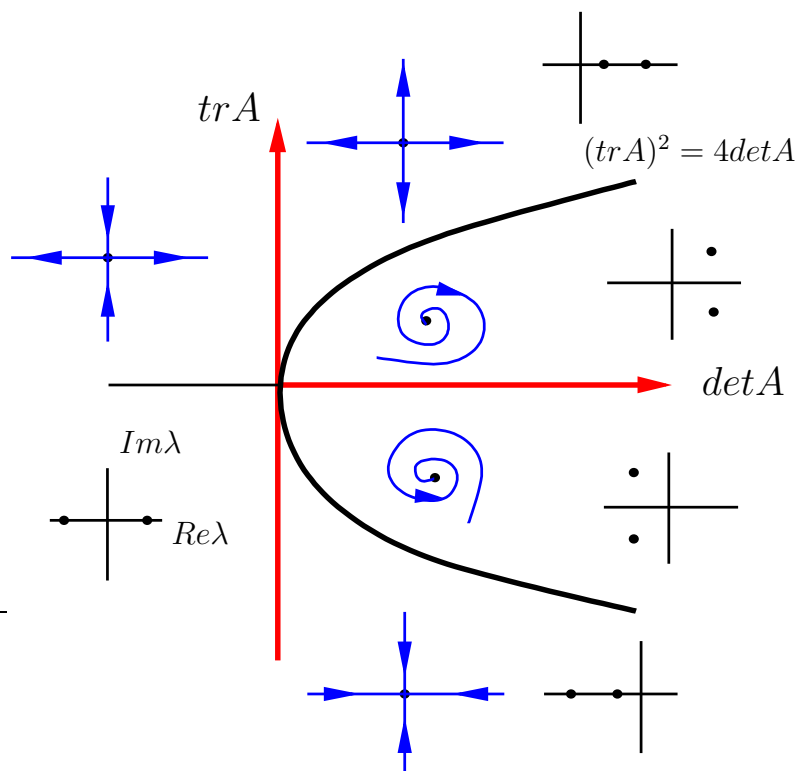


Figure A.4.: The partition of the space of linear 2-dimensional ODE systems according to topological equivalence. Bifurcations occur along the positive  $\det A$ - and the  $\text{tr} A$ -axis (bold, red). The small insets show the qualitative behavior of trajectories (blue lines) near the fixed point and the corresponding position of the eigenvalues in the complex plane.

and  $\text{tr} A$  as long as the system is not located on the positive  $\det A$ -axis or the  $\text{tr} A$ -axis (bold red line) where the system becomes structurally unstable due to the emergence of eigenvalues with zero real part. A point in the  $\det A$ - $\text{tr} A$ -plane where the ODE system is structurally unstable is called a bifurcation point and the crossing of one of the two axis is accompanied by a qualitative change of the local phase portrait near the fixed point for nearby parameter values. For example, when the positive  $\det A$ -axis is crossed from below, the sink turns into a source. However, the two lines along which a bifurcation occurs, constitute a set of (Lebesgue) measure zero in the  $\det A$ - $\text{tr} A$ -plane. Thus, if one generates a two-dimensional linear system by chance, it is almost surely structurally stable which, therefore, is a generic property of such a system. We remark that the same argumentation naturally extends to higher dimensional linear systems.

To the contrary, Smale [80, 81] has shown that structural stability is no generic property for higher dimensional nonlinear systems (i.e. for  $n \geq 3$ ) and much of the complexity in such systems arises from the nontrivial global behavior of the associated nonlinear

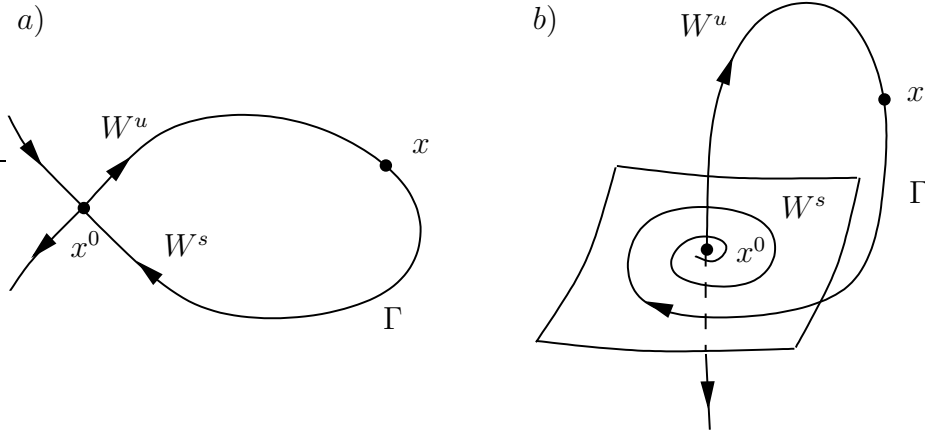


Figure A.5.: Homoclinic orbits in  $\mathbb{R}^2$  (a) and  $\mathbb{R}^3$  (b).

phase flows. Of particular interest are the so-called *homoclinic* orbits (Fig. A.5) where the unstable and the stable manifold of a fixed point bend in such a way that they intersect along the homoclinic orbit, i.e. an orbit  $\Gamma$  starting at  $x \in \mathbb{R}^n$  is called homoclinic to a fixed point  $x^0$  of the ODE system (A.4) if  $\varphi_t x \rightarrow x^0$  as  $t \rightarrow \pm\infty$  which implies that  $\Gamma \subset W^s(x^0) \cap W^u(x^0)$ . In the case that  $x^0$  is a hyperbolic fixed point, one can show that a homoclinic orbit to such a point is structurally unstable, so that one can expect qualitatively different behavior for slightly perturbed systems (cf. Sec. A.5).

### A.2.1. Center manifold theorem

We now consider the case that the ODE system (A.4) has a nonhyperbolic equilibrium point  $x_0$  in which case the Hartman-Grobman and the stable manifold theorems are supplemented by the center manifold theorem. Therefore, we assume that the Jacobian matrix  $f_x(x^0)$  has among  $n_+$  and  $n_-$  eigenvalues with positive and negative real parts, respectively, also  $n_0$  eigenvalues with vanishing real part. The center manifold theorem asserts the existence of a local  $n_0$ -dimensional manifold  $W_{loc}^c(x^0)$  that is tangent to the linear eigenspace  $E^c(x^0)$  at  $x^0$  and locally invariant under the nonlinear flow.  $W_{loc}^c(x^0)$  is called the center manifold and  $E^c(x^0)$  is spanned by the (generalized) eigenvectors associated to the  $n_0$  eigenvalues with zero real part.

The importance of the center manifold results from the fact that it contains the essential dynamics of an ODE system near an equilibrium point no matter what the dimension of the system is. This is a remarkable fact since, as we will later show, the reduced flow on the center manifold for one-parameter families of dynamical systems is generically of dimension one or two.

In order to clarify the ideas involved in the center manifold theorem, let us assume that the original ODE system  $\dot{x} = f(x)$  with  $x \in \mathbb{R}^n$  has been transformed into an

## A. Dynamical Systems and Bifurcation Theory in a Nutshell

eigenbasis of the Jacobian matrix  $f_x(0)$

$$\begin{aligned}\dot{u} &= Bu + g(u, v) \\ \dot{v} &= Cv + h(u, v)\end{aligned}\tag{A.10}$$

where we assumed without loss of generality that the fixed point has been translated to the origin  $x^0 = 0$  and  $u \in \mathbb{R}^{n_0}$ ,  $v \in \mathbb{R}^{n_+ + n_-}$ ,  $n = n_+ + n_- + n_0$ . The eigenvalues of the  $n_0 \times n_0$  matrix  $B$  have all zero real parts while those of the  $(n_+ + n_-) \times (n_+ + n_-)$  matrix  $C$  are all different from zero. The nonlinear functions  $g$  and  $h$  have Taylor expansions starting with at least quadratic terms. The center manifold can be locally represented as a graph of a smooth function:

$$W^c = \{(u, v) | v = V(u), V(0) = 0, V_u(0) = 0\}\tag{A.11}$$

with  $V : U(0) \subset \mathbb{R}^{n_0} \rightarrow \mathbb{R}^{n_+ + n_-}$ .

One of the most important results of the center manifold theorem is the so-called *Reduction Principle* which says that the flow of the  $n$ -dimensional ODE system (A.10) is topologically equivalent near the origin to the ODE system

$$\begin{aligned}\dot{u} &= Bu + g(u, V(u)) \\ \dot{v} &= Cv\end{aligned}\tag{A.12}$$

where the first equation is the restriction of (A.10) to the center manifold (eq. A.11). It describes the essential dynamics near the fixed point while the second equation in (A.12) contains the trivial dynamics since it describes exponentially growing or decaying solutions. However, in practical applications it is desirable to have  $n_+ = 0$  in which case the center manifold is locally attracting and truly describes the long-time behavior of solution curves in its neighborhood. Finally, we remark that by differentiating the defining equation for the center manifold  $v = V(u)$  with respect to time, one can derive the (partial) differential equation

$$CV(u) + h(u, V(u)) = V_u(u) \left( Bu + g(u, V(u)) \right)$$

from which one may obtain an approximation to the center manifold in terms of a power series expansion.

### A.2.2. Parameter dependent systems and normal forms

In the last Subsection, we argued that if a  $n$ -dimensional ODE system has a nonhyperbolic fixed point it is sufficient to study the restriction of the  $n$ -dimensional flow to the center manifold of the nonhyperbolic fixed point in order to determine its stability type. In the following, we consider parameter dependent systems which are naturally used to model experimental situations since the system of interest is usually embedded in some form of environment or subjected to external driving forces. It is clear that hyperbolic fixed points, though they remain hyperbolic under sufficiently small perturbations, may

become nonhyperbolic as parameters in the system are varied; for example, consider a path in the  $trA$ - $detA$ -plane of Fig. A.4 which crosses the  $trA$ -axis.

To this purpose, we describe how the analysis of the previous Subsection can be extended to parameter dependent families of ODE systems

$$\begin{aligned}\dot{x} &= f(x, \alpha), & (x, \alpha) \in \mathbb{R}^n \times \mathbb{R}^k \\ \dot{\alpha} &= 0\end{aligned}\tag{A.13}$$

where we added a trivial dynamics for the parameters  $\alpha$  to make the center manifold theorem applicable to such systems.

Assume that the parameter dependent ODE system (A.13) has at  $\alpha = 0$  a nonhyperbolic fixed point at  $x^0 = 0$  with  $n_0$  eigenvalues having zero real parts. For simplicity, and because it is the most interesting case in real applications, we further assume that all other  $n - n_0$  eigenvalues have a negative real part. In an appropriate eigenbasis of the Jacobian matrix  $f_x(0, 0)$ , the ODE system (A.13) reads

$$\begin{aligned}\dot{u} &= B(\alpha)u + g(u, v, \alpha) \\ \dot{v} &= D(\alpha)v + h(u, v, \alpha), & (u, v) \in \mathbb{R}^{n_0} \times \mathbb{R}^{n-n_0} \\ \dot{\alpha} &= 0, & \alpha \in \mathbb{R}^k.\end{aligned}\tag{A.14}$$

At  $(u, v, \alpha) = (0, 0, 0)$  this ODE system has a  $n_0 + k$ -dimensional (parameter dependent) center manifold  $W_{loc}^c(0, 0)$  that is tangent at the origin to  $E^c(0) \times \mathbb{R}^k$ . It can be represented as the graph of a function  $v = V(u, \alpha)$  which may be approximated by a power series in  $u$  and  $\alpha$ . The invariance properties of center manifolds guarantee that any bifurcating solution near  $(0, 0, 0)$  remains in one of the center manifolds for  $|\alpha|$  being sufficiently small. Thus, the local bifurcations occurring in a family of ODE systems can be studied by restricting (A.14) to the parameter dependent center manifold. As a result, one obtains the topologically equivalent ODE system

$$\dot{u} = B(\alpha)u + g(u, V(u, \alpha), \alpha)\tag{A.15}$$

which is now of dimension  $n_0$ . In one-parameter families,  $n_0$  is typically 1 or 2.

After the center manifold theorem has been applied, the linear part of the ODE system (A.15) is already in a canonical form since the eigenvectors of the Jacobian matrix were used as a basis for the new coordinate system. In order to study the local bifurcations of the flow on the center manifold it is desirable to find a particular simple representative out of the class of topologically equivalent systems which is the aim of *normal form* theory. By successive near identity coordinate transformations, one tries to eliminate as much higher order terms in (A.15) as possible up to a particular order. This procedure guarantees that the linear part of the vector field is retained at each step, so that the resulting (nonlinear) normal form has the same linear degeneracies as the original vector field. Interestingly, it is the linear part of the vector that determines which higher order terms can be removed by a suitable change of coordinates. The nonremovable terms are called *resonances*.

In a next step, one tries to show that neglecting the higher order terms beyond a particular order does not alter the topological class of the system in which case the obtained vector field is called a normal form or a universal unfolding for the considered bifurcation. However, it should be mentioned that normal form theory is far from being complete. So far, it is well developed for one- and two-parameter families of dynamical systems where many universal unfoldings are known.

In the special case that the vector field  $f$  can be obtained as the gradient of a scalar function  $V : \mathbb{R}^n \rightarrow \mathbb{R}$ , i.e.  $f(x) = \text{grad } V(x)$ , all universal unfoldings for generic four-parameter families are known. They are given by Thom's famous seven elementary 'catastrophes' [82].

Finally, we remark that there is a center manifold theorem for fixed points in discrete-time dynamical systems, too, which allows for a similar reduction of the flow near non-hyperbolic limit cycles that arise as fixed points of a suitable Poincarè map.

### A.3. Local bifurcations in one-parameter families

We give a survey of the bifurcations of fixed points and limit cycles that generically occur in one-parameter families of continuous-time dynamical systems.

For each bifurcation, we present a relevant bifurcation diagram together with the bifurcation condition and where appropriate, mention the corresponding normal form vector field. As we have already pointed out, the normal form vector field describes the local behavior of trajectories near a nonhyperbolic fixed point in the center manifold of any generic  $n$ -dimensional system fulfilling the corresponding bifurcation condition. In view of (A.14), 'local' means here both, in a neighborhood of the fixed point in phase space as well as in a neighborhood of the critical parameter value where the bifurcation occurs in parameter space. In order to be called 'generic', the  $n$ -dimensional vector field has to satisfy certain non-degeneracy conditions, such as the nonvanishing of (higher order) derivatives with respect to phase space variables and/or parameters evaluated at the fixed point.

A general bifurcation diagram is usually composed of several bifurcations taking place in different regions of the parameter space. Thus, the generic bifurcations described in the following may be used as building blocks to understand the bifurcation diagrams shown in Part I and II of this thesis. However, it should be noted that the bifurcation diagrams presented there are not drawn with respect to canonical coordinates according to the center manifold theorem and thus, they may appear distorted.

Finally, we make two general remarks: First, we note that the number of independent conditions defining a bifurcation is called its *codimension*. It equals the number of parameters that can be varied independently. Second, the bifurcations described in Section A.3 and A.4 can be detected by analyzing the flow in the neighborhood of a fixed point or a limit cycle and are, therefore, called local bifurcations.

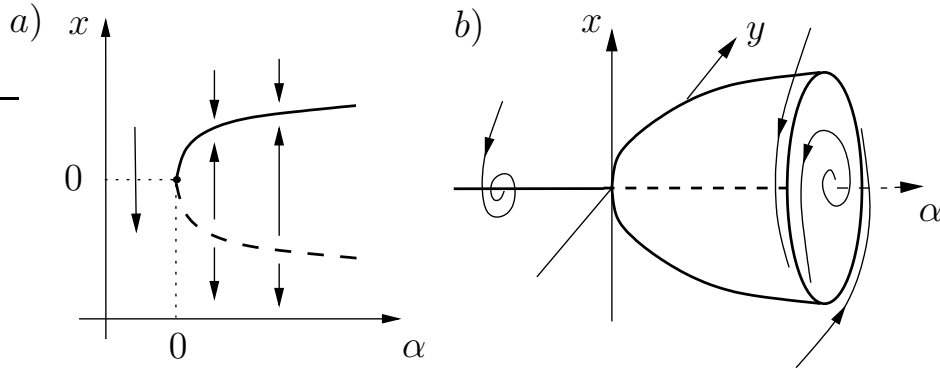


Figure A.6.: Generic bifurcations of equilibria in one-parameter families of ODE systems: the saddle-node (a) and the Hopf bifurcation (b).

### A.3.1. Bifurcations of equilibria

The setting is mostly the same as in Section A.2. We consider parameter dependent ODE systems  $\dot{x} = f(x, \alpha)$  with  $x \in \mathbb{R}^n$ , but only 1-dimensional parameter spaces with  $\alpha \in \mathbb{R}$ . A solution of the fixed point equation  $f(x, \alpha) = 0$  is a smooth curve  $x^0 = x^0(\alpha) \in \mathbb{R}^{n+1}$  and the eigenvalues  $\lambda_i(\alpha)$  of the Jacobian matrix  $f_x(x^0(\alpha))$  depend continuously on the parameter  $\alpha$ . Thus, as long as  $x^0(\alpha)$  is hyperbolic it remains hyperbolic under small parameter perturbations.

However, when a parameter exceeds a critical value, there are generically two possibilities by which  $x^0(\alpha)$  may become nonhyperbolic: First, the Jacobian matrix  $f_x(x^0(\alpha))$  has a simple real zero eigenvalue  $\lambda_1 = 0$  at the critical parameter value or second, a simple pair of complex conjugated eigenvalues approaches the imaginary axis, i.e.  $\lambda_{1/2} = \pm i\omega$ ,  $\omega \geq 0$ . In the former case, a saddle-node bifurcation takes place while the latter corresponds to a Hopf bifurcation.

#### saddle-node bifurcation

The saddle-node bifurcation, also known as tangent or fold bifurcation, describes the appearance and disappearance of a pair of equilibrium points as a critical parameter value is passed (Fig. A.6). The standard form of an ODE system exhibiting a saddle-node bifurcation is given by

$$\dot{x} = \alpha - x^2 \equiv f(x, \alpha), \quad (x, \alpha) \in \mathbb{R} \times \mathbb{R} \quad (\text{A.16})$$

which satisfies the two nondegeneracy conditions

$$\begin{aligned} f_{xx}(0,0) &\neq 0 \\ f_\alpha &\neq 0. \end{aligned} \quad (\text{A.17})$$

The ODE system (A.16) can be thought of as the restricted flow of a  $n$ -dimensional system to its one-dimensional center manifold.

At  $\alpha = 0$ , the ODE A.16 has a nonhyperbolic fixed point  $x^0 = 0$  with eigenvalue  $\lambda = f_x(0, 0) = 0$ . For  $\alpha < 0$ , there is no solution of the fixed point equation  $f(x, \alpha) = 0$  and hence, no fixed point while for  $\alpha > 0$ , there are two stationary points: a saddle (dashed line) and a node (solid line). The arrows in Fig. A.6 show the direction of the one-dimensional flow. Note that in higher dimensional systems with  $n \geq 2$  both of the bifurcating equilibria can be of saddle-type if the number of their unstable directions differs by one.

### Hopf bifurcation

The standard form of the Hopf bifurcation is given by the two-dimensional ODE system:

$$\begin{pmatrix} \dot{x} \\ \dot{y} \end{pmatrix} = \begin{pmatrix} \alpha & -\omega \\ \omega & \alpha \end{pmatrix} \begin{pmatrix} x \\ y \end{pmatrix} - (x^2 + y^2) \begin{pmatrix} x \\ y \end{pmatrix} \quad (\text{A.18})$$

which has a simple pair of complex conjugate eigenvalues  $\lambda_{1/2} = \pm i\omega$  at  $(x, y, \alpha) = (0, 0, 0)$ . For  $\alpha < 0$ , there is only a stable focus (solid line) which becomes unstable for  $\alpha > 0$  (Fig. A.6b). At the same time, a stable periodic solution emerges and coexists with an unstable focus (dashed line). Directly at the bifurcation point, the fixed point remains stable, but the rate of convergence is not exponentially anymore.

The Hopf bifurcation shown in Fig. A.6b is called *supercritical* since the emerging limit cycle is stable. In general, the stability of the bifurcating cycle is determined by the first Liapunov coefficient which must not vanish for a Hopf bifurcation to occur. This coefficient is given by a certain combination of second- and third order derivatives of the vector field evaluated at the bifurcation point (cf. Chapter 3 in [76]). If the Liapunov coefficient is negative, the bifurcating cycle is stable. Otherwise, the sign in front of the nonlinear term in (A.18) is reversed from ‘-’ to ‘+’ and the new born periodic solution is unstable and bifurcates to the left where  $\alpha < 0$ . In this case, the Hopf bifurcation is called *subcritical*.

The existence of the limit cycle is guaranteed only for sufficiently small parameter values in the neighborhood of the bifurcation point. What ‘sufficient’ means, depends on the system under consideration. In particular, the nonlinear terms beyond the third order determine the fate of the limit cycle far away from the bifurcation point.

### A.3.2. Bifurcations of limit cycles

We give a survey of the three generic local bifurcations that a limit cycle may undergo as one-parameter is continuously varied. As we pointed out earlier, the analysis of the local changes in the phase flow near a periodic orbit can be reduced to a local analysis of the associated Poincaré map (cf. Fig. A.3), i.e. to a discrete-time system. In order to discuss the topological changes in the proximity of the bifurcation point, we show representative phase portraits directly at as well as slightly above and below the bifurcation point together with the reduced dynamics on a suitable Poincaré section (Fig. A.7). The

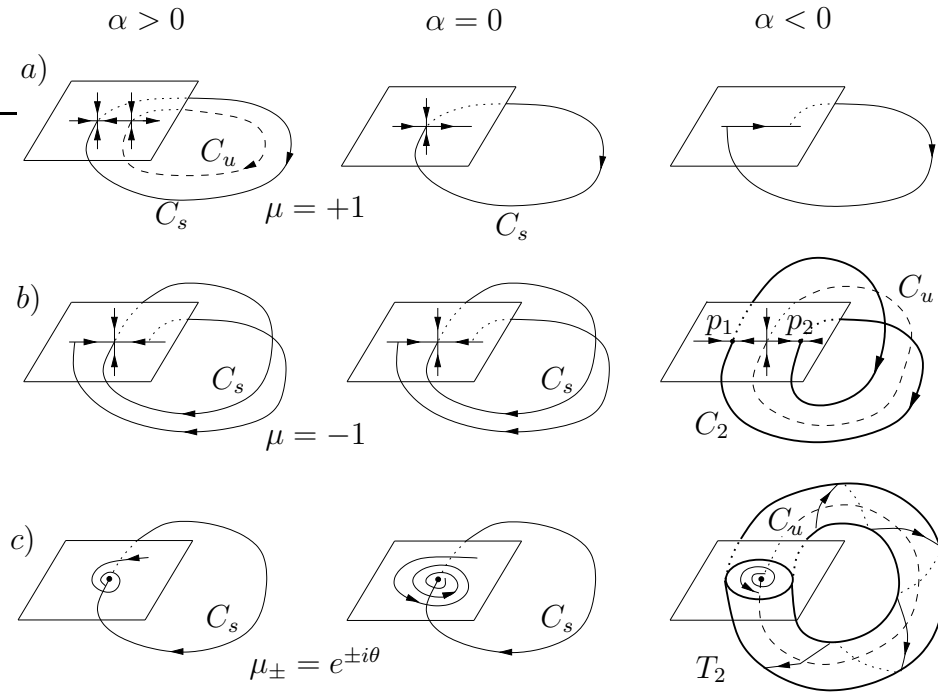


Figure A.7.: Generic one-parameter bifurcations of limit cycles: saddle-node (a), period doubling (b) and Neimark-Sacker bifurcation (c).

definition of ‘above’ and ‘below’ the bifurcation point is somewhat arbitrary as long as the explicit expressions for the corresponding normal form mappings are not taken into account. However, we shall give here only a qualitative description of the corresponding bifurcation phenomena without explicit reference to a particular normal form.

In the following, we describe the saddle-node, the period doubling and the Neimark-Sacker bifurcation for limit cycles in a 3-dimensional phase space. Thus, the associated Poincaré map has two multipliers that determine the stability of its fixed points and thereby the stability of the corresponding cycles. A fixed point of the Poincaré map becomes nonhyperbolic if one of the multipliers lies on the unit circle in the complex plane, i.e.  $|\mu| = 1$ . Generically, there are three possibilities how a multiplier can cross the unit circle as one-parameter is varied and all possibilities lead to topologically different scenarios.

### Saddle-node bifurcation of periodic orbits (SNP)

Assume that the linearized Poincaré map has a simple multiplier  $\mu_1 = +1$  at  $\alpha = 0$  while the other multiplier satisfies  $0 < \mu_2 < 1$ , then a saddle-node bifurcation takes place where, this time, a pair of periodic orbits is created and annihilated as  $\alpha$  passes through zero (Fig. A.7a). For  $\alpha > 0$ , there are two limit cycles, a stable and an unstable one. They merge at  $\alpha = 0$  and disappear for  $\alpha < 0$ . The corresponding Poincaré maps show a node coexisting with a saddle ( $\alpha > 0$ ), a nonhyperbolic fixed point ( $\alpha = 0$ ) and no fixed point at all ( $\alpha < 0$ ). In phase space dimensions  $n \geq 3$ , both of the merging limit cycles can also be of saddle-type if the number of their unstable directions differs by one.

### Period doubling bifurcation

Assume that the linearized Poincaré map has a simple multiplier  $\mu_1 = -1$  at  $\alpha = 0$  while the other multiplier satisfies  $-1 < \mu_2 < 0$ , then a period doubling (or flip) bifurcation takes place where a stable limit cycle, existing for  $\alpha < 0$ , loses its stability and coexists for  $\alpha > 0$  with a newly emerged stable limit cycle  $C_2$  having approximately twice the period of the primary periodic orbit (Fig. A.7b). The associated Poincaré map  $P_\alpha$  has one stable fixed point for  $\alpha < 0$  which becomes unstable for  $\alpha > 0$  where the period-2 cycle  $C_2$  is stable instead. On the transversal cross section, the period-2 cycle consists of two points which are mapped into each other under the application of  $P_\alpha$ , i.e.  $p_1 = P_\alpha p_2$  and  $p_2 = P_\alpha p_1$ . In particular, each of the two points is a fixed point of the second iterate of the Poincaré map, i.e.  $p_1 = P_\alpha^2 p_1$  and  $p_2 = P_\alpha^2 p_2$  where  $P_\alpha^2 \equiv P_\alpha \circ P_\alpha$ .

### Neimark-Sacker bifurcation

Here we consider the case that the linearized Poincaré map has a simple pair of complex conjugate eigenvalues  $\mu_\pm = e^{\pm i\theta}$  located at the unit circle (Fig. A.7c). If the multipliers are away from *strong resonances* defined by  $e^{ik\theta} = 1$  for  $k = 1, 2, 3, 4$  (cf. [9]), the Poincaré map has a two-dimensional invariant manifold on which a closed invariant curve bifurcates from the stable fixed point as  $\alpha$  passes through zero while the fixed

point becomes unstable for  $\alpha < 0$ . The closed invariant curve on the Poincaré section corresponds to a 2-torus  $T_2$  of the original ODE system.

The orbit structure on the torus is basically determined by the properties of a one-dimensional map on the invariant circle. In particular, fixed points and cycles of the circle map correspond to periodic orbits on the torus which always come in pairs of alternating stability. The periodic orbits emerge and disappear in pairs via saddle-node bifurcations as one parameter is varied. Outside these parameter windows, the torus is densely covered by a quasi-periodic orbit.

## A.4. Local bifurcations in two-parameter families

We have shown that along branches of one-parameter equilibrium curves  $x^0(\alpha)$ , a bifurcation may occur at those points  $(x^0, \alpha^0)$  where a simple real or a simple pair of complex conjugate eigenvalues of the Jacobian matrix approach the imaginary axis provided some nondegeneracy conditions such as (A.17) are simultaneously satisfied.

Now, assume that there are two parameters in the system:  $\beta_1$  and  $\beta_2$ . In this case, codimension one bifurcations will generically occur along curves in the two-parameter plane as long as the relevant bifurcation and nondegeneracy conditions are still fulfilled. However, if one of these conditions is violated at some point along the codimension one bifurcation curve, a codimension two bifurcation takes place and one may expect topologically nonequivalent phase portraits for nearby parameter values. Thus, branches of codimension one bifurcations originate in codimension two bifurcation points which, therefore, act as organizing centers for the former. In fact, this is a general feature of higher codimension bifurcation points.

In the remainder of the Section, we shall consider the following three cases leading to topologically distinct codimension two bifurcations in ODE systems:

1. Together with a simple real eigenvalue  $\lambda = 0$ , the first of the nondegeneracy conditions in (A.17) ( $f_{xx}(0,0) \neq 0$ ) does not hold anymore in which case higher order terms beyond the quadratic term are needed to unfold the singularity at  $(0,0)$ . Accordingly, the normal form of the fold bifurcation (A.16) is replaced by a two-parameter family of one-dimensional ODEs exhibiting a cusp bifurcation.
2. Together with a simple real eigenvalue  $\lambda_1 = 0$ , a second simple real eigenvalue  $\lambda_2 = 0$  also approaches the imaginary axis in which case the center manifold becomes two-dimensional and a Bogdanov-Takens bifurcation takes place.
3. Finally, we consider the case that the first Liapunov coefficient vanishes along a Hopf bifurcation curve in which case higher order terms beyond the third order are needed in (A.18) to unfold the Hopf bifurcation. The corresponding codimension two bifurcation is called a generalized Hopf or Bautin bifurcation.

### A.4.1. Cusp bifurcation

The minimal phase space dimension for a cusp bifurcation to occur is one. The corresponding normal form is given by

$$\dot{x} = \beta_1 + \beta_2 x - x^3 \equiv f(x, \beta_1, \beta_2), \quad x \in \mathbb{R}, \quad (\beta_1, \beta_2) \in \mathbb{R}^2. \quad (\text{A.19})$$

The zeros of the vector field  $f$  define the equilibrium manifold

$$M = \{(x, \beta_1, \beta_2) : \beta_1 + \beta_2 x - x^3 = 0\}$$

which is shown in Fig. A.8a. For  $\beta_2 < 0$ , there is a curve (bold line) on  $M$  whose projection onto the  $(\beta_1, \beta_2)$ -plane yields the semicubic parabola

$$SN = \{(\beta_1, \beta_2) : 4\beta_2^3 + 27\beta_1^2 = 0\}$$

along which saddle-node bifurcations take place (Fig. A.8b). The two branches of the semicubic parabola meet in a cusp singularity at  $(\beta_1, \beta_2) = (0, 0)$ . The section along the dotted line in Fig. A.8b is shown in Fig. A.8c where the S-shaped equilibrium curve becomes apparent which is typical for bistable systems. In the wedge-shaped region I of Fig. A.8b, two stable and one unstable fixed point coexist while in region II there is only one stable fixed point. Along the two branches  $SN_1$  and  $SN_2$  in Fig. A.8b, one stable and one unstable fixed point disappear via a fold bifurcation.

### A.4.2. Bogdanov-Takens bifurcation

Here we shall only give a qualitative description of the phase portraits near the Bogdanov-Takens point  $(\beta_1, \beta_2) = (0, 0)$  (Fig. A.9a). There are no equilibria in region I. As region II is entered passing the curve  $SN_2$ , a saddle and a stable node are created by a saddle-node bifurcation. Then the node turns into a focus which does not correspond to a bifurcation. Subsequently, the focus loses stability via a supercritical Hopf bifurcation as region III is entered along H and a stable limit cycle emerges. As one moves inside region III towards HC, the limit cycle grows until it ‘merges’ with the saddle that was created at  $SN_2$  and hence, it becomes a homoclinic orbit by which the limit cycle vanishes as region IV is entered. In region IV a saddle coexists with an unstable focus which turns into a node before it disappears together with the saddle along the second branch  $SN_1$  of saddle-node bifurcations.

The transition from region III into region IV corresponds to a global bifurcation (cf. Sec. A.5) which can not be detected by merely investigating the neighborhood of a fixed point since the homoclinic orbit forms as a result of the intersection of the global stable and unstable manifolds of the saddle-point and thus, involves global aspects of the flow far away from the fixed point. This is a nice example how the local analysis of higher codimension bifurcations may provide information about global bifurcations in the system.

### A.4.3. Bautin bifurcation

Similar to the Bogdanov-Takens bifurcation, we shall restrict to a qualitative discussion of the changes in the local phase portraits as one moves around the Bautin bifurcation point  $(\beta_1, \beta_2) = (0, 0)$  (Fig. A.9b). In region I, there is only one stable focus. It becomes unstable as region II is entered while crossing the curve H where a stable limit cycle emerges via a supercritical Hopf bifurcation. This limit cycle persists as region III is entered crossing the branch SH where an additional unstable limit cycle is created inside the first one while the unstable focus regains its stability. Both limit cycles merge along the curve SNP in a saddle-node bifurcation (cf. A.3) leaving the stable focus as the only attractor in region I.

The stability of the newborn limit cycles is determined by the first Liapunov coefficient. It is negative along H where supercritical Hopf bifurcations take place while it is positive along SH where subcritical Hopf bifurcations occur (cf. [76]).

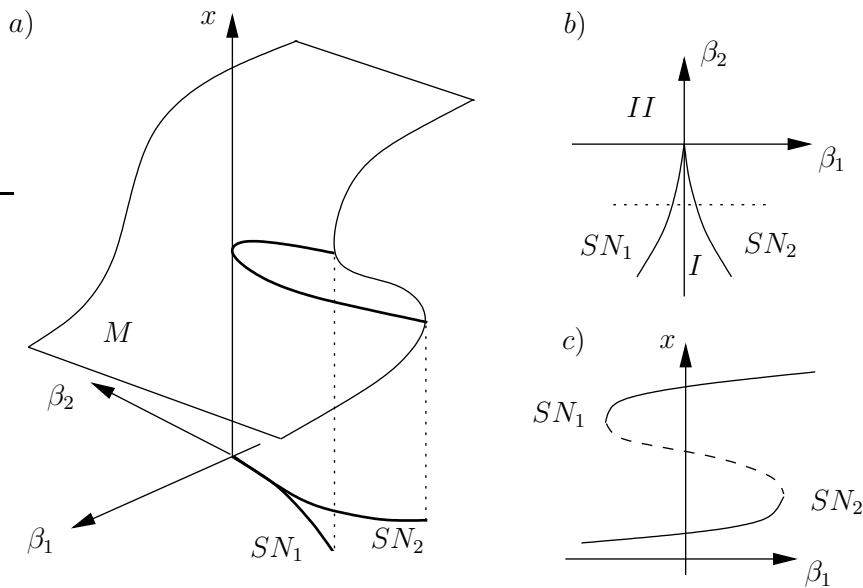


Figure A.8.: The cusp bifurcation:  $M$  is the equilibrium manifold in the direct product space  $\mathbb{R} \times \mathbb{R}^2$  (a). The other two images show different projections of  $M$  onto the parameter plane (b) and the  $x$ - $\beta_1$ -plane (c) which is taken along the dotted line in (b). Region I exhibits bistability (c) while in Region II there is only one stable equilibrium.  $SN_i$  denote curves along which saddle-node bifurcations occur.

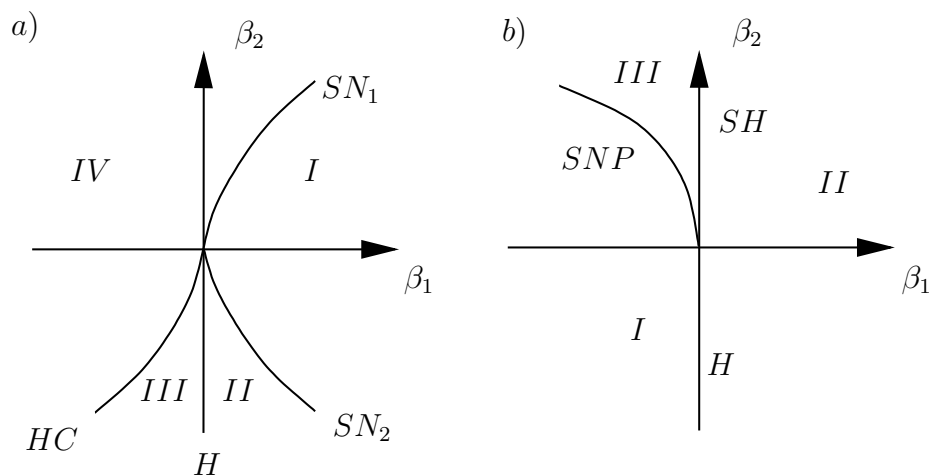


Figure A.9.: Bogdanov-Takens (a) and Bautin bifurcation (b). Symbols denote: H – supercritical Hopf bifurcation, SH – subcritical Hopf bifurcation,  $SN_i$  – saddle-node bifurcation of fixed point, SNP – saddle-node bifurcation of periodic orbits, HC – saddle homoclinic bifurcation.

## A.5. Global bifurcations

So far we have considered bifurcations that can be detected by a local analysis, i.e. by studying the linearized flow in the neighborhood of a fixed point (eq. A.6) or a limit cycle. In contrast, global bifurcations are often associated with homoclinic orbits and thus, involve the global behavior of stable and unstable manifolds of fixed points and limit cycles which, in general, can not be investigated by a local analysis. Note, however, that we have already encountered an example where the local analysis of a codimension two bifurcation (the Bogdanov-Takens bifurcation in Section A.4) led to the prediction of a global bifurcation.

In the remainder of this Section, we shall discuss two global one-parameter bifurcations: the saddle homoclinic bifurcation and the saddle-node homoclinic bifurcation. While the former involves a homoclinic orbit to a hyperbolic fixed point, the latter one is associated with a nonhyperbolic fixed point. The minimal phase space dimension for both bifurcations to occur is two.

### A.5.1. Saddle homoclinic bifurcation

The saddle homoclinic bifurcation is completely characterized by the Andronov-Leontovich theorem (cf. [76]). Here, one considers a 2-dimensional ODE system of the form:

$$\dot{x} = f(x, \alpha), \quad x \in \mathbb{R}^2, \alpha \in \mathbb{R} \quad (\text{A.20})$$

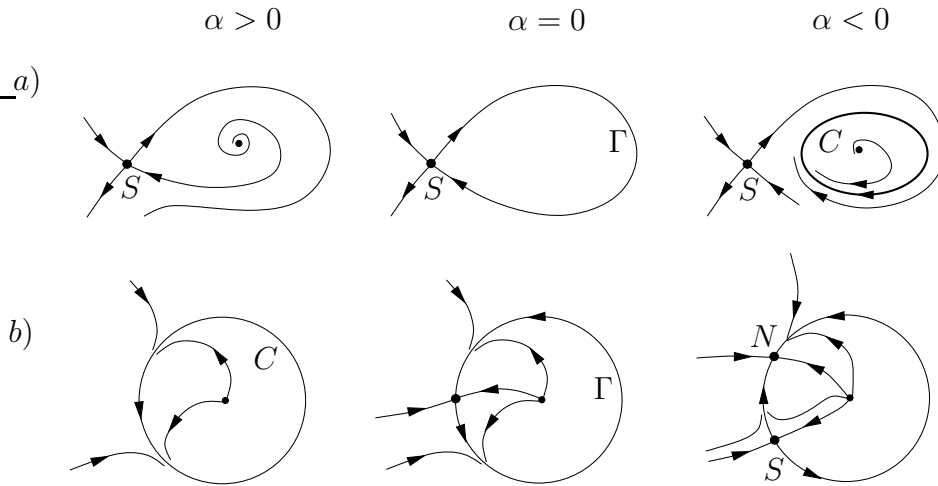


Figure A.10.: Saddle homoclinic bifurcation (a) and saddle-node homoclinic bifurcation (b): Both are global bifurcations that involve a homoclinic orbit  $\Gamma$  to a hyperbolic (a) or a nonhyperbolic fixed point (b) while periodic orbits  $C$  exist for nearby parameter values.  $N$  and  $S$  denote a node and a saddle equilibrium point, respectively.

which at  $\alpha = 0$  has a saddle equilibrium  $S$  at  $x^0 = 0$  with nonvanishing eigenvalues  $\lambda_1(0) < 0 < \lambda_2(0)$ . In addition, the existence of a homoclinic orbit  $\Gamma$  (as in Fig. A.10a for  $(\alpha = 0)$ ) has to be assumed. So the theorem does not prove the existence of a homoclinic orbit. It ‘merely’ describes what happens to this orbit under small perturbations.

First of all, it is clear that the homoclinic orbit  $\Gamma$  in Fig. A.10a is not a structurally stable object since one part of the saddle’s unstable manifold has to bend in such a way that it exactly coincides with one part of its stable manifold. However, the interesting result of the Andronov-Leontovich theorem is the forecast about the existence of a periodic orbit  $C$  for certain perturbations of the homoclinic orbit which is schematically represented in Fig. A.10a for  $\alpha < 0$ . If the perturbation is applied in the other direction ( $\alpha > 0$ ), the homoclinic orbit simply disappears. The stability of the cycle  $C$  in the case  $\alpha < 0$  is determined by the so-called saddle quantity  $\sigma = \lambda_1(0) + \lambda_2(0)$ . If  $\sigma < 0$  the cycle is stable and vice versa.

A frequently observed scenario is the following (see the Bogdanov-Takens bifurcation in Section A.4): A limit cycle is born in a Hopf bifurcation and coexists with a saddle equilibrium which is already present. As the bifurcation parameter increases from the Hopf bifurcation value, the limit cycle grows in magnitude until it merges with the saddle equilibrium in a homoclinic orbit and henceforth vanishes.

### A.5.2. Saddle-node homoclinic bifurcation

The saddle-node homoclinic bifurcation (also known as saddle-loop homoclinic or saddle-node on invariant circle bifurcation) actually involves two events: A local saddle-node bifurcation and the sudden appearance of a stable limit cycle solution after the two equilibria have disappeared. The novel feature of this bifurcation is that the saddle-node bifurcation occurs directly on the limit cycle (Fig. A.10b).

At  $\alpha < 0$ , a saddle  $S$  and a node  $N$  are located on an invariant circle which is formed by the two fixed points and the unstable manifold of the saddle which coincides with the one part of the stable manifold of the node. At  $\alpha = 0$ , the saddle and the node merge in a saddle-node bifurcation leaving a nonhyperbolic fixed point together with a homoclinic orbit  $\Gamma$ . The union of these two sets now constitutes the invariant circle. Small perturbations towards  $\alpha > 0$  cause the homoclinic orbit and the nonhyperbolic fixed point to vanish, but leave the stable limit cycle  $C$  instead.

## B. Investigation Methods and Parameter Settings

The numerical simulations for the hemin and the PO system in Appendix C were performed with the freely available software package XPPAUT [83]. Due to the stiffness of the corresponding ODE systems, the ‘STIFF’ integration routine [83, 84] was chosen with a tolerance of  $10^{-5}$  to ensure numerical stability. For the computation of the one and two-parameter bifurcation diagrams, we used the continuation routines of AUTO which are integrated in the XPPAUT environment as well as two other freely available continuation packages: Content [85] and MatCont [86]. While the AUTO routines are very robust and reliable for the computation of codimension one bifurcations, the other two packages have some advantages for the computation of codimension two bifurcation points since they make use of symbolic algebra packages to compute analytical expressions for the derivatives of the vector field on the right hand side of an ODE system up to the fourth order. The higher order derivatives are required for the detection of certain codimension two bifurcation points such as the generalized Hopf bifurcation [76] and the computation of normal form coefficients. In addition, Content and MatCont allow for an easy monitoring of eigenvalues and multipliers along branches of stationary and oscillatory solutions, respectively.

In the next Section, we shortly introduce the method of numerical continuation which was frequently used throughout this work to obtain most of the presented bifurcation diagrams. The Chapter is concluded by two short Sections containing the necessary technical details to set up the numerical simulations for the hemin and the PO system.

### B.1. The method of numerical continuation

We shall give a rather informal introduction to the basic concepts underlying the method of numerical continuation. A more elaborate presentation can be found in Chapter 10 of the textbook by Kuznetsov [76]. Many of the examples given there can be directly implemented as algorithms.

The numerical continuation method is a tool for studying the parameter dependence of invariant sets of a dynamical system as well as their bifurcations. As a result, a bifurcation diagram is obtained showing the possible asymptotic behavior of typical trajectories in the parameter regions of interest. The mathematical basis for the numerical continuation methods is bifurcation theory (see Appendix A). It is frequently utilized where analytical computations fail or are too intricate, i.e. basically in all cases of practical relevance.

## B. Investigation Methods and Parameter Settings

In the following, we consider a parameter dependent family of ODE systems

$$\dot{x} = f(x, \alpha) \quad x \in M \subset \mathbb{R}^n, \quad \alpha \in N \subset \mathbb{R}^2, \quad f : M \times N \rightarrow \mathbb{R}^n \quad (\text{B.1})$$

where, for convenience, we assume that the parameter space is at most two-dimensional. However, this is not a severe restriction because the bifurcation theory for families of ODE systems involving more than two parameters is only poorly developed. So, from theoretical grounds, it is not clear what typical dynamical changes are to be expected under such circumstances which clearly hampers, for example, the interpretation of experimental results.

The numerical continuation is started from a known or at least approximately known invariant set at a particular point in parameter space. The most commonly used starting point is a stationary state, but in some cases may also be a limit cycle or a homoclinic orbit of the ODE system (B.1). Therefore, one has to compute these sets either analytically or numerically. For example, the fixed points of the ODE system are associated with the singular points of the vector field  $f$ ; the latter are solutions of the (generally nonlinear) algebraic equation system:

$$f(x, \alpha) = 0 \quad (\text{B.2})$$

for which solutions  $x^0(\alpha)$  are rarely found explicitly.

The first strategy to locate at least one of the stable fixed points of an ODE system consists in a straightforward numerical integration of the equations (B.1). To this purpose, one has to choose the initial condition such that the ODE system (B.1) has a fixed point at the corresponding parameter value and the initial point belongs to the basin of attraction of the desired fixed point. A second strategy would be to use some form of the Newton iteration scheme, i.e.

$$x^{(i+1)} = x^{(i)} - f_x^{-1}(x^{(i)})f(x^{(i)}), \quad i = 0, 1, \dots \quad (\text{B.3})$$

which converges to the desired fixed point provided the iteration is started close enough to that point and the Jacobian  $f_x$  has no zero eigenvalue there, i.e. the fixed point is hyperbolic.

The location of limit cycle solutions of the ODE system (B.1) is a more intricate task. If the cycle has no unstable direction, it can be equally found by a straightforward numerical integration provided the parameter and the initial point are chosen appropriately. Otherwise, one relies again on iteration schemes which now are formulated as boundary value problems due to the periodicity of the desired solution. In addition, one has to provide a phase condition to single out a particular periodic solution. This becomes necessary due to the phase invariance of a limit cycle, i.e. every phase-shifted solution is again a periodic solution with the same period.

The most difficult task, however, is to begin the numerical continuation from a homoclinic orbit since it is usually known only approximately; for example in terms of a nearby located limit cycle having a very long period (cf. Sec. A.5). Another possibility is to start a homoclinic continuation from a codimension two bifurcation point such as a Bogdanov-Takens point (cf. Sec. A.4).

Finally, we discuss a typical continuation strategy starting from a stationary state as it was done throughout this thesis. First, we note that the equation system (B.2) consists of  $n$  equations for the  $n+1$  variables  $(x, \alpha) \in \mathbb{R}^n \times \mathbb{R}$ , thus defining generically (i.e. under some regularity conditions for the vector field  $f$ ) a smooth curve  $x^0(\alpha)$  in  $\mathbb{R}^{n+1}$  which describes the dependence of the equilibrium state on the parameter. Beginning with the starting point, the continuation program uses a predictor-corrector algorithm to locate the next point along the curve  $x^0(\alpha)$  and determines its local stability by examining the eigenvalues of the Jacobian matrix. In addition, certain test functions are used to check the occurrence of a particular bifurcation (see Chapter 10 in [76] for details).

From Section A.3 we already know that there are only two generic bifurcations that can be encountered along an equilibrium curve: a saddle-node and a Hopf bifurcation. There are now several possibilities for a further investigation.

If a saddle-node is found, one may simply continue the equilibrium branch or start a new continuation from the saddle-node point using a second parameter of the system. The latter procedure yields a curve in the two-parameter plane along which saddle-node bifurcations occur. Generically, this saddle-node curve meets with a second saddle-node curve in a cusp singularity which is a codimension two bifurcation point.

If, on the other hand, a Hopf bifurcation is encountered along the primary equilibrium curve, one may equally continue this curve (which then consists of unstable equilibrium points after the Hopf bifurcation) or switch to the new branch of periodic solutions which emanates from the Hopf bifurcation point. In the course of traversing the periodic branch, one may now observe three generic bifurcations: The saddle-node, the period doubling and the torus or Neimark-Sacker bifurcation (cf. Sec. A.3). All of these codimension one bifurcations may be continued in a second parameter of the system which leads to a refined partition of the two-parameter plane into regions where different types of complex oscillatory behavior is present.

In addition, one may encounter other codimension two bifurcation points along two-parameter bifurcation curves such as the generalized Hopf or Bautin bifurcation when traversing a branch of Hopf bifurcations. Similarly, on a branch of saddle-node bifurcations of fixed points, a Bogdanov-Takens bifurcation may occur (for details see Sec. A.4).

## B.2. Parameters and settings in the hemin system

The rate constants that were used for the simulations of the ODE system (1.2) and all its derived versions are listed in Table B.1. The variables  $x_1, \dots, x_6$  were rescaled such that the maximal amplitude of the new variables becomes of order unity. In particular, we set

$$\begin{aligned} x'_1 &= 10^4 \cdot M^{-1} x_1 & x'_4 &= 10^4 \cdot M^{-1} x_4 \\ x'_2 &= 10^2 \cdot M^{-1} x_2 & x'_5 &= 10^4 \cdot M^{-1} x_5 \\ x'_3 &= 10^4 \cdot M^{-1} x_3 & x'_6 &= 10^4 \cdot M^{-1} x_6. \end{aligned} \tag{B.4}$$

The method of numerical continuation (see Sec. B.1) was used for the hemin system to compare the original as well as the reduced ODE system according to their local

## B. Investigation Methods and Parameter Settings

Table B.1.: Rate constants (at 25°C) and inflow stream concentrations used for the numerical investigations of the hemin system. The flow rate  $k_0$  was varied between  $1 \cdot 10^{-4} s^{-1}$  and  $4.5 \cdot 10^{-4} s^{-1}$ .

$k_1 = 0.2 M^{-1} \cdot s^{-1}$	$k_2 = 1.5 M^{-1} \cdot s^{-1}$	$k_3 = 8.5 \cdot 10^6 M^{-2} \cdot s^{-1}$	$k_4 = 1000 s^{-1}$
$k_5 = 10^{10} M^{-1} \cdot s^{-1}$	$k_6 = 0.011 s^{-1}$	$k_7 = 2.5 \cdot 10^4 M^{-1} \cdot s^{-1}$	$k_8 = 1.9 \cdot 10^{-4} s^{-1}$
$x_1^0 = 0.025 M$	$x_2^0 = 0.045 M$	$x_4^0 = 2.2 \cdot 10^{-4} M$	$x_5^0 = 3 \cdot 10^{-4} M$

bifurcations. Continuation calculations were always started from a stable fixed point, which we obtained by direct numerical integration of the corresponding ODE system. The parameter region, where the stable fixed point is reached, has to be tested in several runs. We found  $k_0 = 1 \cdot 10^{-4} s^{-1}$  to be a suitable starting value.

The two principal bifurcation parameters in the hemin system are the flow rate  $k_0$  and the decay rate  $k_8$  of hemin which are both simple rate constants having the dimension  $s^{-1}$ . Their order of magnitude is  $10^{-4}$ . Thus, whenever we present numerical values of any of the two parameters, they are to be understood in units of  $10^{-4} \cdot s^{-1}$ . For example, in the ODE system (3.20), we found a subcritical Hopf bifurcation at  $(k_0, k_8) = (1.6461 \cdot 10^{-4} s^{-1}, 2.5 \cdot 10^{-4} s^{-1})$  which due to our convention would simply be denoted as  $(k_0, k_8) = (1.6461, 2.5)$ .

### B.3. Parameters and settings in the PO system

For the numerical simulations of the PO system, we used the BFSO model proposed by *Bronnikova et. al.* [87]. The underlying reaction mechanism, the components of the reaction rate vector  $R$  as well as the numerical values of the corresponding rate constants are listed in Table B.2.  $Per^{n+}$  denotes the different oxidation states of the enzyme peroxidase while coI, coII and coIII are synonyms for  $Per^{5+}$ ,  $Per^{4+}$  and  $Per^{6+}$ , respectively.

In order to obtain a quantitative picture of the asymptotic states in the PO system, we computed bifurcation diagrams by direct numerical integration of the ODE system (C.1) in dependence on the inflow rate  $k_{12}$  of NADH in the parameter range  $k_{12} = 1.1 \cdot 10^{-7} Ms^{-1} \dots 1.345 \cdot 10^{-7} Ms^{-1}$ . For each parameter value, we discarded a transient of 35000 time steps and recorded the successive maxima of the peroxidase compound III (coIII) concentration over the next 15000 time steps. The run for the first parameter value of each simulation was always started from fixed initial conditions. For subsequent runs of the same simulation, but for other parameter values, the final concentrations of the preceding run were used as new initial conditions. By this procedure, it is possible to monitor the changes in the asymptotic states as a parameter is almost continuously varied provided the parameter step size is suitably adapted. For the computation of Fig. C.2, we used a step size of  $10^{-3}$ .

Table B.2.: Detailed (BFSSO) model of the peroxidase-oxidase reaction [87] <sup>a</sup>

reaction	$R_i$	rate constants $k_i$ <sup>f</sup>
(1) $NADH + O_2 + H^+ \longrightarrow NAD^+ + H_2O_2$	$k_1[NADH][O_2]$	$3.0$ <sup>b</sup>
(2) $H_2O_2 + Per^{3+} \longrightarrow coI + H_2O$	$k_2[H_2O_2][Per^{3+}]$	$1.8 \cdot 10^7$ <sup>b</sup>
(3) $coI + NADH \longrightarrow coII + NAD^\bullet$	$k_3[coI][NADH]$	$4.0 \cdot 10^4$ <sup>b</sup>
(4) $coII + NADH \longrightarrow Per^{3+} + NAD^\bullet$	$k_4[coII][NADH]$	$2.6 \cdot 10^4$ <sup>b</sup>
(5) $NAD^\bullet + O_2 \longrightarrow NAD^+ + O_2^-$	$k_5[NAD^\bullet][O_2]$	$2.0 \cdot 10^7$ <sup>b</sup>
(6) $O_2^- + Per^{3+} \longrightarrow coIII$	$k_6[O_2^-][Per^{3+}]$	$1.7 \cdot 10^7$ <sup>b</sup>
(7) $2O_2^- + 2H^+ \longrightarrow H_2O_2 + O_2$	$k_7[O_2^-]^2$	$5.0 \cdot 10^6$ <sup>b</sup>
(8) $coIII + NAD^\bullet \longrightarrow coI + NAD^+$	$k_8[coIII][NAD^\bullet]$	$1.35 \cdot 10^8$ <sup>b</sup>
(9) $2NAD^\bullet \longrightarrow NAD_2$	$k_9[NAD^\bullet]^2$	$5.6 \cdot 10^7$ <sup>b</sup>
(10) $Per^{3+} + NAD^\bullet \longrightarrow Per^{2+} + NAD^+$	$k_{10}[Per^{3+}][NAD^\bullet]$	$1.8 \cdot 10^6$ <sup>b</sup>
(11) $Per^{2+} + O_2 \longrightarrow coIII$	$k_{11}[Per^{2+}][O_2]$	$1.0 \cdot 10^5$ <sup>b</sup>
(12) $\longrightarrow NADH$	$k_{12}$	<i>variable</i> <sup>c</sup>
(13) $O_2(gas) \longrightarrow O_2(liquid)$	$k_{13}[O_2]_{eq}$	$6.0 \cdot 10^{-3}$ <sup>d,e</sup>
(-13) $O_2(liquid) \longrightarrow O_2(gas)$	$k_{-13}[O_2]$	$6.0 \cdot 10^{-3}$ <sup>d</sup>

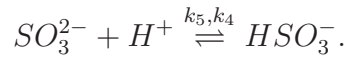
<sup>a</sup> Rate constants are taken from [13]. <sup>b</sup> In  $M^{-1}s^{-1}$ . <sup>c</sup> between  $1.1 \cdot 10^{-7}$  and  $1.345 \cdot 10^{-7} Ms^{-1}$ . <sup>d</sup> In  $s^{-1}$ . <sup>e</sup> The value of  $[O_2]_{eq}$  is  $1.2 \cdot 10^{-5} M$ . <sup>f</sup> The concentrations of  $H^+$  are taken to be constant and absorbed into the rate constants  $k_i$ , since the reaction system runs in a buffer solution at  $pH$  6.3

For the interpretation of the resulting bifurcation diagrams, one has to keep in mind that they are topologically equivalent to a Poincaré map where the cutting section in the extended ‘phase space’ (which is the usual phase space of concentrations augmented by 1 dimension for the time direction) corresponds to the time points at which the trajectory of one of the phase space variables (in our case  $coIII$ ) exhibits a maximum. Thus, limit cycles manifest themselves as fixed points, period-2 cycles as period-2 points, tori as closed invariant loops, etc.

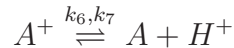


## C. Quasi-Integrals in the Peroxidase – Oxidase System

In Part I of the thesis, we have introduced the method of quasi-integrals as an algorithmic procedure which can be applied in a straightforward manner to any kind of reaction network modeled by ODE systems of the form (3.21). The method was exemplified with the hemin system where we have found one quasi-integral. However, the existence of this quasi-integral is not too surprising since it is associated with one of the reversible reaction steps in the reaction mechanism (1.1), namely with



On the other hand, the existence of the aforementioned quasi-integral is not trivial since the second equilibrium reaction in (1.1)



does not define a quasi-stationary manifold.

In order to demonstrate the fairly wide applicability of the method of quasi-integrals, we additionally investigate the reaction mechanism of the peroxidase – oxidase (PO) system which, in contrast to the hemin system, is entirely composed of irreversible reaction steps. Nevertheless, we shall identify three possible candidates for quasi-stationary manifolds. While two of them lead to reduced systems whose dynamics is in acceptable quantitative agreement with the original system, the third candidate poses an example where the dynamics of the reduced system shows only the qualitative features of the original system.

The PO reaction is the prototypical example of an oscillatory enzyme system (for a review see [88]). Considerable experimental efforts have been devoted to identify the individual reaction steps taking part in this reaction system [89]. In parallel, a series of theoretical investigations aimed at reproducing the observed type of dynamics in numerical simulations [90].

The starting point of our analysis is a reaction mechanism proposed by *Bronnikova, Fed'kina, Schaffer* and *Olsen* [87] (Table B.2) which shows periodic mixed-mode oscillations as well as (homoclinic) chaos [13, 27]. It comprises 14 irreversible reaction steps and involves 10 species. By assuming mass-action kinetics, one can derive the following 10-dimensional ODE system:

### C. Quasi-Integrals in the Peroxidase – Oxidase System

$$\begin{aligned}
\dot{x}_1 &= k_2x_4x_{10} - k_3x_1x_6 + k_8x_3x_5 & (C.1) \\
\dot{x}_2 &= k_3x_1x_6 - k_4x_2x_6 \\
\dot{x}_3 &= -k_8x_3x_5 + k_{11}x_7x_9 + k_6x_8x_{10} \\
\dot{x}_4 &= k_1x_6x_7 + k_7x_8^2 - k_2x_4x_{10} \\
\dot{x}_5 &= k_3x_1x_6 + k_4x_2x_6 - k_5x_5x_7 - k_8x_3x_5 - 2k_9x_5^2 - k_{10}x_5x_{10} \\
\dot{x}_6 &= -k_1x_6x_7 - k_3x_1x_6 - k_4x_2x_6 + k_{12} \\
\dot{x}_7 &= -k_1x_6x_7 - k_5x_5x_7 + k_7x_8^2 - k_{11}x_7x_9 - k_{-13}x_7 + k_{13}[O_2]_{eq} \\
\dot{x}_8 &= k_5x_5x_7 - 2k_7x_8^2 - k_6x_8x_{10} \\
\dot{x}_9 &= k_{10}x_5x_{10} - k_{11}x_7x_9 \\
\dot{x}_{10} &= -k_2x_4x_{10} + k_4x_2x_6 - k_6x_8x_{10} - k_{10}x_5x_{10}.
\end{aligned}$$

The parameter values for the simulations as well as the oxygen concentration  $[O_2]_{eq}$  at equilibrium between the gas/liquid phase are taken from [13] (cf. Table B.2). We used zero initial values for all species except for  $x_{10}^0$ , which was set to the total enzyme concentration of  $1.5 \cdot 10^{-6}M$ .  $k_{12}$  (corresponding to the inflow rate of NADH) was used as a bifurcation parameter ranging between  $1.1 \cdot 10^{-7}Ms^{-1}$  and  $1.345 \cdot 10^{-7}Ms^{-1}$ . The correspondence between phase space variables  $x_1 \dots x_{10}$  and chemical species is as follows:  $x_1 \leftrightarrow \text{Per}^{5+}$  (or co I),  $x_2 \leftrightarrow \text{Per}^{4+}$  (or co II),  $x_3 \leftrightarrow \text{Per}^{6+}$  (or co III),  $x_4 \leftrightarrow \text{H}_2\text{O}_2$ ,  $x_5 \leftrightarrow \text{NAD}^+$ ,  $x_6 \leftrightarrow \text{NADH}$ ,  $x_7 \leftrightarrow \text{O}_2$ ,  $x_8 \leftrightarrow \text{O}_2^-$ ,  $x_9 \leftrightarrow \text{Per}^{2+}$  and  $x_{10} \leftrightarrow \text{Per}^{3+}$ . The notation  $\text{Per}^{n+}$  stands for the different oxidation states of the enzyme peroxidase.

As in the case of the hemin system, we must take care that the chemical constraints, which are expressed by a non-maximal rank of the stoichiometric matrix, are properly taken into account, before the method of quasi-integrals is applied. For the PO system, the rank of the stoichiometric matrix associated with the ODE system (C.1) is 9. The consequential linear relationship between some of the chemical species can be taken as:

$$x_9 = x_{10}^0 - x_{10} - x_3 - x_1 - x_2, \quad (C.2)$$

which simply expresses the conservation of the total amount of enzyme peroxidase in time. Note that the reduction from 10 to 9 dimensions does not lead to any information loss due to (C.2) being an exact conservation relation. Therefore, we shall treat the 9- and 10-dimensional systems on an equal footing in the following.

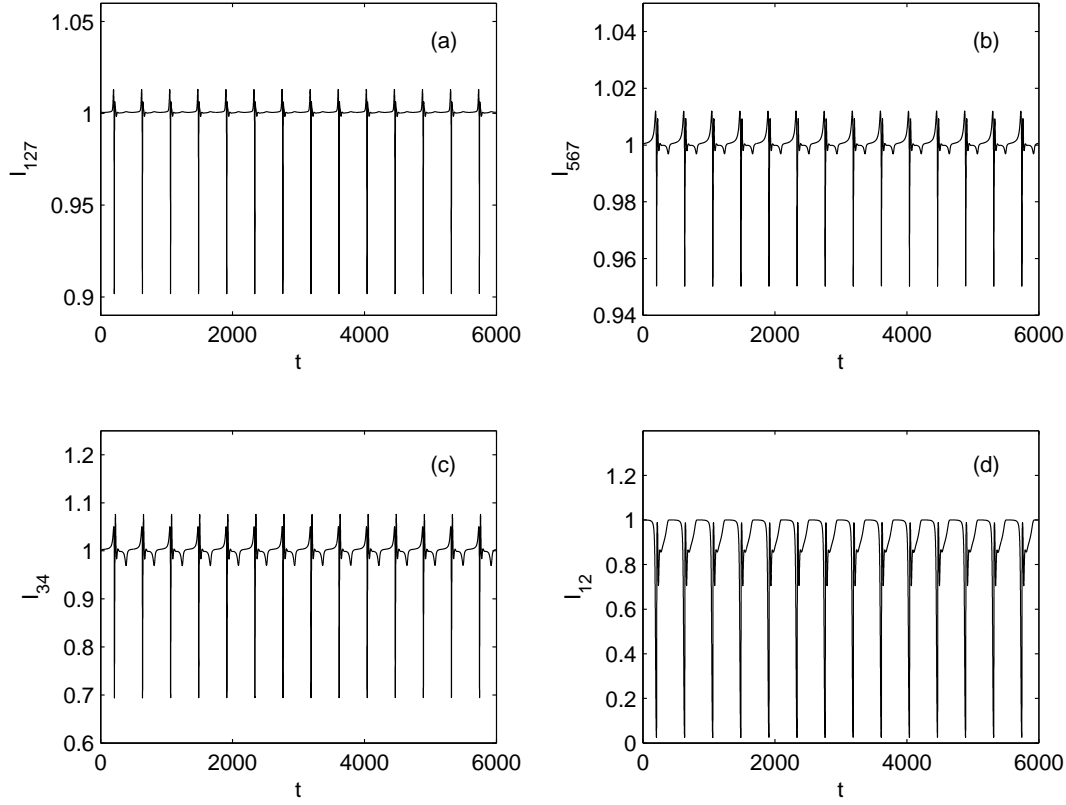


Figure C.1.: Quasi-integrals in the peroxidase–oxidase system. There are three possible candidates for quasi-stationary manifolds given by  $I_{127}$  (a),  $I_{567}$  (b) and  $I_{34}$  (c).  $I_{12}$  (d) shows that it is sometimes not enough to balance only two reaction steps in order to find a quasi-integral: Compare with  $I_{127}$  (a)

In the PO system, there are three candidates for quasi-integrals which are shown in Figs. C.1a-c (cf. Table B.2 for the definition of the  $R_i$ ):

$$\begin{aligned}
 I_{127} &= \frac{R_1 + R_7}{R_2} \sim 1 \leftrightarrow x_4 \sim \frac{k_1 x_6 x_7 + k_7 x_8^2}{k_2 x_{10}} & (C.3) \\
 I_{567} &= \frac{R_5}{R_6 + 2R_7} \sim 1 \leftrightarrow x_8 \sim -\frac{5}{2} \frac{k_6}{k_7} x_{10} + \sqrt{\frac{25}{4} \left(\frac{k_6}{k_7} x_{10}\right)^2 + \frac{1}{2} \frac{k_5}{k_7} x_5 x_7} \\
 I_{34} &= \frac{R_3}{R_4} \sim 1 \leftrightarrow x_2 \sim \frac{k_3}{k_4} x_1.
 \end{aligned}$$

We remark that the first two quasi-integrals in (C.3) are of the form (3.27) (both sides multiplied by  $-1$ ), where we had to balance three terms in order to obtain approximately constant functions. In particular, Fig. C.1d shows that it is not enough to balance only

### C. Quasi-Integrals in the Peroxidase – Oxidase System

$R_1$  with  $R_2$ , because there are time intervals where  $I_{12}$  shows large deviations from the constant value 1.

The attractivity of the quasi-stationary manifolds in (C.3) is evident by direct calculation of the corresponding Jacobian matrices, and the application of the QSSA for  $x_4$ ,  $x_8$  and  $x_2$  yields successively a 8-, 7- and finally the following 6-dimensional ODE system:

$$\begin{aligned}
 \dot{x}_1 &= k_1 x_6 x_7 + k_7 x_8^2 - k_3 x_1 x_6 + k_8 x_3 x_5 & (C.4) \\
 \dot{x}_3 &= k_6 x_{10} x_8 - k_8 x_5 x_3 + k_{11} x_7 x_9 \\
 \dot{x}_5 &= 2k_3 x_1 x_6 - k_5 x_5 x_7 - k_8 x_3 x_5 - 2k_9 x_5^2 - k_{10} x_5 x_{10} \\
 \dot{x}_6 &= -k_1 x_6 x_7 - 2k_3 x_1 x_6 + k_{12} \\
 \dot{x}_7 &= -k_1 x_6 x_7 - k_5 x_5 x_7 + k_7 x_8^2 - k_{11} x_7 x_9 - k_{-13} x_7 + k_{13} [O_2]_{eq} \\
 \dot{x}_{10} &= -k_1 x_6 x_7 - k_7 x_8^2 + k_3 x_1 x_6 - k_6 x_{10} x_8 - k_{10} x_5 x_{10}
 \end{aligned}$$

where  $x_8 = x_8(x_5, x_7, x_{10})$  in (C.4) is given as a function of  $x_5$ ,  $x_7$  and  $x_{10}$  according to the second equation in (C.3).

Let us now address the most prominent dynamical changes that have been observed during the successive reduction from a 10-variable to a 6-variable reaction mechanism. To this purpose, we compare the dynamics of the reduced systems with that of the original one by calculating *Poincaré* maps of successive maxima of the coIII concentration as the NADH inflow rate  $k_{12}$  is continuously varied (cf. Sec. B.3). This procedure yields local bifurcation diagrams which resemble those calculated in [27] due to a similar choice of parameter sets.

Figure C.2a shows the bifurcation scenario in the 10/9-dimensional system as it has already been investigated in [13]. Of particular interest are the mixed mode states  $L^S$ . (The notation  $L^S$  denotes a periodic oscillatory state where one period consists of  $L$  large and  $S$  small amplitude oscillations.) The mixed mode states as well as the alternating periodic and chaotic windows are clearly preserved throughout the reduction procedure. The bifurcation scenarios for the reduced 8- and 7-dimensional systems (Figs. C.2b,c) even show a quantitative agreement with that of the original 10/9-dimensional system (Fig. C.2a).

It is only for the 6-dimensional system that we find quantitative deviations from the original dynamical behavior, since we observe a shift in the parameter space where the first chaotic and the subsequent mixed-mode states appear (Fig. C.2d). Moreover, the order of the MMOs is changed which might be caused by an increased resolution of the periodic windows between two chaotic states. In the 6-dimensional system, the periodic windows also contain Farey progressions of  $1^S$  states with  $S > 1$  which are either absent in the 10/9-, 8- and 7-dimensional systems or occur in too narrow parameter intervals to be resolved numerically.

The reason for the quantitative deviations of the 6-dimensional system from the original dynamical behaviour may be found in the temporarily large deviations (up to 30%) of the function  $I_{34}$  in Fig. C.1c from the constant value 1. In contrast, the quasi-integrals  $I_{127}$  and  $I_{567}$  exhibit only small fluctuations around 1 of at most 10% (cf. Figs. C.1a,b).

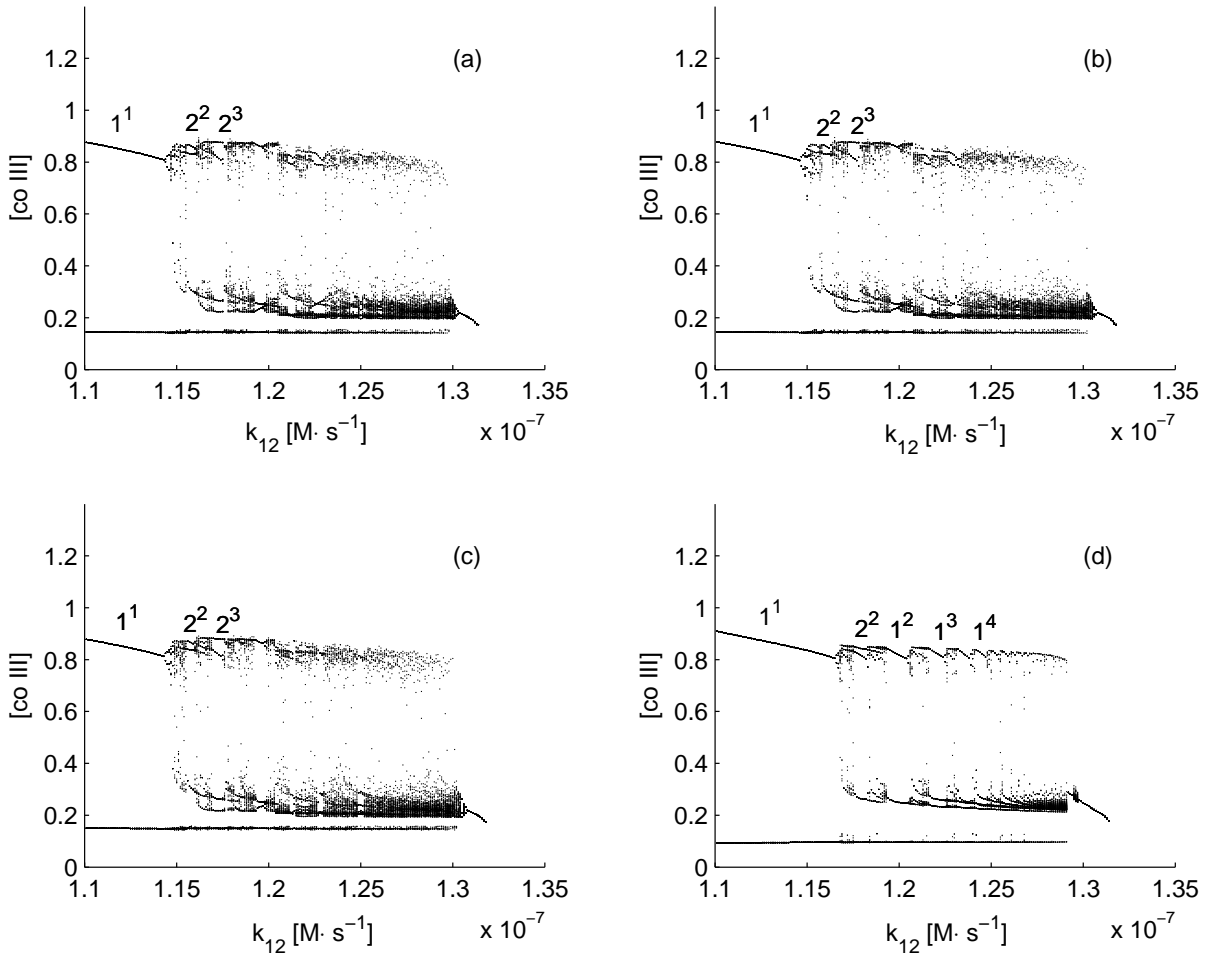


Figure C.2.: Bifurcation diagrams showing the maxima of peroxidase compound III ( $coIII$ ) concentration as the  $NADH$  inflow rate  $k_{12}$  is varied: the original 10-/9-dimensional system (a), the 8-dimensional system (using  $I_{127} \sim 1$ ) (b), the 7-dimensional system (using  $I_{567} \sim 1$ ) (c) and the 6-dimensional system (using  $I_{34} \sim 1$ ) (d). The mixed-mode states as well as the alternating periodic and chaotic windows appear in all of the reduced systems (b,c,d), but at slightly different parameter values (d). The 6-dimensional reduced system exhibits Farey sequences of  $1^S$  states with  $S = 1, 2, 3, 4$  (d).



# Bibliography

- [1] H. Poincare, *Le methodes nouvelles de la mécanique céleste*, Gauthier Villers, Paris, (1892). [1](#)
- [2] A. N. Kolmogorov, *On Conservation of Conditionally-Periodic Motions for a Small Change in Hamilton's Function*, Dokl. Akad. Nauk. USSR **98** (1954) 525. [1](#)
- [3] V. I. Arnold, *Small Denominators II, Proof of a Theorem of A. N. Kolmogorov on the Preservation of Conditionally-Periodic Motions Under a Small Perturbation of the Hamiltonian*, Russ. Math. Surveys **18** (1963) 5. [1](#)
- [4] J. Moser, *Convergent Series Expansions of Quasi-Periodic Motions*, Math. Ann. **169** (1967) 163. [1](#)
- [5] G. Nicolis, I. Prigogine, *Self-Organization in Nonequilibrium Systems*, Wiley, New York, (1977). [1](#)
- [6] H. Haken, *Synergetics*, Springer, Berlin, (2004). [3](#)
- [7] E. N. Lorenz, *Deterministic Nonperiodic Flow*, J. Atmos. Sci. **20** (1963) 130. [3](#)
- [8] S. Smale, *Diffeomorphisms with many periodic points*, in S. Carins, ed., *Differential and Combinatorial Topology*, Princeton University Press, Princeton, (1963), pp. 63. [3](#)
- [9] J. Guckenheimer, P. Holmes, *Nonlinear Oscillations, Dynamical Systems and Bifurcations of Vector Fields*, Springer-Verlag, New York, (1993). [3](#), [63](#), [73](#), [90](#)
- [10] R. A. Schmitz, K. R. Graziani, J. L. Hudson, *Experimental evidence of chaotic states in the Belousov-Zhabotinskii reaction*, J. Chem. Phys. **67** (1977) 3040. [4](#)
- [11] J. Maselko, H. L. Swinney, *Complex periodic oscillations and Farey arithmetic in the Belousov-Zhabotinskii reaction*, J. Chem. Phys. **85** (1986) 6430. [4](#)
- [12] J. L. Hudson, M. Hart, D. Marinko, *An experimental study of multiple peak periodic and nonperiodic oscillations in the Belousov-Zhabotinskii reaction*, J. Chem. Phys. **71** (1979), 1601. [4](#)
- [13] M. J. B. Hauser, L. F. Olsen, *Mixed-Mode Oscillations and Homoclinic Chaos in an Enzyme Reaction*, J. Chem. Soc., Faraday Trans. **92**, (1996) 2857. [4](#), [69](#), [101](#), [103](#), [104](#), [106](#)

## BIBLIOGRAPHY

- [14] C. G. Steinmetz, R. Larter, *The quasiperiodic route to chaos in a model of the peroxidase-oxidase reaction*, J. Chem. Phys. **94** (1991) 1388. [4](#)
- [15] T. Hauck, F. W. Schneider, *Mixed-mode and quasiperiodic oscillations in the peroxidase-oxidase reaction*, J. Phys. Chem. **97** (1993) 391. [4](#)
- [16] X. J. Wang, J. Rinzel, *The Handbook of Brain Theory and Neural Networks* in: M. Arbib (Ed.), The MIT Press, Cambridge, MA, (1995). [4](#)
- [17] L. Glass, M. C. Mackey, *From Clocks to Chaos: The Rhythms of Life*, Princeton University Press, Princeton, NJ, (1988). [4](#)
- [18] L. Brusch, W. Lorenz, M. Or-Guil, M. Bär, U. Kummer, *Fold-Hopf Bursting in a Model for Calcium Signal Transduction*, Z. Phys. Chem. **216** (2002) 487. [4](#)
- [19] M. Falcke, D. Malchow, *Understanding Calcium Dynamics*, Springer, Berlin, (2003). [4](#)
- [20] P. M. Dean, E. K. Mathews, *Glucose-induced electrical activity in pancreatic islet cells*, J. Physiol. (London) **210** (1970) 255. [4](#)
- [21] K. Wierschem, R. Bertram, *Complex bursting in pancreatic islets: a potential glycolytic mechanism*, J. Theor. Biol. **228** (2004) 513. [4](#)
- [22] A. Goldbeter, *Biochemical Oscillations and Cellular Rhythms*, Cambridge University Press, Cambridge, UK, (1996). [4](#)
- [23] J. Rinzel, G. B. Ermentrout, in *Methods in Neuronal Modeling*, C. Koch, I. Segev (eds.), The MIT Press, Cambridge, MA, USA, (1989), *Analysis of neural excitability and oscillations*. [4](#), [13](#), [51](#), [69](#)
- [24] E. M. Izhikevich, *Neural Excitability, Spiking and Bursting*, Int. J. Bifurcat. Chaos **10** (2000) 1171. [4](#), [12](#), [13](#), [53](#), [58](#), [69](#), [70](#)
- [25] D. Barkley, J. Ringland, J. S. Turner, *Observations of a torus in a model of the Belousov-Zhabotinskii reaction*, J. Chem. Phys. **78** (1987) 3812. [4](#), [70](#)
- [26] O. V. Noskov, A. D. Karavaev, V. P. Kazakov, S. I. Spivak, *Quasiperiodic to bursting oscillations transition in the model of the Belousov-Zhabotinsky reaction*, Mendeleev Commun. (1997) 27. [4](#), [70](#)
- [27] M. J. B. Hauser, L. F. Olsen, T. V. Bronnikova, W. M. Schaffer, *Routes to Chaos in the Peroxidase-Oxidase Reaction: Period-Doubling and Period-Adding*, J. Phys. Chem. B **101** (1997) 5075. [4](#), [103](#), [106](#)
- [28] M.T.M. Koper, *Bifurcations of mixed-mode oscillations in a three-variable autonomous Van der Pol-Duffing model with a cross-shaped phase diagram*, Physica D **80** (1995) 72. [4](#), [69](#), [70](#)

- [29] J. Boissonade, P. DeKepper, *Transitions from bistability to limit cycle oscillations. Theoretical analysis and experimental evidence in an open chemical system*, J. Phys. Chem. **84** (1980) 501. [4](#)
- [30] J. Ringland, N. Issa, M. Schell, *From U sequence to Farey sequence: A unification of one-parameter scenarios*, Phys. Rev. A **41** (1990) 4223. [4](#)
- [31] A. Goryachev, P. Strizhak, R. Kapral, *Slow manifold structure and the emergence of mixed-mode oscillations*, J. Chem. Phys. **107** (1997) 2881. [4](#), [69](#)
- [32] M. J. B. Hauser, A. Strich, R. Bakos, Zsuzsanna Nagy-Ungvarai and S. C. Müller, *pH oscillations in the hemin – hydrogen peroxide – sulfite reaction*, Faraday Discuss. **120** (2001) 229. [5](#), [8](#), [33](#)
- [33] M. J. B. Hauser, N. Fricke, U. Storb, S. C. Müller, (2002), *Periodic and Bursting pH Oscillations in an Enzyme Model Reaction*, Z. Phys. Chem. **216** (2002), 375. [5](#), [8](#), [33](#)
- [34] R. Straube, S. C. Müller, M. J. B. Hauser, *Bursting oscillations in the revised mechanism of the hemin – hydrogen peroxid – sulfite oscillator*, Z. Phys. Chem. **217** (2003) 1427. [5](#), [8](#), [9](#), [10](#)
- [35] G. Rabai, K. Kustin, I. R. Epstein, *A systematically designed pH oscillator: the hydrogen peroxide – sulfite – ferrocyanide reaction in a continuous-flow stirred tank reactor*, J. Am. Chem. Soc. **111** (1989) 3870. [5](#), [8](#), [9](#)
- [36] G. Rabai, *Period-Doubling Route to Chaos in the Hydrogen Peroxide – Sulfur(IV) – Hydrogen Carbonate Flow System*, J. Phys. Chem. A **101** (1997) 7085. [5](#), [8](#), [9](#)
- [37] G. A. Frerichs, R. C. Thompson, *A pH-Regulated Chemical Oscillator: The Homogeneous System of Hydrogen Peroxide – Sulfite – Carbonate – Sulfuric Acid in a CSTR*, J. Phys. Chem. A **102** (1998) 8142. [5](#), [8](#), [9](#)
- [38] I. Hanazaki, N. Ishibashi, H. Mori, Y. Tanimoto, *Bifurcation Structure in the Hydrogen Peroxide – Sulfite System*, J. Phys. Chem. A **104** (2000) 7695. [5](#), [8](#), [9](#)
- [39] G. Rabai, N. Okazaki, I. Hanazaki, *Kinetic Role of CO<sub>2</sub> Escape in the Oscillatory H<sub>2</sub>O<sub>2</sub> – HSO<sub>3</sub> – HCO<sub>3</sub> – Flow System*, J. Phys. Chem. A **103** (1999) 7224. [5](#), [8](#)
- [40] T. G. Traylor, F. Xu, *The mechanisms of reaction of hydrogen peroxide and hydroperoxides with iron(III) porphyrins*, J. Am. Chem. Soc. **109** (1987) 6202. [5](#)
- [41] G. Zhang, P. K. Dasgupta, *Hematin as a peroxidase substitute in hydrogen peroxide determinations*, Anal. Chem. **64** (1992) 517. [5](#)
- [42] Q.-Z. Zhu, F.-H. Liu, J.-G. Xu, J.-W. Huang, *Fluorescence immunossay of  $\alpha$  – 1-fetoprotein with hemin as a mimetic enzyme labelling reagent*, Fresenius J. Anal. Chem. **362** (1998) 537. [5](#)

## BIBLIOGRAPHY

- [43] G. Rabai, A. Kaminaga, I. Hanazaki, *Chaotic pH oscillations in the hydrogen peroxide-sulfite-ferrocyanide-hydrogen carbonate flow system*, Chem. Commun. **18** (1996) 2181. [5](#), [8](#)
- [44] G. Rabai, I. Hanazaki, *Chaotic pH Oscillations in the Hydrogen Peroxide-Thiosulfate-Sulfite Flow System*, J. Phys. Chem. A **103** (1999) 7268. [5](#)
- [45] G. Michal, *Biochemical Pathways*, Spectrum, Heidelberg, (1999). [6](#)
- [46] J. Keener, J. Sneyd, *Mathematical Physiology*, Springer, New York, (1998). [6](#)
- [47] P. Warneck, *The relative importance of various pathways for the oxidation of sulfur dioxide and nitrogen dioxide in sunlit continental fair weather clouds*, Phys. Chem. Chem. Phys. **1** (1999) 5471. [6](#)
- [48] H. Geiger, I. Barnes, K. H. Becker, B. Bohn, T. Brauers, B. Donner, H.-P. Dorn, M. Elend, C. M. Freitas Dinis, D. Grossmann, H. Hass, H. Hein, A. Hoffmann, L. Hoppe, F. Hülsemann, D. Kley, B. Klotz, H. G. Libuda, T. Maurer, D. Mihelcic, G. K. Moortgat, R. Olariu, P. Neeb, D. Poppe, L. Ruppert, C. G. Sauer, O. Shestakov, H. Somnitz, W. R. Stockwell, L. P. Thüner, A. Wahner, P. Wiesen, F. Zabel, R. Zellner, C. Zetzsch, *Chemical Mechanism Development: Laboratory Studies and Model Applications*, J. Atm. Chem. **42** (2002) 323. [6](#)
- [49] D. L. Allara, D. Edelson, *A Computational Modeling Study of the Low Temperature Prolysis of n-Alkanes; Mechanisms of n-Propane, n-Butane and n-Pentane Prolysis*, Int. J. Chem. Kin. **7** (1975) 479. [6](#)
- [50] J. Warnatz, *Hydrocarbon oxidation high-temperature chemistry*, Pure Appl. Chem. **72** (2000) 2101. [6](#)
- [51] L. Györgyi, T. Turányi, R. J. Field, *Mechanistic details of the oscillatory Belousov-Zhabotinskii reaction*, J. Phys. Chem. **94**, (1990) 7162. [6](#)
- [52] B. D. Aguda, B. L. Clarke, (1987), *Bistability in chemical reaction networks: Theory and application to the peroxidase – oxidase reaction*, J. Chem. Phys. **87** (1987) 3461. [6](#)
- [53] M. Eiswirth, A. Freund, J. Ross, *Mechanistic classification of chemical oscillators and the role of species*, Adv. Chem. Phys. **80** (1991) 127. [6](#)
- [54] Y.-F. Hung, I. Schreiber, J. Ross, *New Reaction Mechanism for the Oscillatory Peroxidase – Oxidase Reaction and Comparison with Experiments*, J. Chem. Phys. **99** (1995) 1980. [6](#)
- [55] A. Sensse, M. Eiswirth, *Feedback loops for chaos in activator-inhibitor systems*, J. Chem. Phys. **122** (2005) 044516. [6](#)

- [56] B. L. Clarke, *Stability of complex reaction networks*, Adv. Chem. Phys. **43** (1980) 1. [6](#)
- [57] T. Turányi, *Sensitivity analysis of complex kinetic systems: Tools and applications*, J. Math. Chem. **5** (1990) 203. [7](#)
- [58] N. D. Price, J. L. Reed, J. A. Papin, S. J. Wiback, B. O. Palsson, *Network-based analysis of metabolic regulation in the human red blood cell*, J. Theor. Biol. **225** (2003) 185. [7](#)
- [59] S. Vajda, T. Turányi, *Principal component analysis for reducing the Edelson-Field-Noyes model of the Belousov-Zhabotinsky reaction*, J. Phys. Chem. **90** (1986) 1664. [7](#)
- [60] N. Fenichel, *Geometric Singular Perturbation Theory for Ordinary Differential Equations*, J. Diff. Eq. **31** (1979) 53. [7](#), [12](#), [19](#), [39](#)
- [61] R. E. O'Malley, *Singular Perturbation Methods for Ordinary Differential Equations*, Springer, New York, (1991), pp. 83. [7](#)
- [62] G. Li, A. S. Tomlin, H. Rabitz, J. Tóth, *Determination of approximate lumping schemes by a singular perturbation method*, J. Chem. Phys. **99** (1993) 3562. [7](#)
- [63] M. R. Roussel, S. J. Fraser, *Invariant manifold methods for metabolic model reduction*, Chaos **11** (2001) 196. [7](#)
- [64] S. H. Lam, *Using CSP to understand complex chemical kinetics*, Combust. Sci. Technol. **89** (1993) 375. [7](#)
- [65] C. C. Lin, L. A. Segel, *Mathematics applied to deterministic problems in the natural sciences*, SIAM, Philadelphia, (1994). [7](#), [10](#), [18](#)
- [66] M. Schauer, R. Heinrich, *Quasi-steady-state approximation in the mathematical modeling of biochemical reaction networks*, Math. Biosci. **65** (1983) 155. [8](#)
- [67] M. Stiefenhofer, *Quasi-steady-state approximation for chemical reaction networks*, J. Math. Biol. **36** (1998) 593. [8](#)
- [68] G. Rabai, R. Orban, I. R. Epstein, *Systematic design of chemical oscillators: A model for the pH-regulated oscillatory reaction between hydrogen peroxide and sulfide ion*, J. Phys. Chem. **96** (1992) 5414. [8](#)
- [69] M. L. Kremer, *Decomposition of Hydrogen Peroxide by Haemin*, Trans. Faraday Soc. **61** (1965) 1453. [9](#)
- [70] S. B. Brown, P. Jones, *Reactions between haemin and hydrogen peroxide. 2. Destructive oxidation of haemin*, Trans. Faraday Soc. **64** (1968) 994. [9](#)

## BIBLIOGRAPHY

- [71] C. Bartocci, F. Scandola, A. Ferri, V. Carassiti, *A spectrophotometric investigation on iron(III)protoporphyrin-IX in water/alcohol/pyridine solvent systems*, Inorg. Chim. Acta **37** (1979) L473. [10](#)
- [72] N. G. van Kampen, *Stochastic Processes in Physics and Chemistry*, North-Holland, (1992). [10](#)
- [73] R. Straube, D. Flockerzi, S. C. Müller, M. J. B. Hauser, *Reduction of chemical reaction networks using quasi-integrals*, J. Phys. Chem. A **109** (2005) 441. [12](#), [23](#)
- [74] S. Schuster, R. Schuster, *A generalization of Wegscheider's condition. Implications for properties of steady states and for quasi-steady-state approximation*, J. Math. Chem. **3** (1989) 25. [29](#)
- [75] D. Hilbert, S. Cohn-Vossen, *Anschauliche Geometrie*, Springer, (1996). [29](#)
- [76] Y. Kuznetsov, *Elements of Applied Bifurcation Theory*, Springer, Heidelberg, (1998). [35](#), [73](#), [88](#), [93](#), [94](#), [97](#), [99](#)
- [77] G. Jetschke, *Mathematik der Selbstorganisation*, VEB Deutscher Verlag der Wissenschaften, Berlin, (1989). [73](#)
- [78] P. Holmes, J. L. Lumley, G. Berkooz, *Turbulence, Coherent Structures, Dynamical Systems and Symmetry*, Cambridge University Press, Cambridge, UK, (1996). [75](#)
- [79] H. Stephani, *Differentialgleichungen: Symmetrien und Lösungsmethoden*, Spektrum Akademischer Verlag, (1994). [75](#)
- [80] S. Smale, *Structurally stable systems are not dense*, Amer. J. Math. **88** (1966) 491. [82](#)
- [81] S. Smale, *Differentiable Dynamical Systems*, Bull. Amer. Math. Soc. **73** (1967) 747. [82](#)
- [82] R. Thom, *Structural Stability and Morphogenesis*, Benjamin, London, Amsterdam, Sidney, (1976). [86](#)
- [83] B. Ermentrout, *Simulating, Analyzing and Dynamical Systems: A Guide to XPPAUT for Researchers and Students*, SIAM, Philadelphia, (2002). <http://www.math.pitt.edu/~bard/xpp/xpp.html> [97](#)
- [84] W. H. Press, S. A. Teukolsky, W. T. Vetterling, B. P. Flannery, *Numerical Recipes in C. The Art of Scientific Computing*, 2nd ed., Cambridge University Press, Cambridge, UK, (1992). [97](#)
- [85] Yu. A. Kuznetsov, V. V. Levitin, *content: A multiplatform environment for analyzing dynamical systems*, Dynamical Systems Laboratory, CWI, Amsterdam, The Netherlands, (1995-1997), Available at <ftp.cwi.nl/pub/CONTENT>. [97](#)

- [86] A. Dhooge, W. Govaerts, Yu. A. Kuznetsov, *MATCONT: A MATLAB package for numerical bifurcation analysis of ODEs*, ACM Trans. Math. Softw. **29** (2003) 141. [97](#)
- [87] T. V. Bronnikova, V. R. Fed'kina, W. M. Schaffer, L. F. Olsen, *Period-doubling bifurcations and chaos in a detailed model of the peroxidase – oxidase reaction*, J. Phys. Chem. **99** (1995) 9309. [100](#), [101](#), [103](#)
- [88] M. J. B. Hauser, L. F. Olsen, in *Transport versus Structure – Their Competitive Roles in Biophysics and Chemistry*, Müller, S. C.; Parisi, P.; Zimmermann, W. (eds.), Springer, Heidelberg, (1999), pp. 252. [103](#)
- [89] A. Scheeline, D. L. Olson, E. P. Williksen, G. A. Horras, M. L. Klein, R. Larter, *The Peroxidase – Oxidase Oscillator and Its Constituent Chemistries*, Chem. Rev. **97** (1997) 739. [103](#)
- [90] R. Larter, L. F. Olsen, C. G. Steinmetz, T. Geest, in *Chaos in Chemical and Biological Systems*, Field, R. J.; Györgyi, L. (eds.), World Scientific, Singapore, (1993), pp. 175. [103](#)



# Publikationsliste

1. R. Straube, S. C. Müller, M. J. B. Hauser, *Bursting oscillations in the revised mechanism of the hemin – hydrogen peroxide – sulfite oscillator*, Z. Phys. Chem. **217** (2003) 1427.
2. R. Straube, D. Flockerzi, S. C. Müller, M. J. B. Hauser, *Reduction of chemical reaction networks using quasi-integrals*, J. Phys. Chem. **109** (2005) 441.
3. R. Straube, D. Flockerzi, S. C. Müller, M. J. B. Hauser, *Origin of bursting ph oscillations in an enzyme model system*, Phys. Rev. E. **72** (2005) 066205.



# Danksagung

An dieser Stelle sei all denjenigen gedankt, ohne deren aktive und passive Unterstützung nicht an eine Umsetzung der hier vorliegenden Arbeit zu denken gewesen wäre.

Insbesondere möchte ich Prof. Stefan C. Müller für die großzügigen Freiräume danken, die er mir für meine tägliche Arbeit gelassen hat, ohne dabei stets den Blick für das Wesentliche zu verlieren.

Marcus Hauser verdanke ich das Thema meiner Dissertation im engeren Sinne. Ursprünglich “nur” als Modellsystem zur Einarbeitung in die Theorie der nichtlinearen Dynamik gedacht, wurde das von ihm entwickelte Hämin System schon bald zum Hauptgegenstand meiner Untersuchungen, wobei die erzielten Ergebnisse teilweise weit über den ursprünglich gesteckten Rahmen hinaus gingen und damit den Grundstein für diese Arbeit legten.

Des weiteren möchte ich mich bei Prof. Dietrich Flockerzi vom Max-Planck-Institut für komplexe technische Systeme in Magdeburg für die unzähligen Diskussionen bedanken, in denen er mir (und Marcus) die Theorie singular gestörter Systeme näher gebracht und durch entscheidende Hinweise die Qualität unserer gemeinsamen Veröffentlichungen gesteigert hat.

Dank sei schlussendlich auch an meine Frau und meine Mutter gerichtet, die mir während der letzten drei Jahre meiner Promotion und insbesondere während der dreimonatigen Fertigstellungsphase der Dissertationsschrift den Rücken frei gehalten und somit den Termin bis zur Abgabe erheblich zu verkürzen geholfen haben.



# Deutsche Zusammenfassung

Die vorliegende Arbeit ist in der Theorie dynamischer Systeme angesiedelt. Sie befasst sich einerseits mit der Modellreduktion komplexer (bio-)chemischer Reaktionsnetzwerke, wobei die wesentlichen dynamischen Eigenschaften der ursprünglichen Systeme weitestgehend erhalten werden sollen und andererseits mit einer Untersuchung über den Ursprung burstartiger Oszillationen im Hämin-Wasserstoffperoxid-Sulfit-Reaktionssystem (Hämin-System). Das Hämin-System ist ein so genanntes minimales Ein-Enzym-Modell-System, das nur aus einem Enzym-Modellkomplex (Hämin) und seinen Substraten besteht. Es gehört zu einer Familie von pH Oszillatoren, die periodische Änderungen des pH Wertes in ihrer Umgebung hervorrufen können, was im Weiteren zur Änderung physiologischer Parameter wie der Permeabilität von Membranen oder der Aktivität anderer Enzyme führen kann. Somit besitzt das Hämin-System als pH Oszillator eine gewisse biologische Bedeutung, insbesondere da der Enzym-Modellkomplex Hämin in ähnlicher Form in vielen natürlich vorkommenden Enzymen vorhanden ist.

Neben einfachen periodischen Oszillationen wurden im Hämin-System experimentell auch sogenannte burstartige Oszillationen beobachtet. Letztere sind periodische Zyklen, innerhalb derer einer gewissen Anzahl an Oszillationen großer Amplitude, eine im Allgemeinen davon verschiedene Anzahl an Oszillationen kleinerer Amplitude folgen. Wegen ihrer typischen Wellenform mit abwechselnd großen und kleinen Amplituden jeweils unterschiedlicher Frequenz werden sie oft mit Signalübertragungsvorgängen in zellulären Netzwerken in Verbindung gebracht und besitzen deshalb potentiell eine gewisse physiologische Bedeutung.

Entsprechend ihrer thematischen Ausrichtung, ist die vorliegende Arbeit in zwei Teile gegliedert, die durch einen Anhang ergänzt werden.

Im ersten Teil wird die Methode der *Quasi-Integrale* beispielhaft anhand des Hämin-Systems entwickelt. Diese Methode ist numerischer Art und dient dem Auffinden langsamer invarianter Mannigfaltigkeiten in Systemen gewöhnlicher nichtlinearer Differentialgleichungen, welche häufig zum Modellieren räumlich homogener chemischer Reaktionsnetzwerke verwendet werden. Sie erweist sich insbesondere bei realistischen und deshalb meistens höher dimensionalen Systemen von Vorteil, da jene analytischen Methoden im Allgemeinen nicht mehr zugänglich sind.

Die Existenz langsamer Mannigfaltigkeiten ist charakteristisch für dissipative Systeme, in denen sich die Zustände auf zwei stark unterschiedlichen Zeitskalen entwickeln. Um diese zu finden, prüfen wir systematisch, ob Verhältnisse bestimmter Komponenten des Reaktionsgeschwindigkeitsvektors, welche die nichtlineare Kinetik der Elementarreaktionen beschreiben, entlang der durch numerische Integrationsroutinen gewonnenen Lösungskurven einen annähernd konstanten Wert annehmen. Jedem annähernd konstanten Verhältnis entspricht ein Quasi-Integral und damit eine langsame Mannigfaltigkeit.

Letztere sind durch algebraische Gleichungen gegeben und können im Folgenden dazu benutzt werden, die Dimension des ursprünglichen Differentialgleichungssystems und damit die Anzahl dynamischer Freiheitsgrade um die Anzahl gefundener Quasi-Integrale zu verringern. Dieses Vorgehen wird durch die Theorie singular gestörter Systeme motiviert, deren Grundideen wir zu Beginn des ersten Teiles der Arbeit kurz darstellen, um im Anschluss daran auch den Bezug zu den Quasi-Integralen aufzuzeigen.

Die Dynamik des Hämin-Systems wird aufbauend auf einem experimentell gut bestätigten Reaktionsmechanismus durch ein 6-dimensionales gewöhnliches Differentialgleichungssystem modelliert. Die Methode der Quasi-Integrale liefert in Anwendung auf das Hämin-System die Existenz einer langsamen Mannigfaltigkeit. Diese wird, unter Berücksichtigung zweier Massen-Erhaltungsgrößen, zur Reduktion des ursprünglich 6-dimensionalen Systems auf ein Drei-Variablen-Modell benutzt. Im Folgenden vergleichen wir die dynamischen Eigenschaften beider Systeme auf der Grundlage ihrer lokalen Bifurkationen, die als quantitatives Maß für die topologische Äquivalenz beider Systeme angesehen werden können. Dazu berechnen wir mit Hilfe numerischer Kontinuationsroutinen Ein- und Zwei-Parameter Bifurkationsdiagramme, die für beide Systeme praktisch identisch sind.

Im zweiten Teil der Arbeit untersuchen wir den Ursprung der burstartigen Oszillationen im Hämin-System in seiner 3-dimensionalen Approximation. Dazu benutzen wir eine von Rinzel und Ermentrout entwickelte Methode, bei der eine langsame dynamische Variable als quasi-statischer Bifurkationsparameter für das restliche, sich auf einer schnelleren Zeitskala entwickelnde Untersystem fungiert. In Abhängigkeit vom aktuellen Wert der langsamen Variablen gibt es unterschiedliche anziehende Zustände im schnellen Untersystem, denen die Trajektorien des 3-dimensionalen Flusses folgen, was ein geometrisches Verständnis des Flusses im Phasenraum ermöglicht. Insbesondere läßt sich der das Bursting-Verhalten charakterisierende Mechanismus nach einem von Izhikevich vorgeschlagenen Schema durch gewisse Bifurkationen im schnellen Untersystem erklären, die zum Entstehen und Verschwinden der burstartigen Oszillationen führen.

Entsprechend diesem Schema, zeigt das Hämin-System an einem fest gewählten Satz von Parameterwerten, so genanntes SubHopf/Fold-Cycle Bursting, da eine subkritische Hopf-Bifurkation zusammen mit einer Sattel-Knoten Bifurkation periodischer Lösungen, die für dicht benachbarte Werte der langsamen Variablen im schnellen Untersystem auftreten, für das Bursting-Verhalten des Hämin-Systems verantwortlich sind.

Durch eine systematische Zwei-Parameter-Bifurkationsanalyse des schnellen Untersystems, die in dieser Form bisher noch nicht benutzt worden zu sein scheint, finden wir einen Übergang im Bursting-Verhalten des Hämin-Systems von einem sogenannten SubHopf/Fold-Cycle Burster zu einem Fold/SubHopf Burster entsprechend der Klassifikation von Izhikevich. Solche Übergänge im Bursting-Verhalten in Abhängigkeit von äusseren Parametern können von physiologischer Bedeutung sein.

Schließlich untersuchen wir mit der von Rinzel und Ermentrout entwickelten Analyse-methode den Phasenfluß auf einem 2-Torus im Hämin-System und finden dadurch eine Erklärung für den Ursprung quasi-periodischen Verhaltens in diesem System, die auch für andere dynamische Systeme mit ähnlichen Tori von Bedeutung sein sollte.

# Lebenslauf

Name	Ronny Straube
geboren	am 17. September 1975 in Borna
Nationalität	deutsch
Familienstand	verheiratet, 2 Kinder

## Studium

seit 07/2005	wissenschaftlicher Mitarbeiter am Hahn-Meitner-Institut Berlin
04/2005 – 06/2005	Doktorand in der Abteilung Biophysik an der Otto-von-Guericke-Universität Magdeburg
05/2002 – 03/2005	Wissenschaftlicher Mitarbeiter und Doktorand in der Abteilung Biophysik an der Otto-von-Guericke-Universität Magdeburg Betreuer: Prof. Stefan C. Müller
November 2001	Diplomarbeit in der Arbeitsgruppe von Prof. Andreas Wipf zum Thema “Solitonen und Knoten im Faddeev-Niemi Modell”
10/1996 – 11/2001	Studium der Physik an der Friedrich-Schiller-Universität Jena

## Schulbildung

07/1994	Abitur am Bismarck Gymnasium Genthin
---------	--------------------------------------